

**Development of effective antimicrobial
nanocomposites / nanomaterials.**

Afshin Karami

A thesis submitted for the degree of master of philosophy

School of Chemical Engineering

The University of Adelaide

Australia

September 2018

Table of contents

Preface	IV
Acknowledgement	V
Declaration	VI
Abstract	VII
Chapter 1 : Introduction	1
1.1 Background	2
1.2 Bacteria structure and properties	3
1.3 Fighting back against antimicrobial resistant bacteria	5
1.4 Aim and objectives	8
1.5 Thesis structure	8
Chapter 2 : Literature review	10
2.1 Antimicrobial coating surfaces	11
2.1.1 Antimicrobial surfaces	12
2.1.2 Fabrication of a coating surface	16
2.2 Antimicrobial nanomaterials	19
2.2.1 Synthesis of NPs	20
2.2.2 Antimicrobial mechanisms of NPs	22
Chapter 3 : Antimicrobial coating surfaces	30
3.1 Introduction	31
3.2 Materials and methods	33
3.3 Results	34
3.3.1 XPS	34
3.3.2 XRD	36

3.3.3	Nanoindentation.....	39
3.3.4	Antimicrobial.....	40
3.4	Discussion	43
3.5	Conclusion.....	44
Chapter 4 : Antimicrobial nanomaterial paper		45
4.1	Introduction	46
4.2	Experimental	48
4.2.1	Raw material.....	48
4.2.2	Synthesis and processing	48
4.2.3	Characterization of as-prepared NPs	49
4.2.4	Antimicrobial evaluation of NPs	50
4.3	Results and discussion.....	51
4.3.1	XRD.....	51
4.3.2	XPS.....	53
4.3.3	Morphology	56
4.3.4	UV-Vis spectroscopy.....	60
4.3.5	Photoluminescence (PL).....	61
4.3.6	Antimicrobial efficacy	63
4.4	Antimicrobial mechanisms by Ag/I doped ZnO NPs.....	66
4.5	Conclusions	71
Chapter 5 : Conclusions and future directions.....		72
Appendix		75
References		80

Preface

This thesis is prepared in a publication format according to the specifications for the thesis of the University of Adelaide. The thesis includes publications submitted for publication and prepared in publication format:

1. A. Karami et al. “Cr-Ag coatings: synthesis, microstructure and antimicrobial properties”, *Surface Engineering Journal* (submitted and under review, reference number: SUR4539R2).
2. A. Karami et al. “Insight into antimicrobial mechanism of ZnO nanoparticle derivatives under visible light”, *Materials Science and Engineering C Journal* (submitted and under review, reference number: MSEC_2018_1919).

Acknowledgement

I would like to thank my supervisors Dr Hu Zhang and Prof Zonghan Xie for all their support, patience, encouragement and knowledge.

I am grateful to my siblings and parents, who are my life.

I would like to thank the staff from the research centre for Infectious Diseases, School of Molecular and Biomedical Sciences, the University of Adelaide for allowing me to work in their facilities for my research project. I especially thank Dr Victoria Pederick for her technical support in my research project.

I am grateful to the Adelaide University staff, the School of Chemical Engineering and Adelaide Microscopy for their support and assistance.

Also, support from the Australian Government Research Training Program Scholarship is acknowledged. The funding support from the Australian Research Council is also acknowledged.

And finally, to all the friends in the school of chemical engineering, it was great sharing laboratory with all of you during my study.

Declaration

I certify that this work contains no material which has been accepted for the award of any other degree or diploma in my name, in any university or other tertiary institution and, to the best of my knowledge and belief, contains no material previously published or written by another person, except where due reference has been made in the text. In addition, I certify that no part of this work will, in the future, be used in a submission in my name, for any other degree or diploma in any university or other tertiary institution without the prior approval of the University of Adelaide and where applicable, any partner institution responsible for the joint-award of this degree.

I acknowledge that copyright of published works contained within this thesis resides with the copyright holder(s) of those works.

I also give permission for the digital version of my thesis to be made available on the web, via the University's digital research repository, the Library Search and also through web search engines, unless permission has been granted by the University to restrict access for a period of time.

I acknowledge the support I have received for my research through the provision of an Australian Government Research Training Program Scholarship.

Afshin Karami

Signature:

Date: 20/09/2018

Abstract

Microbial infections have a long history of causing serious illnesses for human and animals. The presence of harmful bacteria, especially on the surface of the objects and equipment in hospitals, causes many mortalities for ill patients and is a major global challenge.

The inappropriate usage of antibiotics has lead to antimicrobial resistance development in bacteria. The global concern about antimicrobial resistance has triggered the development of new and more effective antimicrobial agents. A promising method is the use of novel nanomaterials against bacteria in a rapid way so that these bacteria may not be able to develop resistance. The nanoparticles (NPs) possess enhanced physicochemical properties compared with their bulk counterparts owing to a high surface to volume ratio. The metal and metal oxide nanoparticles (NPs) such as Ag, Cu and TiO₂ NPs have proven to be effective in killing bacteria through various mechanisms such as ion originating from the dissolution of NPs and reactive oxygen species (ROS) generated from the photocatalytic process. This research project is focused on synthesizing of effective antimicrobial nanocomposites/nanomaterials with novel characteristics such as rapidness, multi-mode mechanisms and induction in the visible light range.

Chapter 1 : Introduction

1.1 Background

The antibiotics have been used to combat bacteria since the 1940s (with the introduction of Penicillin) and lead to dramatic reduction of the mortality. It introduced an ambitious hope in human history that antibiotics can be expected to eliminate all infectious bacteria. However, this hope did not last long as the battle between antibiotics and bacteria became more complicated as bacteria use different mechanisms to resist antibiotics.

The main motivation to produce effective antibiotics is a relatively high number of infections caused by antimicrobial-resistant bacteria. The research survey from world health organization (WHO) has shown that only in the United States, an estimated number of two million people annually is reported to be infected with antimicrobial-resistant bacteria and 23,000 of these people die from infections [1]. The *Clostridium (C.) difficile* bacteria alone in United State infects 250,000 people annually and 14,000 of these infected people do not survive from infections eventually. The healthcare-associated infections (HCAIs), mainly caused by antimicrobial-resistant bacteria, would require the patient with a prolonged hospital stay and this brings additional burden to the health system. The HCAIs cause an estimated annual financial loss of approximately 7 billion British Pounds in Europe [2]. The culprit in these cases is bacterial resistance to the antibiotics. The overuse and/or inappropriate usage of antibiotic agents leads to the development of antimicrobial resistant bacteria. *Staphylococcus (S.) aureus* is a common pathogen in hospital environments and is one of several bacterial strains resistant to antibiotics and responsible for nosocomial infections [3].

The bacteria become resistant to antimicrobial agents by several mechanisms such as: blocking entry of the drug into the cell, inactivation of the drug by enzymes, alteration of the drug target site, efflux of the drug from the cell or alteration of metabolic pathways of the host. For example, natural antimicrobics agents such as penicillins and cephalosporins are mainly

inactivated by the enzymatic destruction. However, synthetic antimicrobial agents such as fluoroquinolones are less likely to be affected by the enzyme inactivation mechanism [3].

1.2 Bacteria structure and properties

The structure and properties of bacteria play a significant role in developing resistance against drugs. Bacteria are normally a single cell. The size of bacterial cells is very small, typically less than 2 μm in diameter. The bacteria have different cell shapes including spherical, rod-like and spiral shapes [3]. The major parts of a bacterium are flagellum, cytoplasm, ribosomes, plasma membrane, DNA, capsule, pilus and cell wall. The simplified sketch of a bacterium is shown in the following Figure 1 [4].

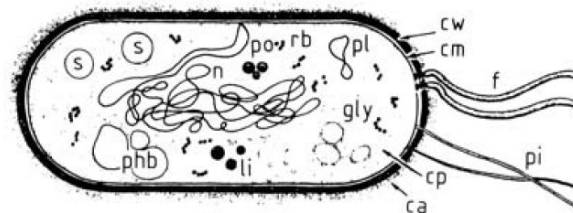


Figure 1 Bacterial cell, ca: capsule, cm: cytoplasmic membrane, cp: cytoplasm, cw: cell wall, f: flagellum, gly: glycogen, li: lipid droplets, n: nuclear material or bacterial chromosome, phb: poly (b-hydroxybutyric acid), pi: pili or pilus, pl: plasmid, po: polyphosphate, rb: ribosomes, s: sulphur granules [4].

The architectural structure, thickness and chemical compositions of each layer of the cell wall play an important role in the interaction between bacteria and antimicrobial surface agents. In 1884 Hans Christian Gram devised a method for differentiating bacteria cell walls based on their retention of violet crystal dye. The bacteria that retain the violet dye are called Gram-positive. The Gram-negative bacteria do not retain the violet dye and change the colour to red. It is also discovered that a relationship exists between the thickness of the cell wall layer (20 to 50 nm) in Gram-positive bacteria and the extent of retention of violet dye. The common antimicrobial-resistance bacteria which have been studied extensively are *Escherichia (E.) coli*

and *Pseudomonas (P.) aeruginosa* as Gram-negative bacteria and *S. aureus* and *Enterococcus (E.) faecalis* as Gram-positive bacteria. The bacteria cell wall structure for Gram-positive and Gram-negative bacteria is shown in Figure 2.

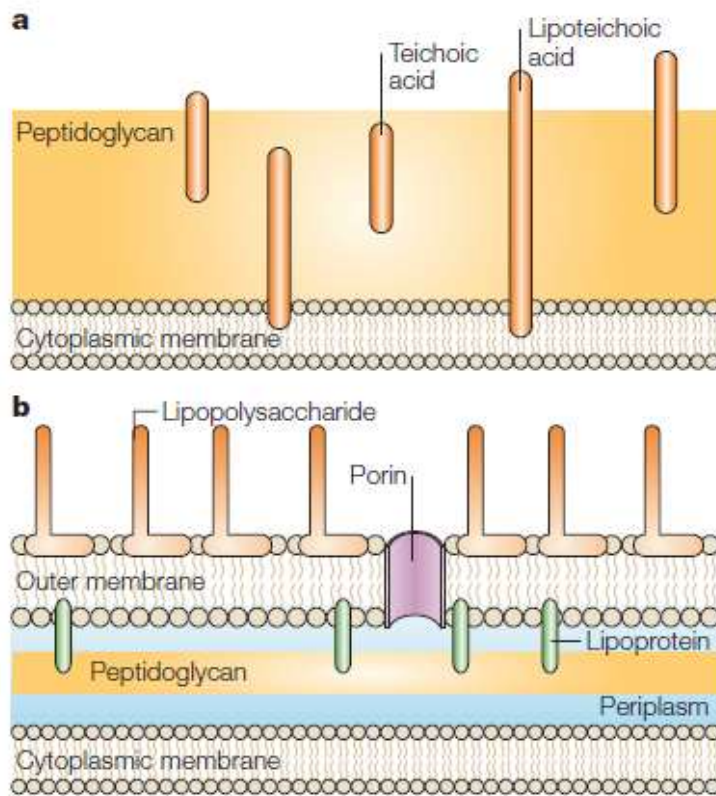


Figure 2 Bacterial cell wall structure, a: Gram-positive, b: Gram-negative [5]

The cell wall in bacteria has an essential role in controlling the osmotic pressure of the cytoplasm, providing a shape to the cell and protect the cell internals from damages. The cell wall in Gram-positive bacteria consists of a thick layer of peptidoglycan polymers with a single cytoplasmic membrane. However, the cell wall in Gram-negative bacteria is more complex. It consists of an outer membrane, two cell membranes, a plasma membrane and a thin layer of peptidoglycan [6, 7]. The difference in bacterial cell wall between Gram-positive and Gram-negative bacteria has an impact on the effectiveness of nanomaterials-based antimicrobial agents. The Gram-negative bacteria are inherently resistant to most antibiotics and biocides (e.g. detergents, heavy metals) due to their outer layer which forms a barrier to inhibit the entry of biocides into the bacteria. The major factor in selective toxicity of antibiotics is the

lipopolysaccharide (LPS) layer in the outer layer of Gram-negative bacteria. The LPS layer also contains porins protein that forms a channel across the LPS layer in order to uptake nutrients required for bacterial cell metabolism. The porins allow the passage of nucleotides, disaccharides and amino acids into Gram-negative bacteria. However, drugs with a large size and lipophilic properties, for example an affinity for lipids, could not enter into Gram-negative bacteria easily [3]. The antibiotics that have been developed in the past decades are more effective in Gram-positive bacteria but very poor for Gram-negative bacteria, which increases the demands for new antibiotics and novel antimicrobial agents.

1.3 Fighting back against antimicrobial resistant bacteria

Several core strategies are in place in order to fight against antimicrobial resistance. These strategies include preventing infections, preventing the spread of resistance, tracking/reducing antibiotic prescriptions and developing new drugs and diagnostics tests.

Preventing infections and the spread of resistance will reduce the need for an antibiotic. As the main cause of antibiotic resistance is the overuse of antibiotics, a reduction in usage of antibiotics will slow down the pace of antimicrobial resistance. New antibiotics are continuously developed as the antibiotic resistance occurs as part of a natural evolution process. Ceftaroline developed in 2010 is an example of a new antibiotic to battle against *S. aureus* and *Streptococcus* infections [8, 9]. However, production of new antibiotics is a time consuming and costly process, therefore, other strategies should be employed to prevent the spread and eliminating antimicrobial-resistant bacteria.

The most common physical methods for eliminating bacteria are heat, low temperature, desiccation, osmotic pressure and radiation. The sterilization method is a common method to eliminate the most persistent bacteria from an object, regardless of different types and different growth phases [3]. It could be applied in dry and moist (steam) forms. The advantages of

thermal sterilization are availability, ease of control and economic cost. The main mechanism of action is denaturation, destroying the enzymes in bacteria. The mechanism for the dry method is oxidation of chemical bonds, while the moist method is based on breaking the hydrogen bonds of cell proteins by water. The typical conditions for sterilization by heat requires a temperature of 121 °C for 15 minutes. At a low temperature, most microorganisms stop reproduction. Therefore, the main mechanism for a low temperature is to reduce the growth rate of the microorganisms. However, most bacteria can still grow at a much lower rate even at a low temperature. The desiccation method removes water from bacteria which is crucial for bacterial growth and reproduction. However, bacteria are viable again and resume growth and reproduction when water is present. The osmotic method has a similar mechanism as desiccation to dewater from bacteria. A high concentration of salts is applied to bacteria, and the osmotic pressure drives water from bacteria cells to the salt solution, and bacteria become non-viable after losing water [3]. The radiation method in ionizing and non-ionizing forms can eliminate bacteria. The wavelength, intensity and treatment duration are important factors for this antimicrobial method by radiation. X-ray and gamma rays are examples of ionizing radiation. They have a short wavelength with very high energy which can penetrate through the bacteria to damage them. The ionizing radiation causes ionization of water molecules to form free radicals which are lethal to bacteria due to breaking the DNA strands in bacteria. The ultraviolet (UV) light as nonionizing radiation has a higher wavelength with lower energy. The mechanism of action for UV light is based on damaging the DNA in the bacteria, which leads to binding between thymines in the DNA chains and then disrupts DNA replication [3]. All these physical methods have their own limitations. For example, the heat method cannot be applied to all surfaces such as hospital walls and doors. The ionizing light like gamma rays uses very high energy which can bring damage to most objects. The UV lights have limited penetration into objects due to a much lower energy supply.

Chemical agents such as phenol and phenolic agents, biguanides, halogens, alcohols and aldehydes have proven to be effective in controlling the bacterial growth. However, a single chemical agent cannot be used for all types of microbes. The liquid (aqueous) and gaseous chemical agents are frequently used for disinfection of surfaces from harmful bacteria. The glutaraldehyde solution ($C_5H_8O_2$) and ethylene oxide (C_2H_4O) gas are examples of common chemical agents widely used to sterilize the medical devices. The phenol and phenolic compounds such as biphenols (e.g. Triclosan and Hexachlorophene), oranges (e.g. carvacrol and limonene) and O-phenylphenol have antimicrobial properties, normally at a concentration greater than 1 % v/v. The phenolic compounds are especially effective against Gram-positive bacteria, for example, Hexachlorophene is often used to eliminate the growth of Gram-positive staphylococci and streptococci. The antimicrobial mechanism of phenolic compounds depends on the chemical structure of the compounds, especially the substitution position of the benzene ring and the saturated chain length. Inhibition of the cellular fatty acids enzymes by compromising the integrity of the plasma membrane in the bacterial cell wall has been reported as the main antimicrobial mechanism of action for the phenolic compounds [10]. The phenolic compounds have several advantages including stability and persistence for a long period of time and activity in the presence of other organic materials. The main disadvantages include irritation of skin and odour [3]. The biguanides agents such as chlorhexidine and alexidine have been reported to be effective against Gram-positive bacteria. The antimicrobial mechanism of biguanides is mainly based on the alteration of the bacterial cell wall membrane [11-13]. The halogens such as iodine (I_2), chlorine (Cl_2) are strong antimicrobial agents both as pure or constituents of other compounds. Povidone-iodine, calcium hypochlorite ($Ca(OCl)_2$) and sodium hypochlorite ($NaOCl$) and chloramine (NH_2Cl) are several examples of antimicrobial halogens compounds. The antimicrobial mechanism of action is based on impairing protein synthesis and alteration of cell membrane via binding with amino acids and unsaturated fatty acids of bacteria [14-16].

Alcohols such as ethanol (C_2H_5OH) and isopropanol (C_3H_7OH) are very effective antimicrobial agents. The alcohols normally eliminate bacteria by disrupting the bacterial membrane, denaturing the protein and dissolving the lipids within bacteria. However, pure alcohol is not effectively antimicrobial as denaturation requires water, therefore an aqueous solution with a concentration of 70 % is normally used in surface disinfection. Aldehydes are another group of chemical agents with strong antimicrobial properties. The antimicrobial mechanism is based on the formation of covalent cross-links with functional groups on proteins leading to inactivation of proteins. Formaldehyde (CH_2O) and glutaraldehyde ($C_5H_8O_2$) are two commonly used aldehydes in disinfection of hospital instruments [17, 18]. These chemical methods for eliminating bacteria also have limitations. For example, they could cause significant damage to the main material of the object, therefore their use is limited.

1.4 Aim and objectives

The aim of this research project is to develop effective nanocomposites/nanomaterials for antimicrobial purposes. The Ag and TiO_2 NPs have been evaluated for antimicrobial properties with promising efficacy. The ZnO NP (especially in visible light range) is the least tested nanomaterial for antimicrobial application and has a great potential due to high photocatalytic characteristics. The main objectives of this research project are:

- Evaluation of antimicrobial efficacy for a surface coated with a nanostructure manufactured by magnetron sputtering.
- Synthesis of a novel nanomaterial by doping zinc oxide nanoparticles in the visible light range for its application as an antimicrobial agent.

1.5 Thesis structure

The thesis is prepared in a publication format. In the first chapter, introduction and some backgrounds are described. The second chapter includes a literature review related to the

research topic. The third chapter presents the antimicrobial coating surfaces paper submitted for publication in the Journal of Surface Engineering. The fourth chapter covers antimicrobial zinc oxide (single and doped) nanoparticles. In the end, the conclusion is presented to summarise the finding on research conducted as part of this degree of Master of Philosophy - chemical engineering.

Chapter 2 : Literature review

2.1 Antimicrobial coating surfaces

In hospitals, bacteria can survive on different surfaces such as beds, doorknobs, surgical equipment and medical implants, despite widespread use of terminal cleaning such as sterilization, wiping with ethanol etc. The most common material which is used in making the surfaces for hospital setup surfaces is stainless steel (SS) due to its good corrosion resistance and high hardness, as well as low cost and ease of cleaning. However, SS is not antimicrobial.

The bacteria could form biofilm when they attach and grow on a surface. The infections caused by biofilm are especially important for the indwelling devices. The biofilms are normally resistant to antibiotics and the host immune system as they delay the penetration or diffusion of antimicrobial agents [19]. The presence of biofilms on SS in hospital settings is extremely threatening due to the presence of patients with weak or compromised immune systems. Several studies have shown the difficulties of removing bacterial biofilms through cleaning by disinfectants [20].

The biofilm is formed by a polymer-shaped matrix constituted of polysaccharide, protein and DNA which are self-produced by bacteria. The bacteria then use the biofilm as a physical barrier against antimicrobial agents for growth and colonization, therefore the biofilm acts as a protective layer for bacteria.

The biofilm formation has been investigated extensively so that antimicrobial surfaces can be prepared to prevent biofilm formation. Surface contamination often starts with bacterial adhesion to the surface. The bacteria cannot colonise on the surface if they cannot attach to the surface. Bacteria adhere to the surface via different mechanisms, involving complex chemical interactions that lead to biofilm formation. Four stages of formation of the biofilms are attachment to a surface, sessile growth, colonization and dispersion, as shown in the following

schematic [21].

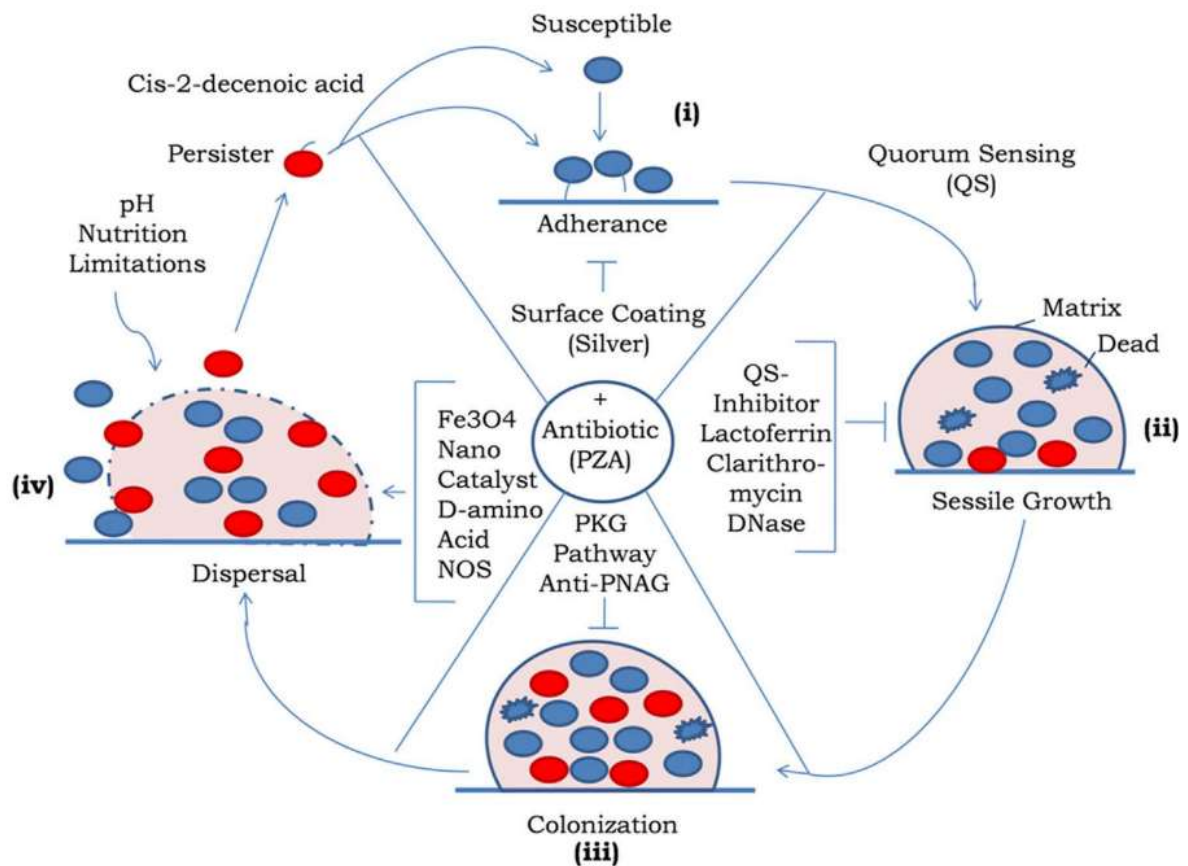


Figure 1 Biofilm formation stages: attachment to a surface, sessile growth, colonization and dispersion [21]

Adhesion of a bacterial cell to the surface is initiated by interactions of the cell with the surface and these interactions are influenced by several forces such as electrostatic and Van der Waals forces. The hydrophobicity of the surface and the bacteria cell, for example, *Staphylococcus (S.) aureus* bacteria [22], plays a crucial role in the initial adhesion of the bacteria to the surface. The hydrophobicity of the surfaces could be manipulated by synthesis methods.

2.1.1 Antimicrobial surfaces

The antimicrobial surfaces could be categorized into two main groups: (1) antifouling or bacterial repellent surfaces, i.e. preventing bacterial attachment, and (2) bactericidal surfaces,

i.e. releasing antimicrobial agents upon contact with bacteria [23]. The following table from Davide Campoccia et al. [24] presents important factors for bacterial adhesion to a surface in the aqueous phase.

Table 1 Variables affecting bacterial adhesion to a surface (David Campoccia et al. [24])

Surface morphometry	macroporosity, microporosity, micro-roughness and nano-roughness
Physico-chemical properties	surface energy, hydrophilicity/superhydrophilicity, hydrophobicity/superhydrophobicity, hydrophobic functional groups, polar functional groups, charged functional groups, functional groups with specific activities, the degree of hydration
Environmental conditions	electrolytes, pH, temperature, host proteins/host, adhesins, shear rate/fluid viscosity, fluid flow rate
Pathogen	Gram-positive/Gram-negative, genus/species, bacterial shape, surface energy, strain type and specific set of expressed adhesins

The bacteria-repellent surfaces are normally realized by surface chemistry modification, for example, surface polymerisation. Some examples of polymers for surface coating are polyethylene, polypropylene, and polyethylene glycol. The challenge of the surface polymerisation method is to control the molecular weight of the coated polymers [23]. Tiller et al. [25] synthesized poly(4-vinyl-N-alkylpyridinium bromide) on a glass substrate for the antimicrobial application. They reported a 94 % reduction of *S. aureus* using this synthesised

polymeric surface. In another study [26], the interaction between polymers and the phospholipid membrane of the bacterial cells was evaluated using poly(2-methyl-1,3-oxazoline)s (PMOX) with a N,N-dimethyldodecylammonium (DDA) end group and methyl, decyl, hexadecyl groups. Hume et al. [27] investigated the efficacy of covalently bound furanones to polymers against *Staphylococcus (S.) epidermidis*. The efficacy of furanone-coated catheters produced by co-polymerisation with styrene and plasma-1-ethyl-3-(dimethylaminopropyl) carbodiimide (EDC) reaction was 89 % and 78 % inhibition of *S. epidermidis*, respectively. Roosjen et al. [28] investigated bacterial adhesion to poly(ethylene oxide) (PEO)-brushes. They found bacterial adhesion decreased on this polymeric surface and suggested attenuation in Lifshitz–Van der Waals attractive energies was responsible for the reduction in bacterial adhesion.

The bactericidal surfaces are normally fabricated as a coating that is loaded with antimicrobial agents, such as silver, zinc, copper, and chitosan. Silver is the extensively studied metal for eliminating microorganisms due to its high efficacy, but silver is often used as an alloy coating because of its high cost and the corrosion issue. Other coatings, such as hydroxyapatite (HA) and quaternary ammonium compounds (QACs), are often reported as anti-microorganism agents [29, 30]. Zhi et al. [31] evaluated a dual-function thin film coating consisting of two layers: one layer as a reservoir to release the antimicrobial agents and the second layer of a nanoparticle cap with immobilized antimicrobial properties. The following Table 2 shows some examples for a different type of antimicrobial coatings.

Table 2 Antimicrobial coating examples (David Campoccia et al. [24])

Type of coating	Coating material	Tested bacteria	References
Antiadhesive coating	2-Methacryloyloxyethyl phosphorylcholine (MPC) polymer (Polymerization)	<i>Pseudomonas (p.) aeruginosa, S. aureus, S. epidermidis</i>	[32]
	Poly(2-methyl-2-oxazoline) (PMOXA) (Polymerization)	<i>Escherichia (E.) coli</i>	
	Trimethylsilane (Plasma polymerization)	<i>S. epidermidis</i>	[33]
Bioactive coating	Chlorhexidine (1,10-hexamethylenebis[5-(4-chlorophenyl)biguanide]) on PE (Cold Plasma)	<i>E. coli, S. aureus</i>	[34]
	Silver/hydroxyapatite composite coatings (Polymer impregnating)	<i>E. coli, S. epidermidis</i>	[35]
Nitric oxide (NO)-releasing coatings	NO-storing Zn(2p)-exchanged zeolite in a polytetrafluoroethylene polymer	<i>P. aeruginosa, S. aureus</i>	[36]

Type of coating	Coating material	Tested bacteria	References
	Quaternary ammonium (QA)-functionalized silica nanoparticles	<i>P. aeruginosa, S. aureus</i>	[37]
Reactive oxygen species-releasing coatings	Nanofibers of polycaprolactone (PCL) incorporating calcium peroxide (Electrospinning technique)	<i>E. coli, S. epidermidis</i>	[38]
	Carboxyl-ethylselen immobilized polyethylenimine (e-PEI) and alginate (Alg) alternatively assembled layer-by-layer (LbL) film	<i>E. coli, P. aeruginosa, S. aureus</i>	[39]

2.1.2 Fabrication of a coating surface

The coating surfaces can be fabricated through different methods such as electrostatic deposition [40], electrophoretic deposition [41, 42] and chemical vapour deposition (CVD), plasma polymerization and physical vapour deposition (PVD) [40, 43], [44].

In the electrostatic deposition method, a negative electrical charge is placed on the coating particles either by direct charging or by ionizing the air around the coating particles. The coating particles are then attracted to the surface when passing alongside the surface. A voltage source between 60 to 125 kV is typically used in the electrostatic deposition method [45]. The electrophoresis method is a combination of electrophoresis and deposition processes. The

electrophoresis is based on the motion of electrically charged particles in a suspension using an electric field. This method is used only to deposit ionic particles [46, 47].

The chemical vapour deposition (CVD) technique is used to produce layers with a thickness of 0.1 to 10 μm from the gas phase using a chemical reaction. The precursor can be either organic or inorganic materials. The solid precursors are converted into gaseous phase before deposition on the surface of the material to be coated. The deposition process occurs inside a chemical reactor. The quality of coating by the CVD technique is subjected to various steps within the process including adsorption and desorption of precursors, surface reaction, surface dilution, nucleation, growth of the critical nuclei, layer formation and aging process. Thermal CVD and plasma CVD are two common methods based on the CVD technique [48, 49].

The plasma polymerization technique is used to fabricate a polymeric coating of organic or organometallic materials on the surface of substrates. The plasma polymerization process occurs inside a reactor. The reactor has two internal electrodes: one electrode on which the substrate is placed is grounded; the other electrode is connected to a radio frequency power supply. The organic monomer gas, alone or combined with a carrier gas (e.g. argon) is fed into the reactor to form plasma then deposited as a coating on the surface of the substrate. The plasma polymerization method has an advantage of producing coatings with a controlled thickness of approximately 2 μm and acceptable adhesion to a variety of substrates. However, plasma polymerization requires reactors with very good vacuum integrity. Control and measurement of the pressure in the plasma polymerization reactor is also a challenging task as the pressure in the reactor could change significantly when the discharge is turned on [49].

The PVD method is a process to fabricate a thin film on a substrate. In this method, the atoms or molecules of the target material are vaporised and then deposited onto the substrate in vacuum conditions. The method can be used to deposit metals, compounds and alloys. The advantages of this method are its accuracy in depositing a very thin coating and its controlled

properties which are required for antimicrobial purposes. The PVD process can be realised through vacuum evaporation, sputter deposition, ion plating and pulsed laser deposition [50]. Figure 2 below shows a simplified configuration of the physical sputtering deposition technique.

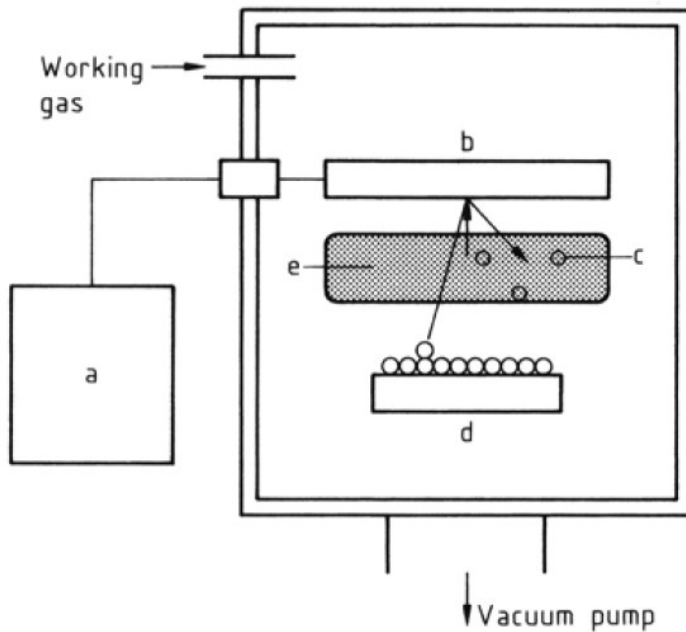


Figure 2 The physical sputtering deposition process. a- power supply, b- cathode, c- ion, d- substrate and e- plasma [49]

The magnetron sputtering deposition has also been explored to fabricate antimicrobial coating surfaces. Magnetron sputtering deposits the target atoms in a non-thermal vaporization process. In this technique, a magnetic field parallel to the cathode surface traps the electron and restrict the primary electron motion into the vicinity of a cathode. The magnetic field in this technique only influences the plasma electrons but not the ions. The high efficiency of ionization mechanism allows the process running at a very low pressure (approximately 0.15 Pa) with high current densities and at a low voltage resulting in a high sputtering rate. This technique provides a faster deposition rate compared with other techniques and can be used to create very strong adhesive coatings on substrates with very complex geometries including biomedical equipment [49, 51]. The following Figure 3 displays a simplified planar configuration of the

magnetron sputtering deposition technique [49].

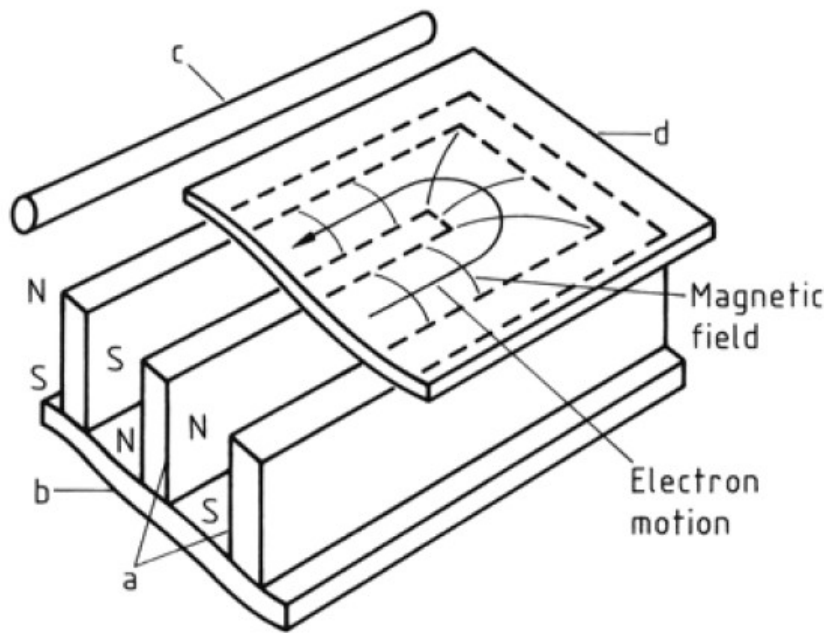


Figure 3 Planar magnetron sputtering sources a- magnets, b- pole piece, c- anode and d- cathode [49]

The magnetron sputtering deposition has the following advantages: a- a wide range of materials including metals, alloys and even components can be deposited, b- very durable deposition, c- the flexibility of deposition conditions which allow great control over the properties of the deposited coatings.

2.2 Antimicrobial nanomaterials

The nanoparticles (NP) are the material with a crystal form at a size less than 100 nm. Although the NPs have the same chemical composition as the bulk materials, they show different properties such as different conductivity and melting points. The nano size of NPs and the quantum mechanic effects contribute to the variation in these properties [52]. The NPs for antimicrobial applications have attracted attention by researchers for decades. One of the main advantages of NPs compared with its bulk materials especially for antimicrobial purposes is related to their morphology: a high ratio of surface area to volume due to their nanoscale size.

Ag, Au, copper (Cu), titanium oxide (TiO₂) and zinc oxide (ZnO) have been studied extensively for their antimicrobial purposes.

2.2.1 Synthesis of NPs

The NPs can be synthesized through various methods. The most common methods for synthesis of NPs are solvothermal, sol-gel, precipitation, sonochemical, microwave-assisted, laser ablation and combustion [53].

The solvothermal method is the most common method for synthesising NPs. In this method, NPs are formed in a small Teflon lined SS autoclave in a high pressure and temperature in the presence of a solvent. In the case of using water as the solvent, the method is called hydrothermal. The morphology of the NPs can be controlled by selecting different solvents, surfactants, pressures and temperatures. Metal oxides NPs such as zinc oxide (ZnO) and titanium oxide (TiO₂) can be readily synthesised by this method.

Precipitation and sol-gel depend on the Brownian motion of particles. The Brownian motion is a force keeping the particles suspended in liquid or gas. This force can be exerted on the particles in the form of thermal energy and it is normally greater than gravity in order to suspend the particles in the fluid. Two possible scenarios exist for the colloidal particles. In the first scenario, a bond is established between the colloidal particles upon collisions, leading to particles aggregation (known as coagulation or flocculation). The aggregated particles are then deposited at the bottom of the reactor. This is the basis for precipitation method for synthesising the NPs. Co-precipitation occurs when a couple of different materials are used. The second scenario applies to the sol-gel method. No bond is established between the colloidal particles when colliding. However, a solution colloid is normally produced after a few days and it is used as a precursor to building NPs network. The sol-gel method is often used to synthesize metal oxide NPs (e.g. TiO₂) and can also be used to make discrete NPs or polymers [54].

Ag NPs have been synthesised by different methods, each method with advantages and disadvantages. The common method to synthesise Ag NPs is to reduce silver nitrate (AgNO_3) by sodium borohydride (NaBH_4) or sodium hydroxide (NaOH). It is also common to use a capping agent to prevent aggregation and agglomeration of the NPs during the synthesis process. Aggregation happens when single particles are strongly bonded with each other, and the surface area of the resulting aggregated particles is less than the summation of the surface area of individual particles. Agglomeration, on the other hand, occurs when the bonding between single particles is not strong. The resulting surface area of the agglomerated particles is equal to the summation of the surface area of individual particles. Typical capping agents include polyethylene glycol (PEG), ethylenediaminetetraacetic acid (EDTA), polyvinyl pyrrolidone (PVP) and polyvinyl alcohol (PVA).

Rose Amal et al. [55] have synthesised Ag-doped TiO_2 NPs and evaluated the as-prepared NPs against *E. coli*. They have shown the NPs at a concentration of 50 mg/l killed 100 % of *E. coli* in 6 h. The antimicrobial mechanism of action is suggested to be silver ions produced from the synthesised NPs. The Ag ions have the bactericidal efficacy by binding them with thiol, sulfur and phosphorus groups of the bacterial cell wall to produce holes on the cell wall, which allow the Ag ions to enter the bacterial cell and bind with DNA which leads to cell death [56, 57].

A green method, using non-toxic and environmentally-safe chemicals, was used to synthesise Ag NPs by Vigneshwaran et al. [58]. In this method, AgNO_3 was reduced by starch in a one-step process at 121 °C and 15 psi. However, the synthesised NPs were polydispersed. The Ag NPs can also be synthesized using UV light. Guang-nian et al. [59] synthesised very small Ag NPs (4 to 6 nm) by irradiation of $[\text{Ag}(\text{NH}_3)_2]^+$ with UV light in the presence of PVP as the reducing and stabilizing chemicals.

2.2.2 Antimicrobial mechanisms of NPs

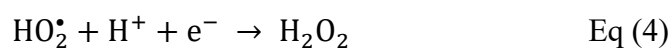
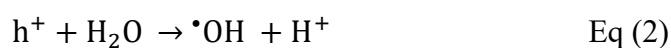
The NPs use various mechanisms to produce localised toxicity for killing microorganisms such as generation of active ions and reactive oxygen species (ROS). Metallic Ag has been used historically in a medical application, without knowing the exact mechanism of the action, over thousands of years. Different compounds of Ag such as nitrates and sulphides have also been used in dentistry, treatment of wounds and water treatment [60-62]. The mechanisms of the antimicrobial function of Ag NPs have been investigated by the scientists, however, it is still an area of debate [63-66].

One of the antimicrobial mechanisms for silver NPs is related to the accumulation of the metallic silver NPs on the bacterial membrane. The accumulated NPs form aggregation within the bacterial membrane which disturbs bacterial normal interactions leading to bacterial death [67-69]. The average size of bacteria is 1 μm (e.g. *E. coli*), while the NPs are less than 100 nm and normally have a non-uniform size distribution. This mechanism is only applicable to the fractions of the particles which are in nano-metre size.

Another antimicrobial mechanism of silver is related to ROS generated from silver-containing products [70, 71]. The mechanism of bacterial inactivation by ROS involves different actions: (1) The ROS induce pits on the bacterial membrane, which lead to leaking the intracellular organelles out of the bacteria; (2) The ROS may penetrate into bacteria internal structures through these pits and then bind with DNA and enzymes, which prevents reproduction of the bacteria.

The third mechanism of the action for silver NPs is ascribed to Ag^+ ions produced from silver [72-74]. In this mechanism, the metallic silver NPs generate Ag^+ by oxidative dissolution upon reaction with water. Ag^+ is an active cation and can bind with thiol and amino groups of bacterial proteins, resulting in deactivating the bacteria.

The photocatalytic materials such as TiO₂ and ZnO in the NP form have been intensively investigated for antimicrobial applications due to ROS emission upon illumination with light. One of the motivations for using these materials is their relatively low cost, which is ideal for making antimicrobial coatings. The photocatalytic material absorbs photons (hν) with an energy equivalent or greater than their band gap (E_G). The band gap is defined as the potential differences between the conduction band (CB) and valence band (VB). Upon absorption of the photon by the photocatalytic NPs, the electron from VB promotes to CB, which results in the formation of CB electron (e⁻) and a VB hole (h⁺). The VB hole, in fact, is lack of the electron in the CB. The electron-hole pair then simultaneously reacts with the surrounding molecules, for example, water (H₂O) and oxygen (O₂), to form ROS through the following equations [75].



TiO₂ and ZnO are both considered as semiconductors with a wide band gap. The band gap energy for TiO₂ is 3.2 eV, which requires light with a wavelength of equal to or less than 388 nm to be excited, while a light with a wavelength equal to or less than 369 nm is required to induce ZnO with a band gap of 3.37 eV. The wavelengths of 369 and 388 nm are both in the UV light wavelength range. In nature, only a small fraction of the solar light spectrum is in the UV wavelength range. The artificial UV lights can damage eyes and skins due to a very high energy level when the lights are used for medical applications.

The photocatalytic activity of TiO₂ and ZnO can be modified so that photocatalysis occurs in a higher or visible range of light wavelengths (higher than 400 nm). There are three main theories for this process: bandgap narrowing, impurity energy level and oxygen vacancies [76]. The

bandgap narrowing method is the most common method of doping NPs with another element(s). The doping process leads to a reduction in the CB energy or an increase in the VB energy or both. For example, Asahi et al. [77] have narrowed the band gap of TiO₂ NPs using a nitrogen (N) dopant. Doping of TiO₂ with different elements has been explored to produce novel NPs for antimicrobial evaluation. The following table presents doped TiO₂ NPs for antimicrobial applications. The table also includes doped novel materials whose photocatalytic activity is in the visible light condition.

Table 3 TiO₂ NP dopants for antimicrobial and photocatalytic applications

Authors	Dopants	Bacteria tested or photocatalytic evaluation	References
Duran-Alvares et al.	Au, Ag and Cu	-	[78]
Gopinath et al.	Au, Pt	<i>S. pneumoniae</i> , <i>B. subtilis</i> , <i>S. dysenteriae</i> , <i>P. aeruginosa</i> , <i>E. coli</i> , <i>K. pneumoniae</i>	[79]
Hamad et al.	Ag	<i>E. coli</i>	[80]
Jia et al.	Bi ₂ WO ₆	<i>E. coli</i>	[81]
Sood et al.	Bi ₂ O ₃	degradation of an aqueous solution of ofloxacin drug	[82]
Dhanapandian et al.	Sn	<i>Bacillus (B.) subtilis</i>	[83]
Dhineshababu et al.	SiO ₂	<i>S. aureus</i> and <i>E. coli</i>	[84]
Leyland et al.	F, Cu	<i>S. aureus</i> (ATCC 6538)	[85]
Parvathi et al.	MgO, Ag	<i>E. coli</i> and <i>B. subtilis</i>	[86]

Authors	Dopants	Bacteria tested or photocatalytic evaluation	References
Wang et al.	Y, B	<i>E. coli</i> and <i>S. aureus</i>	[87]
Sutassana et al.	V-N pair	degradation of organic pollutants	[88]
He et al.	Sr-Ag	<i>E. coli</i> and <i>S. aureus</i>	[89]
Wang et al.	Zn, Ce, Y, B, Zn/RE, Zn/B	-	[90]
Raja et al.	N, (porous TiO ₂)	Photocatalysis against methylene blue degradation	[91]
Duo et al.	BiOCl	photocatalysis against degradation of phenol	[92]
Tobaldi et al.	Cu	-	[93]
Naghibi et al.	Fe	<i>E. coli</i> , <i>S. aureus</i> , Saccharomyces cerevisiae (yeast) and Aspergillus niger (fungus)	[94]
Prabha et al.	Cd, (AC-Cd) pair	<i>Bacillus (B.) subtilis</i> , <i>S. aureus</i> , <i>E. coli</i> , <i>Pseudomonas aeruginosa</i> (<i>P. aeruginosa</i>)	[95]
Lin et al.	I	<i>E. coli</i>	[96]
Zhang et al.	Na, Pd	-	[97]

Authors	Dopants	Bacteria tested or photocatalytic evaluation	References
Yang et al., Wang et al.	B ₂ O ₃ , B, Zn	<i>Candida albicans</i> (yeast), <i>E. coli</i> , <i>S. aureus</i>	[98-100]
Kongsong et al.	N, SnO ₂	<i>E. coli</i> , <i>Salmonella typhi</i> , <i>S. aureus</i>	[101]
Yuzheng et al.	C, (C, B) pair	<i>E. coli</i> and <i>S. aureus</i>	[102]
Wang et al.	S	Photocatalysis against methyl orange	[103]
Duran-Alvares et al.	Au, Ag, Cu and Ni	<i>Aliivibrio fischeri</i> (marine Gram-negative bacteria)	[78]
Amna et al.	Co	<i>S. aureus</i> , <i>Salmonella typhi</i>	[104]
Ramya et al.	Eu, Ag	<i>P. aeruginosa</i>	[105]
Yu et al.	N	<i>E. coli</i>	[106]

The antimicrobial activity of ZnO NPs is dependent on several factors such as shape, particle size and particle charge. Different shapes of ZnO NPs are synthesised, such as sphere [107], flower, dumbbell [108], rod [109] and flake [110] shapes. Some shapes are presented in the

following images from Talebial et al. [111].

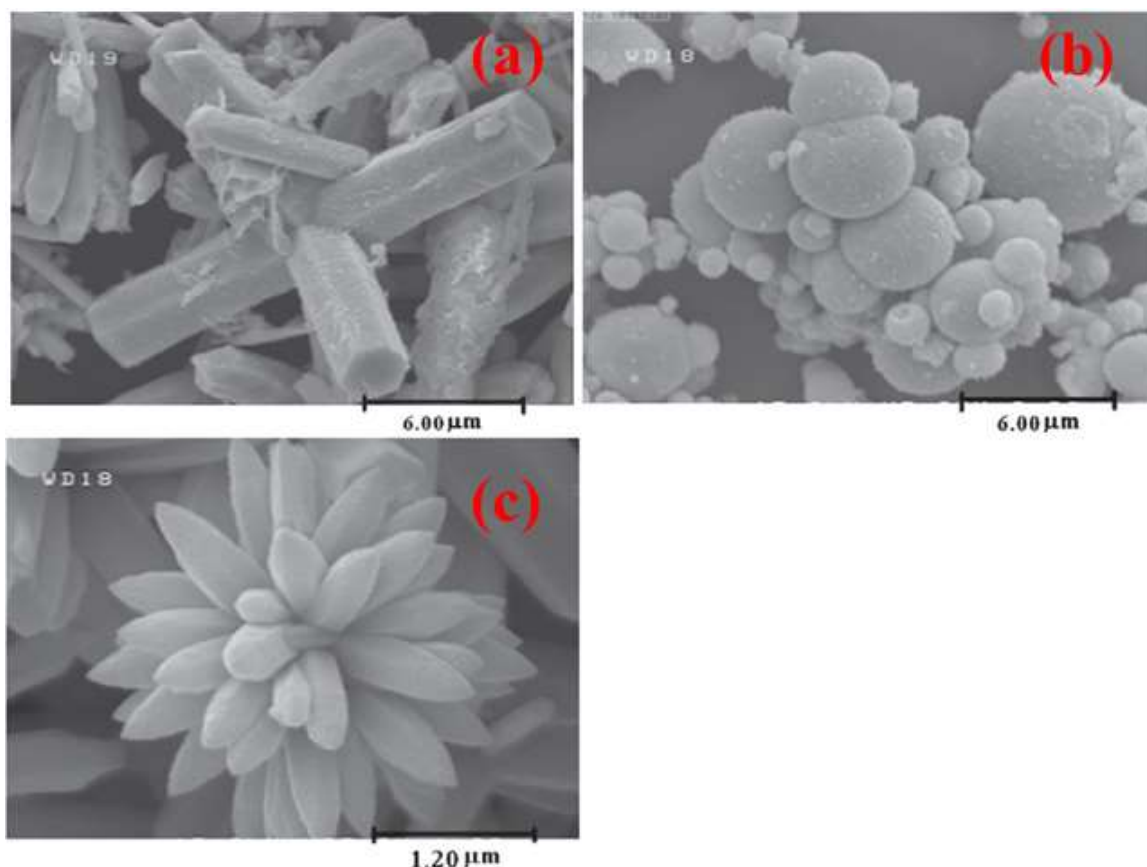


Figure 4 SEM images of ZnO NPs with different shapes synthesised by Solvothermal method. a- ZnO NPs synthesised using 1-hexanol as solvent, b- ZnO NPs synthesised using ethylene glycol as solvent, c- ZnO NPs synthesised using water as solvent [111]

ZnO NPs, similar to TiO₂ NPs, have been explored for their antimicrobial properties. The following table shows selective ZnO NPs synthesised for antimicrobial evaluations.

Table 4 Selected doped ZnO NPs for antimicrobial evaluations

Authors	Dopants	Synthesis method	Bacteria tested	References
Azizi et al.	Ag	green method	<i>E. coli</i> , <i>S. aureus</i> , <i>B. subtilis</i> ,	[112]

Authors	Dopants	Synthesis method	Bacteria tested	References
			<i>S. epidermidis</i> , <i>Salmonella choleraesuis</i> , <i>Acinetobacter anitratus</i>	
Sharma et al.	Mn, Fe	co-precipitation	<i>E. coli</i> , <i>S. aureus</i> , <i>K. pneumoniae</i> , <i>Salmonella typhi</i> , <i>P. aeruginosa</i> , <i>B. subtilis</i> . <i>Candida albicans</i> , <i>Aspergillus fumigatus</i> , <i>Cryptococcus neoformans</i> , <i>Trichophyton</i> <i>mentegrophytes</i> .	[113]
Arul Mary et al.	Ce-Cu	microwave assisted combustion	<i>E. coli</i> , <i>P. aeruginosa</i> , <i>S. aureus</i> , <i>K. pneumonia</i> , <i>B. subtilis</i>	[114]
Ravichandran et al.	(Ag- Mn) and (Ag- Mn-F)	combustion	<i>E. coli</i> , <i>Klebsiella Oxytoca</i>	[115]

In summary, healthcare-associated infections caused by antimicrobial resistance bacteria is a global challenge. The SS as the main material used in hospital setups do not have antimicrobial properties and there is an increasing demand of creating coatings to improve its antimicrobial properties. Several strategies have been employed to produce antimicrobial coatings, however, more efficient coatings by combining different technologies are continuously pursued. Metal alloy coating has been used for other applications, but very few research efforts are placed for the antimicrobial application.

The nanomaterials with their special properties compared with bulk materials have shown promising results in combating antimicrobial resistance bacteria. Several different types of nanoparticles with a variety of morphologies have been synthesised by different methods. ZnO NPs-derived NPs have received attractive attention in the antibacterial arena, especially under the illumination of visible light.

Statement of Authorship

Title of Paper	Cr-Ag coatings: synthesis, microstructure and antimicrobial properties
Publication Status	<input type="checkbox"/> Published <input type="checkbox"/> Accepted for Publication <input checked="" type="checkbox"/> Submitted for Publication <input checked="" type="checkbox"/> Unpublished and Unsubmitted work written in manuscript style
Publication Details	

Principal Author

Name of Principal Author (Candidate)	Afshin Karami				
Contribution to the Paper	Design the experiment, performed analysis on samples, interpreted data and wrote manuscript.				
Overall percentage (%)	90 %				
Certification:	This paper reports on original research I conducted during the period of my Higher Degree by Research candidature and is not subject to any obligations or contractual agreements with a third party that would constrain its inclusion in this thesis. I am the primary author of this paper.				
Signature	<table border="1" style="width: 100%;"> <tr> <td style="width: 80%;"></td> <td style="width: 20%;">Date</td> </tr> <tr> <td></td> <td>13.03.18</td> </tr> </table>		Date		13.03.18
	Date				
	13.03.18				

Co-Author Contributions

By signing the Statement of Authorship, each author certifies that:

- i. the candidate's stated contribution to the publication is accurate (as detailed above);
- ii. permission is granted for the candidate to include the publication in the thesis; and
- iii. the sum of all co-author contributions is equal to 100% less the candidate's stated contribution.

Name of Co-Author	Dr. Hu Zhang				
Contribution to the Paper	Design the experiment, interpreted data, co-wrote the manuscript and acted as corresponding author.				
Signature	<table border="1" style="width: 100%;"> <tr> <td style="width: 80%;"></td> <td style="width: 20%;">Date</td> </tr> <tr> <td></td> <td>13.03.18</td> </tr> </table>		Date		13.03.18
	Date				
	13.03.18				

Name of Co-Author	Prof. Zonghan Xie				
Contribution to the Paper	Design the experiment, interpreted data, co-wrote the manuscript and acted as corresponding author.				
Signature	<table border="1" style="width: 100%;"> <tr> <td style="width: 80%;"></td> <td style="width: 20%;">Date</td> </tr> <tr> <td></td> <td>13/03/18</td> </tr> </table>		Date		13/03/18
	Date				
	13/03/18				

Name of Co-Author	Mohammad Sharear Kabir		
Contribution to the Paper	Performed analysis on samples, Interpreted data, co-wrote the manuscript.		
Signature		Date	03/04/18

Name of Co-Author	Prof. Paul Munroe		
Contribution to the Paper	Interpreted data and co-wrote the manuscript.		
Signature		Date	3/4/18

Chapter 3 : Antimicrobial coating surfaces

Paper title: Cr-Ag coatings: synthesis, microstructure and antimicrobial properties

Afshin Karami, Hu Zhang, Mohammad Sharear Kabir, Paul Munroe, and Zonghan Xie

Journal of Surface Engineering, (submitted and under review, manuscript number: SUR4539R2)

Abstract

Cr-Ag coatings for antimicrobial surface applications were fabricated by magnetron sputtering. The coating microstructure and mechanical properties were characterised using XPS, XRD, FESEM, TEM and nanoindentation measurement as a function of Ag content. The antimicrobial efficacy of these Cr-Ag coatings was evaluated against the pathogenic bacteria *Escherichia coli* and *Staphylococcus aureus*, revealing varied levels of bacterial killing. This study warrants further investigation into the antimicrobial mechanism of action of silver and future applications of Cr-Ag as antimicrobial coating for healthcare settings.

Keywords: antimicrobial surfaces, coating, silver, chromium

3.1 Introduction

Nosocomial bacterial infections are a significant reason for morbidity and mortality worldwide. Estimated 4,131,000 individuals within Europe acquire nosocomial infection each year [1]. Together these infections result in 147,000 deaths, either directly or indirectly [2]. The rates of nosocomial infections are also increasing due to the development of bacterial strains which are resistant to available antibiotics. Within hospitals, bacteria are capable of surviving on a range of surfaces thereby facilitating transmission. This is despite the widespread utilisation of terminal cleaning following discharge of patients. Nosocomial infections commonly arise from bacteria present on surfaces such as beds, doorknobs, surgical equipment and medical implants. Many of these are made of stainless steel (SS) due to its good corrosion resistance and high hardness, as well as low cost and ease of cleaning. However, SS is not antimicrobial [116]. Bacteria antiadhesive surfaces [117-119], intrinsically antimicrobial biomaterials [120, 121], bioactive antimicrobial coatings [34, 38, 122-125], nanostructured biomaterials [126, 127] and bioactive molecules [24, 128, 129] all form the current surface antimicrobial arsenal. However, these surfaces are generally polymer-based, mechanically weak and susceptible to heat and

environmental damage and so they are not suitable for biomedical applications. Therefore, development of an antimicrobial coating which maintains the advantageous mechanical properties of a material such as SS would be highly beneficial in preventing the transmission of bacterial infections within healthcare settings.

Silver (Ag), in metallic [61], salt [130] and nanoparticle forms [131, 132] has proven to be antimicrobial. Several studies have suggested silver ions (Ag^+) released from the dissolution of metallic silver to be the basis for its antimicrobial effects [44, 56, 68, 132]. Metallic silver is a noble metal with the standard reduction potential (E°) of 0.7996 V [133]. Upon contact with water molecules in the environment, silver is oxidized by dissolved oxygen (O_2) in the water and generates a silver ion (Ag^+) that serves as an active antimicrobial species [44, 68]. Silver is an attractive antimicrobial material due to its potent antimicrobial activity, relatively low toxicity to humans, and durability in the environment. However, employing pure silver (as an antimicrobial agent) in biomedical applications is limited. This is primarily due to the increased cost and decreased corrosion resistance of silver by comparison to SS. Further, pure silver could also cause the uncontrolled release of the Ag^+ ions, which could also result in localised toxicity [24].

Silver-containing surfaces for biomedical application have been investigated in multiple studies. Textiles containing Ag [134], Ag-doped titanium dioxide (TiO_2) surfaces [135-137], Ag-doped zinc oxide (ZnO) nanocomposite textiles [138], Ag-copper (Cu) alloy [139] and Ag-hydroxyapatite [140] are several examples of silver-containing surfaces investigated as antimicrobial surfaces. The selection of materials and synthesis methods to produce precise thin coatings with the required mechanical properties are important factors in manufacturing antimicrobial coatings suitable for healthcare applications.

Hard alloy coatings with a small, optimised quantity of silver (acting as a reservoir for release of the Ag^+ ions) could be engineered onto SS for biomedical applications. Here, we report the

synthesis and characterisation of chromium-silver (Cr-Ag) alloy coatings. Chromium (Cr)-based coatings were utilised as they show excellent mechanical characteristics such as hardness and corrosion resistance. However, Cr has not been extensively characterised as an antimicrobial agent.

3.2 Materials and methods

Magnetron sputtering is an advanced method for producing very thin coatings with controlled properties. This technique was used to deposit the antimicrobial alloy coatings onto glass microscope slides (76 x 26 mm and a thickness of approximately 1 mm), and the microstructure properties of the coatings were characterised. In this experiment, a magnetron sputtering system (closed field unbalanced UDP650, Teer Coatings Ltd., UK) was utilised to deposit the Cr-Ag coatings. The magnetron with the configuration of a pure Ag (99.99 %) target, two Cr (99.5 %) target and a dummy target were used in this process. The dimensions of the targets were 345 mm x 145 mm x 8 mm. The substrates were cleaned using an ultrasonic bath, polished then dried by nitrogen gas. The substrates were placed on the holder then the distance between the substrate and target adjusted to 170 mm. The pulse DC with a frequency of 250 kHz was used to bias the substrates. The chamber pressure reduced to a background pressure of 4×10^{-4} Pa. The high purity Argon (Ar) gas with a flow rate of 50 sccm and pressure of 0.18 Pa was added to the chamber through mass flow controller (MKS). The Cr-Ag coating deposition process occurs in two steps of plasma ion cleaning followed by Cr-Ag layer deposition. The substrates were cleaned in order to remove contaminants from their surfaces hence superior adhesion of coatings. The substrates were cleaned by ion etching at a temperature of approximately 200 °C and a bias voltage of -450 V for 30 minutes. After that, the Cr-Ag coatings with approximately 0.8 µm thickness were prepared by co-sputtering the Cr target and the Ag target. The sputtering power of the Cr target was 1.3 kW at a fixed target current of 4.0 A. The bias voltage of -60 V was used during the deposition stages. In order to prepare the Cr-Ag coatings with different

percentages of Ag, the Ag target currents of 0, 0.3 and 1.0 A were selected in the deposition stage. The deposition times between 30 and 60 min was used to ensure the total coating thickness reached approximately 0.8 μm . The pure Ag and pure Cr coatings were also prepared by only sputtering Ag or Cr at a target current of 2.0 A for 30 min. All the depositions were carried out at the ambient temperature, with the substrate holder rotating at a speed of 10 rpm. The composition, microstructure and mechanical properties of as sputtered coatings were examined using XPS, XRD, FESEM, TEM and nanoindentation tests.

3.3 Results

3.3.1 XPS

The X-ray photoelectron spectroscopy (XPS) is a tool to define and study the chemical bonding structure in the coatings. To do so, Al $K\alpha$ radiation (photon energy, $h\nu = 1,468.68$ eV) was applied as the excitation source. The high resolution (HR) scans were carried out at 100 eV while the spectrometer calibration was performed using binding energy levels of Au4f7 (83.96 eV), Ag3d5 (368.21 eV) and Cu2p3 (932.62 eV). From the XPS graphs in Fig. 1, the deconvolution of HR spectra of Cr3p clearly indicates the presence of metallic chromium and chromium (III) oxide [141]. The existence of Cr (III) oxide is further confirmed by the deconvolution of O 1s HR spectra [141] indicating the highly oxidizing nature of the Cr-Ag coatings since the enthalpy of formation of Cr (III) oxide is quite high (-1134.70 kJmol⁻¹ [142]). Furthermore, Cr3p and Ag3d5 spectra clearly show the absence of bonding between Cr and Ag. Studies on the Cr-Ag system by Hindrichs [143], Allen [144] and Grigorev et al. [145] confirm the immiscibility of Cr and Ag in both solid and liquid states indicating the absence of any stable intermediate phases.

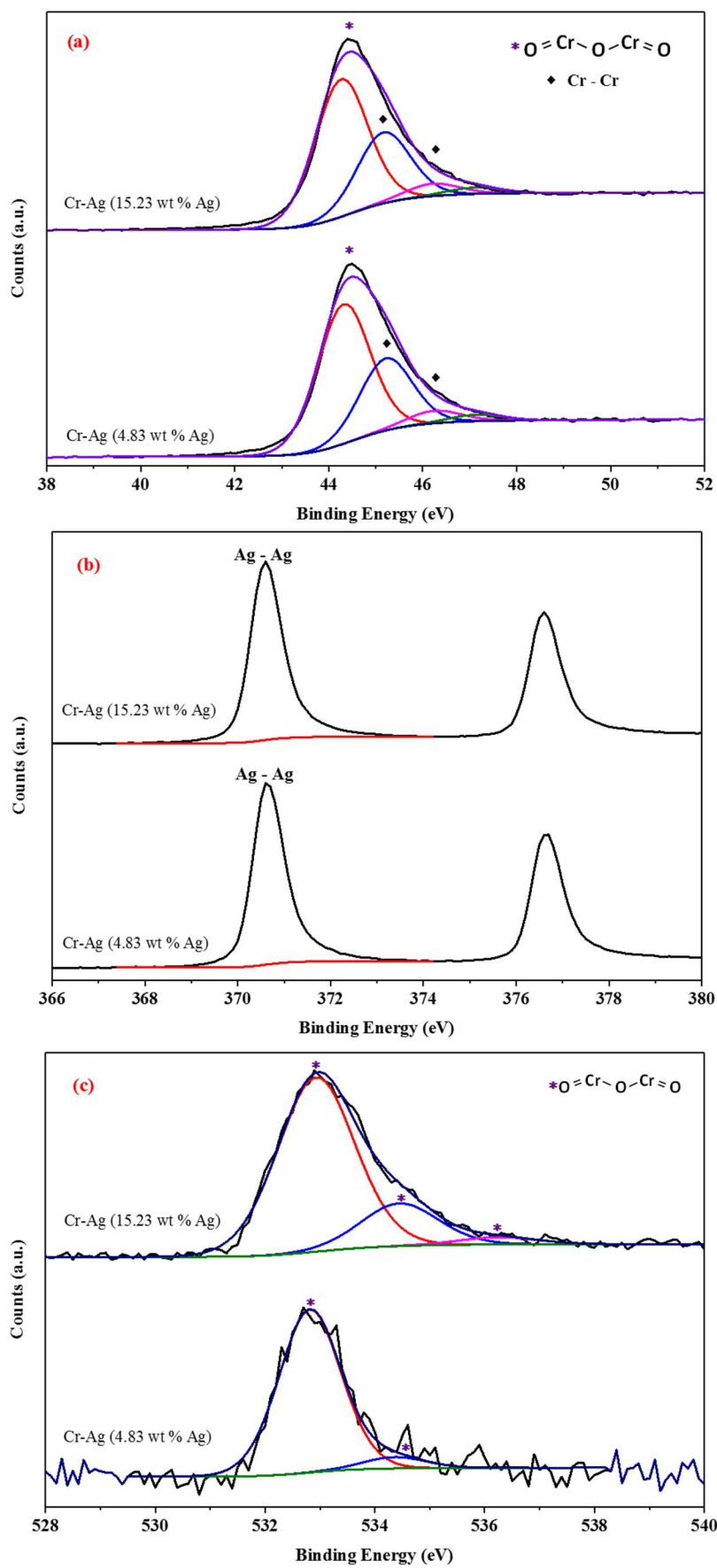


Figure 1 Deconvoluted HR spectra of (a) Cr3p, (b) Ag3d5 and (c) O1s

3.3.2 XRD

The X-ray diffraction (XRD) patterns for the Cr-Ag coatings along with pure Ag and Cr coatings are shown in Fig. 2. Diffraction peaks corresponding to Ag are absent in the pure Cr coating [Fig. 2(a)] and even after the addition of 4.83 wt.% Ag [Fig. 2(b)]. However, diffraction peaks corresponding to face-centre cubic (FCC) Ag (111) is observed in Cr-Ag coating surfaces [Fig. 2(a)] after addition of 15.23 wt.% Ag, accompanied by a slight shift towards higher 2θ angles. The majority of the diffraction peaks are representative of BCC polycrystalline Cr. This can be further confirmed from selected area electron diffraction (SAED) patterns. The SAED analyses were carried out using transmission electron microscopy (TEM) micrographs presented in Fig. 4. The structure and morphology of the pure Ag and Cr coatings were also investigated by focused ion beam microscopy (FIB, FEI xT Nova Nanolab USA) and TEM (Philips CM 200). Figure 3 presents the ion-induced secondary electron (SE) images. Pure Ag coating consists of a coarse-grained structure with a rough coating surface, whereas pure Cr coating consists of the columnar grained structure. The size of the columnar grains in the Cr rich coatings decreases with the addition of Ag which can be seen from FIB micrographs in Fig. 3(d) and in the TEM micrographs in Fig. 4.

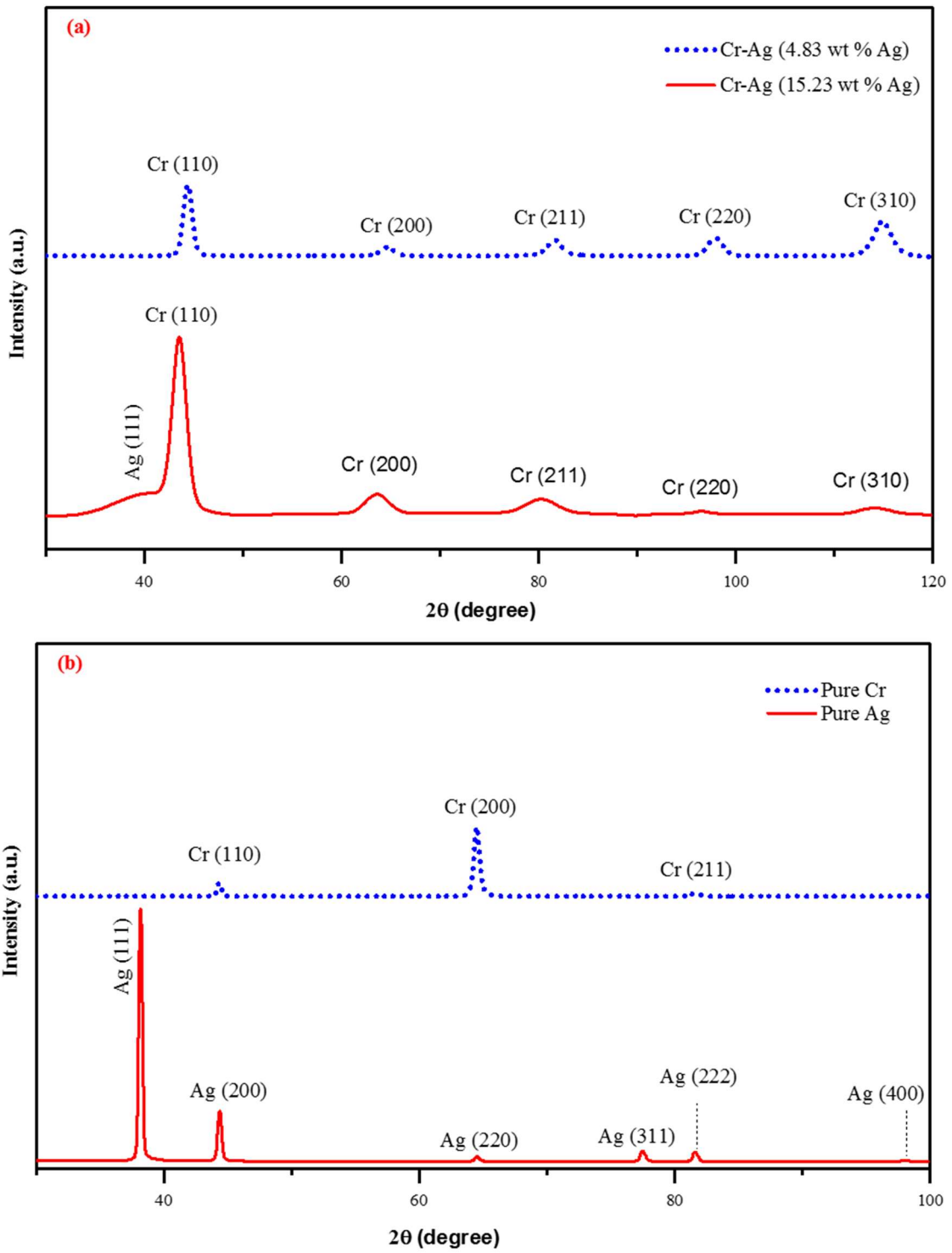


Figure 2 GI-XRD patterns of (a) Cr-Ag coatings and (b) Pure Cr and Ag

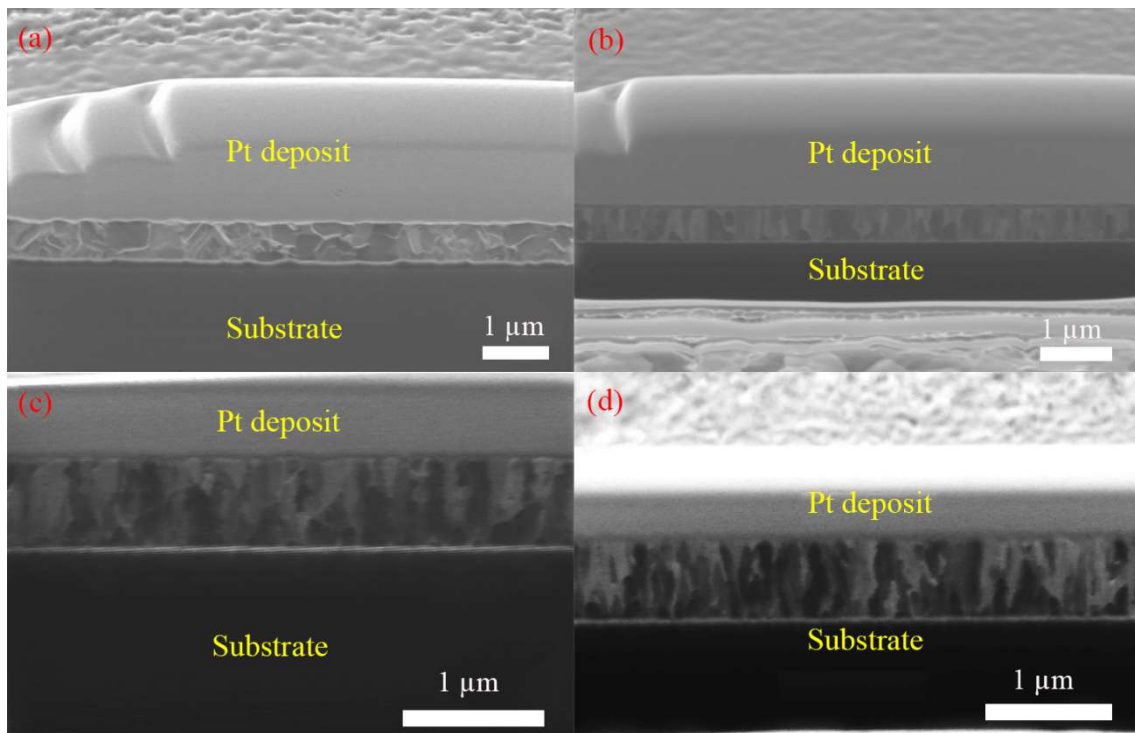


Figure 3 Ion induced SE micrographs of: (a) Pure Ag, (b) Pure Cr, (c) Cr-Ag 4.83 wt.% and (d) Cr-Ag 15.23 wt.%. Substrate refers to microscope glass, the platinum (Pt) coating has been used to facilitate SEM measurement.

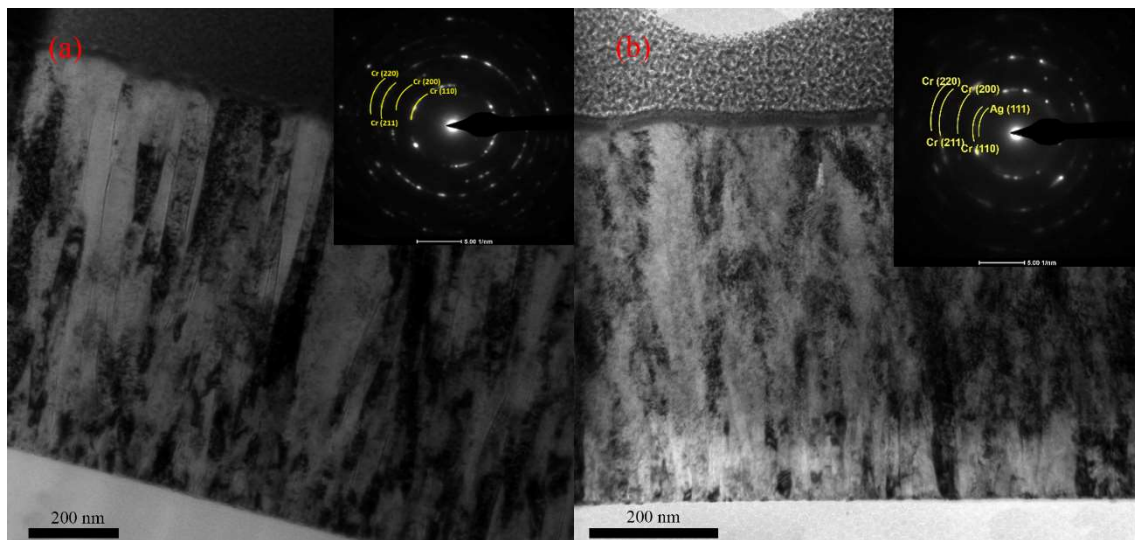


Figure 4 Bright field TEM micrographs of (a) Cr-Ag 4.83 wt.% and (b) Cr-Ag 15.23 wt.%

3.3.3 Nanoindentation

The nanoindentation tests were performed using a Hysitron Triboindenter (Hysitron TI900, USA) to determine several mechanical properties of the coatings, including hardness (H), elastic modulus (E), elastic strain to failure (H/E), plastic deformation resistance (H^3/E^2) and energy required to plastically deform the coating (E_p). The coating samples were indented, where the load-unload segments were carried out at a maximum load of 8 mN with each in 10-second duration in a linear fashion. Each sample was subjected to more than twelve indents at different locations. The Oliver-Pharr method was utilised to determine the modulus and hardness [146-148] and are presented in Table 1. From the results, it can be seen that an increase in the Ag content in Cr-Ag coatings leads to an increase in the hardness and a decrease in the modulus of the coatings by almost 24 GPa. As a result, the H/E and H^3/E^2 ratios increase by almost 1.5 and 2 times, respectively. This means a potential increase in coating toughness, which is further confirmed by an increase in plastic deformation energy, E_p , derived from the area under the load-displacement curves.

Table 2 Nanoindentation measurements (hardness (H), elastic modulus (E), elastic strain to failure (H/E), plastic deformation resistance (H^3/E^2) and energy required to plastically deform the coating (E_p). Data are presented as mean \pm standard deviation

Samples	H (GPa)	E (GPa)	H/E	H^3/E^2 (GPa)	E_p (NJ)
Pure Ag	1.3 ± 0.32	103.7 ± 2.8	0.012536	0.000204	0.11
Pure Cr	9.0 ± 0.58	208.6 ± 4.9	0.043145	0.016753	0.44
4.83 % Ag	7.1 ± 0.43	132.3 ± 3.5	0.053666	0.020448	0.34
15.23 % Ag	8.1 ± 0.45	108.3 ± 3.3	0.074792	0.04531	0.41

3.3.4 Antimicrobial

A modified method based on the Japanese standard JIS Z 2801:2010 [149] was used to determine the antimicrobial efficacy of samples. Microscope slides coated with pure Cr, pure Ag, 4.83 % Ag, or 15.23 % Ag and a glass microscope slide without any coating were used. The pure Ag coating was used as a positive control and the glass slide without coating was used as a negative control. The antimicrobial properties of each surface were assessed against both the Gram-negative bacterium *Escherichia (E.) coli* MG1655 and the Gram-positive bacterium *Staphylococcus (S.) aureus* USA300.

Cells were grown to the mid-logarithmic phase in Mueller Hinton Cation-Adjusted media (Becton Dickinson), prior to dilution in phosphate buffered saline (PBS) solution to 10^7 colony forming units per ml (CFU/mL) for use in each assay.

The coatings were sterilized by wiping with 100 % ethanol and left to dry inside a biosafety cabinet. Each antimicrobial test was performed inside a sterilized petri-dish, with moist Whatman filter paper placed at the bottom of the petri-dish to provide sufficient humidity and to avoid evaporation of PBS used in the assay. Four glass microscope slides were placed on the paper filter, to ensure the test coatings did not contact the paper and absorb the test solution. 50 μ L of diluted bacteria (10^7 CFU/ml) was added to the coating surface. A sterile glass microscope slide was placed on the coating to spread the bacteria evenly on the surface of the coating. The petri-dishes were then placed at 37 °C for 1 hour. Upon completion of the treatment, PBS was used to wash the coating surface and cover slide. The collected samples were spread on luria bertani 1.5 % agar plates allowing for bacterial enumeration and determination of antimicrobial efficacy. Bacterial survival after 1hr was assessed on each surface in at least biological triplicate for at least 3 separate coated slides of each Cr-Ag formulation (Figure 5). Statistical analysis was performed by one-way ANOVA by comparing

the survival of each surface relative to the glass control, with significance indicated by * for $P < 0.05$; *** for $P < 0.001$; and **** for $P < 0.0001$.

The pure Ag coatings were very effective in killing *E. coli*, resulting in 2.74 log CFU reduction in survival relative to the glass control, while the pure Cr showed 0.26 log CFU reduction of survival cells. Of the two Cr-Ag alloys tested, the coating with 4.83 % Ag exhibited greater antimicrobial activity (0.82 log CFU reduction) compared to the glass control, with a 0.32 log CFU reduction of viable cells the Cr-Ag coating with 15.23 % Ag. The antimicrobial efficacy of the coatings followed a similar pattern with *S. aureus*, however, all surfaces were less antimicrobial against this organism, with the pure silver resulting in an 0.92 log CFU reduction and the 4.83 % Ag and 15.23 % Ag coatings resulting in 0.67 log CFU reduction and 0.26 log CFU reduction, respectively.

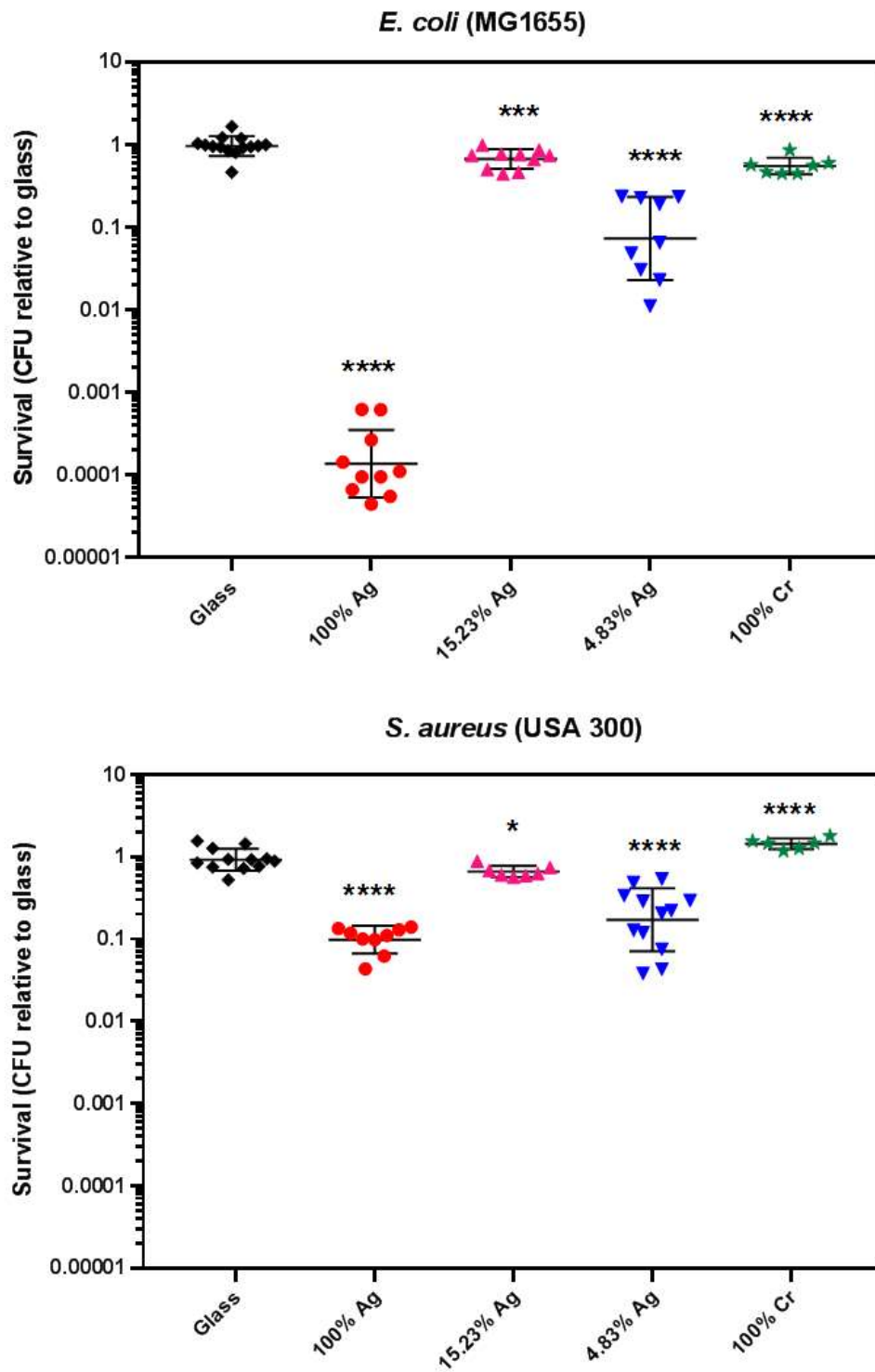


Figure 5 Antimicrobial efficacy of the Cr-Ag surfaces against *E. coli* (MG1655) and *S. aureus* (USA300). Statistical analysis was performed by one-way ANOVA by comparing the cell survival on each surface relative to the glass control, with significance indicated by * for P <0.05; *** for P <0.001; and **** for P <0.0001

3.4 Discussion

Despite the inclusion of silver as an antimicrobial in wound dressings, the exact antimicrobial mechanism(s) of silver remain unclear. Several studies [44, 56, 68, 132] have suggested that the possible mechanism of action for metallic silver might be via Ag^+ ions, which can be generated by oxidative dissolution of silver. These Ag^+ ions can then bind phosphorus, thiol and sulfur groups of the bacterial cell membrane, increasing permeability [56]. Ag^+ ions may also be able to penetrate the membrane, and bind to DNA, thereby inhibit DNA replication and resulting in cell death [56, 57, 150-153]. Our results also demonstrate that Ag^+ ions released from the coating surface may be the key factor for reducing viable cells.

According to the Japanese standard JIS Z 2801:2010 [149], the treatment time for the bacteria on the sample surfaces is 24 ± 1 h. However, examination of bacterial survival after 24 h on Cr-Ag coatings using either 4.83 % or 15.23 % Ag resulted in 4 log CFU reduction against both tested bacteria (data not presented). Rather, in the present study, the treatment time was set to be 1 h to enable comparison of the antibacterial efficacy for different Cr-Ag coatings. Also, within a hospital setting, it is likely that a time-frame for the bacterial killing of more than 1 h would be beneficial for reducing bacterial transmission from contaminated surfaces. Our analyses demonstrated bacterial survival had an order of $15.23\% \text{ Ag} > 4.83\% \text{ Ag} > 100\% \text{ Ag}$. Whilst this was consistent across both the Gram-negative bacterium *E. coli* and the Gram-positive bacterium *S. aureus*, the level of survival for *S. aureus* on the surfaces was greater than that for *E. coli*. This may indicate that the differences in the cell envelope structure play a role in resistance to killing on the tested surfaces. Gram-positive bacteria featuring a single membrane and a thicker protective peptidoglycan cell wall, and this is in contrast to the cell envelope of Gram-negative bacteria, which features both inner and outer membranes with a thin peptidoglycan layer between the membranes [5, 154]. Further analysis is required to

determine the relative antibacterial efficacy of these surfaces against different bacterial genera, including examples of both Gram-positive and Gram-negative organisms.

3.5 Conclusion

In conclusion, Cr-Ag coatings were manufactured by magnetron sputtering to evaluate their applicability as an antibacterial coating on medical surfaces. The nanoindentation measurements revealed an acceptable level of mechanical properties for these coatings. The results confirmed that an increase in the Ag content in Cr-Ag coatings will increase the hardness and decrease the modulus of the coatings. As a result, a potential increase in coating toughness was observed, and confirmed by an increase in plastic deformation energy (E_p). Consistent with previous studies which have characterised the antimicrobial nature of Ag, the 100 % Ag coating had a very strong antimicrobial efficacy against *E. coli*. Contrary to expectations, the 15.23 % Ag coating did not have a greater antimicrobial efficacy than the 4.83 % Ag coating against either *E. coli* or *S. aureus*. Together, this study confirmed the antimicrobial properties of Cr-Ag coatings, which can be adjusted by varying the Ag content. This warrants further investigation into their mechanism of antimicrobial action and future potential as an antimicrobial coating for healthcare settings.

Acknowledgements

Afshin Karami thanks the support of Australian Government Research Training Program Scholarship. This work was supported by Australian Research Council Discovery Project [DP160104632] to Z.X. and H.Z. Australian Research Council Discovery Project [DP170102102] and a Future Fellowship [FT170100006] to C.A.M.


Conflicts of interest

There are no conflicts to declare.

Statement of Authorship

Title of Paper	Insight into the antimicrobial mechanism of ZnO nanoparticle derivatives under visible light	
Publication Status	<input type="checkbox"/> Published	<input type="checkbox"/> Accepted for Publication
	<input type="checkbox"/> Submitted for Publication	<input checked="" type="checkbox"/> Unpublished and Unsubmitted work written in manuscript style
Publication Details		


Principal Author

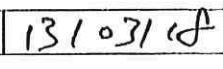
Name of Principal Author (Candidate)	Afshin Karami	
Contribution to the Paper	Design the experiment, performed analysis on samples, interpreted data, wrote manuscript and acted as corresponding author.	
Overall percentage (%)	95 %	
Certification:	This paper reports on original research I conducted during the period of my Higher Degree by Research candidature and is not subject to any obligations or contractual agreements with a third party that would constrain its inclusion in this thesis. I am the primary author of this paper.	
Signature		Date 13.03.18

Co-Author Contributions

By signing the Statement of Authorship, each author certifies that:

- i. the candidate's stated contribution to the publication is accurate (as detailed above);
- ii. permission is granted for the candidate to include the publication in the thesis; and
- iii. the sum of all co-author contributions is equal to 100% less the candidate's stated contribution.

Name of Co-Author	Dr. Hu Zhang	
Contribution to the Paper	Design the experiment, interpreted data, co-wrote the manuscript and acted as corresponding author.	
Signature		Date 13/03/18

Name of Co-Author	Prof. Zonghan Xie	
Contribution to the Paper	Design the experiment, interpreted data, co-wrote the manuscript.	
Signature		Date 13/03/18

Name of Co-Author	Mohammad Sharear Kablr		
Contribution to the Paper	Performed analysis on samples, Interpreted data, co-wrote the manuscript.		
Signature		Date	03/04/18

Name of Co-Author	Prof. Paul Munroe		
Contribution to the Paper	Interpreted data and co-wrote the manuscript.		
Signature		Date	3/4/18

Chapter 4 : Antimicrobial nanomaterial paper

Paper title: Insight into the antimicrobial mechanism of ZnO nanoparticle derivatives under visible light

Afshin Karami, Hu Zhang, Mohammad Sharear Kabir, Paul Munroe, and Zonghan Xie

Materials Science and Engineering C (submitted and under review, manuscript number: MSEC_2018_1919)

Abstract

ZnO nanoparticles doped with I and Ag were prepared via a solvothermal method. Characterizations of as-synthesised samples were carried out using X-ray diffraction (XRD), X-ray photoelectron spectroscopy (XPS), UV-Vis spectrometry, Photoluminescence (PL), transmission electron microscopy (TEM) and scanning electron microscopy (SEM). The nanoparticles exhibited wide-spectrum light absorption from ultra-violet (UV) to visible light. The antimicrobial efficacy was evaluated against *Escherichia coli* (MG1655) and *Staphylococcus aureus* (USA300) as models of Gram-negative and Gram-positive microorganisms respectively. The double-doped nanoparticles had demonstrated their potent efficacy against both types of microorganisms and they may have great potential application in combating infectious diseases. More importantly, the mechanisms underlying the antimicrobial samples were revealed: synergistic effect of reactive oxygen species (ROS) generation and Ag⁺ release. However, ROS generation was more dominant in the I:Ag:ZnO sample, while Ag⁺ release played an important role in the Ag:I:ZnO. We also confirmed that a small fraction of Ag in the AgO form in the sample was enough to eliminate these pathogenic bacteria.

Keywords: antimicrobial; nanomaterial; ZnO; visible light

4.1 Introduction

Healthcare-associated infection (HCAI) caused by antimicrobial-resistant bacteria is a global health challenge. For example, more than 4 million individuals within Europe acquire HCAI each year which directly or indirectly results in 147, 000 mortalities [2]. The antimicrobial resistance occurs when bacteria develop genetic mutations to protect themselves against conventional antibiotics. The overuse and/or inappropriate usage of antibiotics has been suggested as the main reason for antimicrobial resistance development in bacteria [155].

The global concern about antimicrobial resistance has triggered the development of new multi-functional antimicrobial agents. A promising method is the use of novel nanomaterials against bacteria in a rapid way so that these bacteria may not be able to develop resistance. The nanoparticles (NPs) possess enhanced physicochemical properties compared with their bulk counterparts owing to a high surface-to-volume ratio [156]. Metal oxide NPs such as titanium oxide (TiO₂), zinc oxide (ZnO), selenium oxide (SnO₂) and cerium oxide (CeO₂) NPs have been reported to be effective antimicrobial agents when they are exposed to ultra-violet (UV) light [6, 157-160]. Among metal oxide NPs, ZnO NPs with different morphologies and crystal structures have been examined for their antimicrobial properties due to attractive features such as low cost, ease of synthesis, high photocatalytic activities and good biocompatibility [6].

The antimicrobial mechanisms vary among different types of NPs. Although the exact antimicrobial mechanism of ZnO NP remains unclear, several bacteria-killing pathways have been proposed. The toxicity of Zn²⁺ ion originating from the dissolution of ZnO NPs, reactive oxygen species (ROS) generated from the photocatalytic process, and bacterial membrane dysfunction have been reported as possible antimicrobial mechanisms for the ZnO-based NPs [60, 161-167]. Based upon these pathways, the antimicrobial efficacy of ZnO NPs would be strongly dependent on their physical properties such as size, morphology and surface energy [6]. Among these properties, the morphology of ZnO NPs may be manipulated by synthesis techniques, such as solvothermal, precipitation and sol-gel methods. The details of different synthesis methods and the resulting morphologies for ZnO NPs have been reviewed by Kolodziejczak-Radzimsk et al. [168] and Sirelkhatim et al. [6]. ZnO NPs in a pure form have been demonstrated to be less effective in antimicrobial efficacy, mainly due to their wide band-gap and a high recombination rate of charge carriers which result in limited efficiency under solar irradiation [162, 169, 170]. The photocatalytic activity of ZnO NPs can be improved by modification of their crystal structure via insertion of defects and impurities. Doping of ZnO

NPs with other elements such as B, Mn, Mo, Ce, Cu, Pd has been explored as an effective strategy in improving the antimicrobial properties of ZnO NPs in the visible light regime [170-174]. In this study, ZnO-based NPs were synthesised using a solvothermal method. Iodine (I) and silver (Ag) were used as single and double dopants with different combinations (I-ZnO, Ag-ZnO, I-Ag-ZnO, and Ag-I-ZnO) in order to improve the antimicrobial properties of ZnO NPs. The synthesised NPs were then characterized with a range of techniques including X-ray diffraction (XRD), X-ray photoelectron spectroscopy (XPS), UV-Vis spectrometry, photoluminescence (PL), transmission electron microscopy (TEM) and scanning electron microscopy (SEM). The antimicrobial efficacy of the synthesised NPs was investigated against Gram-negative *Escherichia (E.) coli* (MG1655) and Gram-positive *Staphylococcus (S.) aureus* (USA300) bacteria as model microorganisms.

4.2 Experimental

4.2.1 Raw material

The zinc acetate dihydrate ($\text{Zn}(\text{CH}_3\text{COO})_2 \cdot 2\text{H}_2\text{O}$, purity > 98 %), ethylene glycol ($\text{C}_2\text{H}_6\text{O}$, 99.8 %), hydriodic acid (HI, 57 wt. % in H_2O , 99.95 % HI) and cetyltrimethylammonium bromide (CTAB, 99 %) were supplied from Sigma-Aldrich. The zinc nitrate hexahydrate ($\text{Zn}(\text{NO}_3)_2 \cdot 6\text{H}_2\text{O}$, 99.5 %), sodium hydroxide (NaOH, 97 %) and silver nitrate (99.99 %) were purchased from Chem-supply. All reagents were of analytical grade and used as received.

4.2.2 Synthesis and processing

ZnO NPs were synthesised via the solvothermal method using zinc acetate dihydrate as a precursor and ethylene glycol as the solvent. In a typical synthesis, 5.6 g of zinc acetate dihydrate was dissolved in 50 ml pure ethylene glycol and the mixture was vigorously stirred at 60 °C for 45 min. The mixture solution was then added to a Teflon-lined autoclave to react at 170 °C for 18 h. Upon completion of the synthesis, the precipitated ZnO NPs were collected

by centrifugation, washed with ethanol and deionized water several times and then dried at 80 °C for 12 h. The synthesised ZnO NPs were used later as a precursor for I:ZnO NPs.

The Ag:ZnO NPs were synthesised via the following procedure. In a typical process, 5.6 g zinc nitrate hexahydrate, 0.637 g silver nitrate, 0.309 g CTAB and 40 ml of absolute ethanol were mixed in a flask. The mixture was vigorously agitated at room temperature for 15 min and then 0.6 g sodium hydroxide was gradually added. The mixture was stirred for 1 h. The mixture solution was then added to a Teflon-lined autoclave to react at 120 °C for 3 h. The precipitated silver doped zinc oxide NPs were collected by centrifugation, washed with ethanol and deionized water several times and then dried at 80 °C for 12 h.

The I:ZnO NPs were synthesised by mixing 25 ml of absolute ethanol with hydriodic acid (HI) and previously synthesised ZnO NPs at a molar ratio of HI to ZnO of 1:1. The mixture was vigorously stirred at room temperature for 4 h and then added to a Teflon-lined autoclave to react at 160 °C for 12 h. The I:Ag:ZnO NPs were synthesised from the similar procedure, but Ag:ZnO NPs were served as a precursor. The Ag:I:ZnO NPs were also synthesised by doping the I:ZnO NPs (as a precursor) with Ag using the above procedure.

4.2.3 Characterization of as-prepared NPs

The crystal structure of the synthesised NP samples was analysed by X-ray diffraction (XRD) on MiniFlex 600 (Rigaku, Cu K α , $\lambda = 0.15418$ nm). The XRD was operated at 40 kV and 15 mA and the X-ray diffractions were collected at the scanning range from 10° to 80° with a step size of 0.02°. X-ray photoelectron spectroscopy (XPS) was employed to investigate the surface chemistry of the NPs using ESCALAB250Xi (Thermo Scientific, UK). Al K α radiation (photon energy, $h\nu = 1486.68$ eV) was used as the excitation source. The high resolution (HR) scans with a pass energy of 100 eV were carried out. The spectrometer calibration was performed using binding energy levels of Cu2p₃ (932.62 eV), Ag3d₅ (368.21 eV) and Au4f₇ (83.96 eV).

The particle size and morphology of synthesised NPs were investigated by a scanning electron microscopy (SEM, Quanta 450) and transmission electron microscopy (TEM) FEI Tecnai G2 Spirit TEM operated at 120 kV accelerating voltage. The hydrodynamic size and zeta potential of the synthesized NPs in aqueous suspensions (Milli Q water) were evaluated by dynamic light scattering (DLS) using Zetasizer Nano (Malvern Instruments Ltd., UK). A He-Ne laser with a wavelength $\lambda = 633$ nm was used as the light source. The intensity of light was scattered at 173° angle. The optical property of the NPs was evaluated by a spectrophotometer UV-3600 Plus, Shimadzu with an integrated sphere and a Renishaw inVia Raman Microscope integrated with Photoluminescence at an excitation wavelength of 325 nm. The band gap energy of the synthesised NPs was calculated by the Tauc plot using the following equation: $(h\nu\alpha)^{1/n} = A (h\nu - E_g)$, where h is Planck's constant, ν is the frequency of vibration, α is the absorption coefficient, E_g is the band gap, A is a proportion constant and n is the nature of sample transition ($n = 2$ for indirect allowed transition) [169, 175, 176].

4.2.4 Antimicrobial evaluation of NPs

The antimicrobial efficacy of NPs samples was determined in two modes: illumination by exposure to visible light and no illumination under the dark conditions. The dark conditions were used as a control to evaluate the potential bacterial reduction due to the light source which was used to activate ZnO NPs. The antimicrobial efficacy results in dark conditions also assist in elucidating the mechanism(s) other than ROS of the as-synthesized ZnO NPs. The NP concentration of 1 mg/ml in PBS was applied in all antimicrobial evaluation experiments. Five NP samples of ZnO, I:ZnO, Ag:ZnO, I:Ag:ZnO and Ag:I:ZnO were used. Bacterial growth without any NPs was used as the control for bacterial behaviour under illumination and dark conditions. The antimicrobial properties of NPs were assessed against both the Gram-negative bacterium *E. coli* MG1655 and the Gram-positive bacterium *S. aureus* USA300. Cells were grown to the mid-logarithmic phase in Mueller Hinton Cation Adjusted media (Becton

Dickinson), and diluted in phosphate buffered saline (PBS) solution to obtain 10^5 colony forming units per ml (CFU/ml) in each assay.

Each antimicrobial test was performed inside a sterilized 4 ml glass vial. The glass vial was selected due to its light transparency of the glass materials. A LED light source (U9090 LED) with a peak wavelength at 420 nm and a radiant flux of 6,500 mW was used for the illumination mode in a distance of about 10 cm from bacterial growth samples inside the shaker incubator. For the dark conditions, the vials were placed in 50 ml tubes with a black colour. The experiments were performed simultaneously in separate incubators under illumination and dark conditions. Shaking was performed to prevent sedimentation of the NPs. Each assay included 950 μ L of normalised bacteria with the viable cell number of 10^5 CFU/ml with 50 μ L of a specific NP sample. The vials were mixed by a vortex mixer and then placed into a shaker at 37 °C for 1 h under either an illumination or a dark condition. Upon completion of the treatment, samples were spread on Luria Bertani 1.5 % agar plates for bacterial enumeration and the determination of the antimicrobial efficacy in that test. Each sample was assessed in triplicate. Statistical analysis was performed using a one-way ANOVA, with a statistical significance indicated by ns for $P > 0.05$; * for $P < 0.05$; ** for $P < 0.01$; *** for $P < 0.001$; and **** for $P < 0.0001$, respectively.

4.3 Results and discussion

4.3.1 XRD

XRD is an analytical technique to characterize the crystalline material and evaluate the crystal structure, crystal orientation and crystal defects. The XRD patterns for the synthesised NP samples are presented in Figure 1. The XRD pattern for the ZnO NPs confirms the sample is crystalline in nature. The diffraction peaks for ZnO NPs are located at 32°, 34°, 36°, 47°, 56°, 63°, 66°, 68° and 69° which correspond to the ZnO wurtzite structure indexed with (100), (002),

(101), (102), (110), (103), (200), (112) and (201), respectively. The indices of ZnO NP are in agreement with those in the ZnO standard powder diffraction file (PDF) code number: 00-036-1451 that has been referenced in several studies [154, 177, 178]. The XRD patterns for I:ZnO and Ag:ZnO NPs samples are similar to those of the ZnO NP sample without any distinctive peaks for I and Ag species or any significant shift in the location of the diffraction peaks. This indicates that the lattice structure of the ZnO NP crystal has not significantly changed, which may be due to a low concentration of dopants used in the synthesis. Both Ag and I dopant concentrations may also be below the detection limits of the XRD equipment for I:ZnO and Ag:ZnO NP samples [96]. The XRD of the I:Ag:ZnO and Ag:I:ZnO NP samples present a similar pattern as the ZnO sample but they have additional peaks at 30°, 38° and 44°. The additional peaks are partially assigned to Ag and AgI using the PDF card numbers 5000218 and 9011698, respectively.

The XRD peaks confirm the presence of Ag and I elements within the crystal structure of synthesised ZnO-based NPs (I:Ag:ZnO; Ag:I:ZnO). Modification of the crystal structure of ZnO-based NPs may improve the photocatalytic activities of ZnO NPs and potentially lead to

generation of ROS in the visible light region.

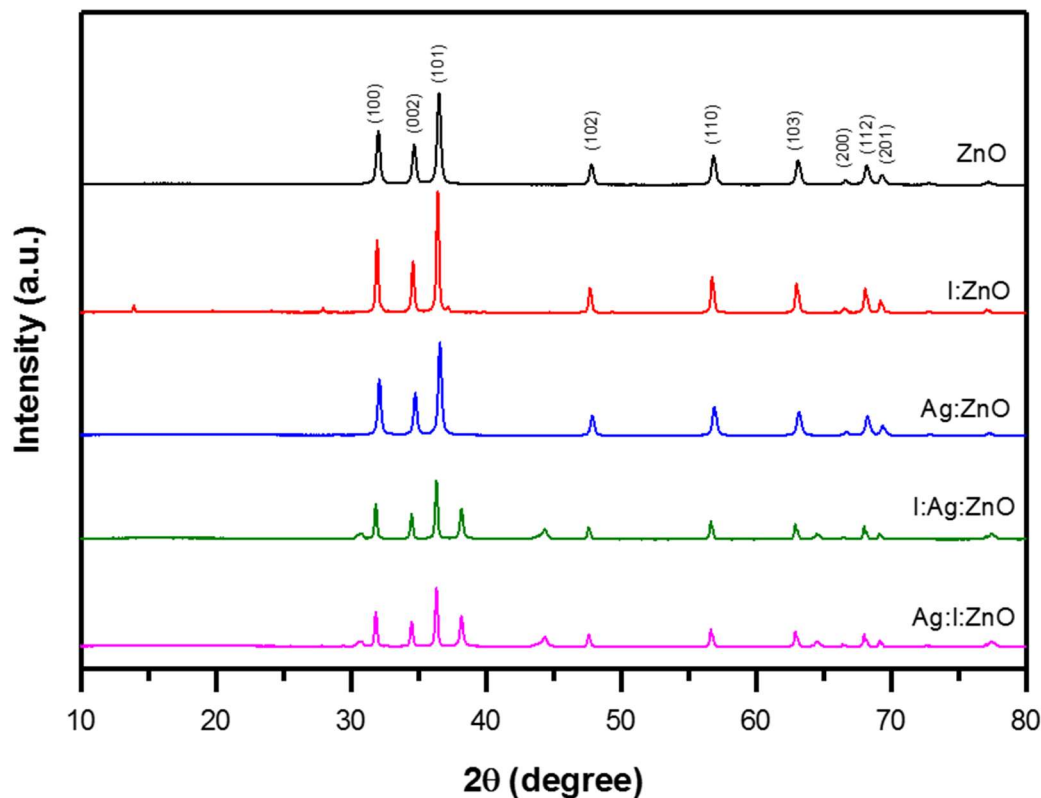


Figure 1 XRD patterns of ZnO, I:ZnO, Ag:ZnO, I:Ag:ZnO and Ag:I:ZnO NP samples

4.3.2 XPS

Apart from XRD, we also employed XPS as a tool to evaluate the elemental compositions, concentrations and chemical bindings of the synthesized NPs. The XPS spectra for the I:Ag:ZnO NP sample is presented in Figure 2, while the spectra for ZnO, I:ZnO, Ag:ZnO and Ag:I:ZnO NP samples are provided in Supplementary Information (SI).

The XPS survey spectra confirm the presence of Zn, O, Ag and I elements in both I:Ag:ZnO and Ag:I:ZnO synthesised NP samples. The binding energy peaks for Zn 2p $3/2$ and 2p $1/2$ are found at 1,022 and 1,045 eV, respectively, for all five samples (Fig 2b, S.F.1-4b). The well-defined peak at 1,022 eV for the binding energy is accurately assigned to the ZnO compound [179]. Three peaks at 530 eV, 531 eV and 532 eV appear in the spectrum for O 1s (Fig 2c, S.F.1-4c), indicating different oxygen species in the samples. The binding energy at

530 eV is assigned to the oxygen-zinc bonding for ZnO and I:ZnO NP samples, while the peak is assigned to the oxygen-silver bonding for Ag:ZnO, I:Ag:ZnO and Ag:I:ZnO NP samples. The other two peaks of 531 eV and 532 eV are associated with the oxygen-zinc bonding for all five NP samples. The Ag 3d binding energy spectrum for Ag:ZnO, I:Ag:ZnO and Ag:I:ZnO NP samples has two peaks at 367 eV and 373 eV (Fig 2d, S.F.3-4d). The first peak at 367 eV is due to the silver-oxygen bonding. The I 3d binding energy spectrum for I:ZnO, I:Ag:ZnO and Ag:I:ZnO NP samples holds two peaks at 619 eV and 630 eV (Fig 2e, S.F.2d, S.F.4e). The 619 eV peak corresponds to the iodine-iodine bonding.

The XPS spectra for the I:Ag:ZnO and Ag:I:ZnO NP samples (Fig 2 b-e and S.F.4 b-e) show a similar spectral pattern of the binding energies for Zn 2p₃, O 1s, Ag 3d and I 3d, indicating the presence of the ZnO NPs, Ag and I elements in these two NP samples.

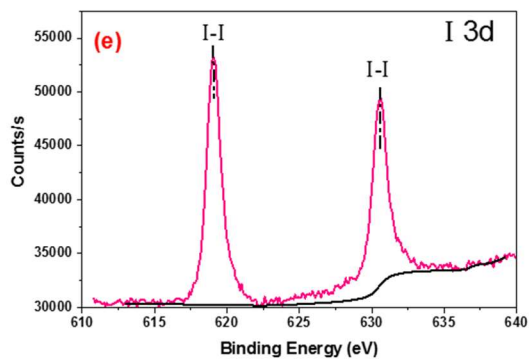
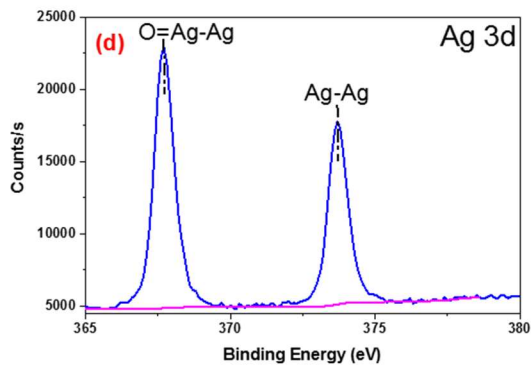
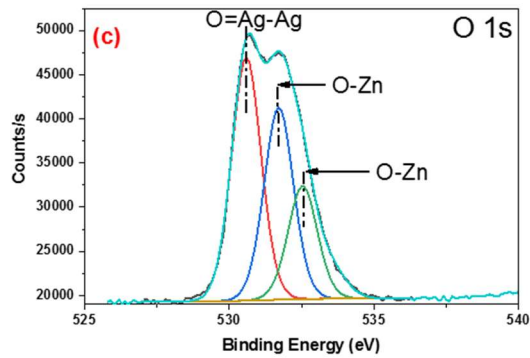
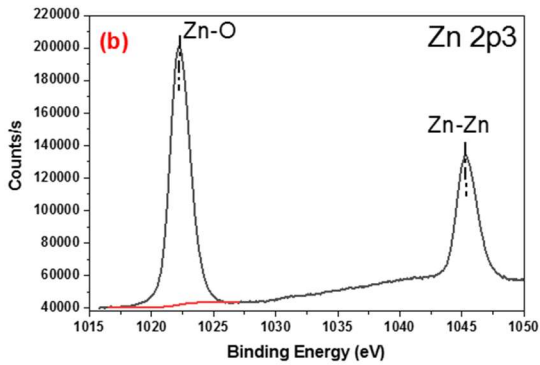
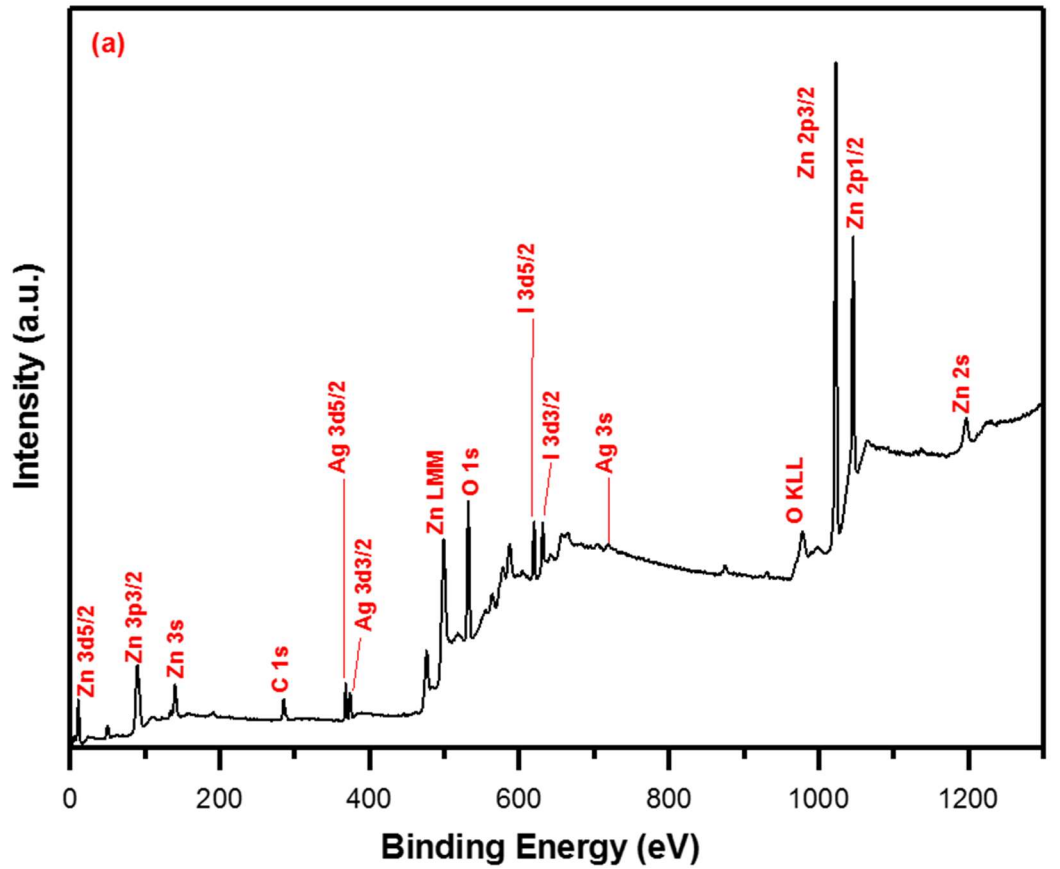


Figure 2 XPS spectra, I:Ag:ZnO XPS survey (a), I:Ag:ZnO XPS spectra (b-e). The binding energy spectra for Zn 2P3 (b), binding energy spectra for O 1s (c), binding energy spectra for Ag 3d (d) and binding energy spectra for I 3d (e).

4.3.3 Morphology

The morphology of the ZnO NPs synthesised via the solvothermal method could be controlled by different parameters including the type of precursors, solvents and surfactants employed for the synthesis as well as the processing conditions such as temperature and the reaction time [168]. The morphology of the synthesised NPs was investigated by TEM and SEM analysis and is presented in Figures 3 and 4. In addition, the hydrodynamic size and zeta potential for the synthesised NPs were evaluated and presented in Table 1. The TEM images confirm a polycrystalline structure with a main shape of hexagonal prisms for all NPs. However, the Ag:ZnO sample (Fig 3c) presents a distorted crystal form. The images also reveal aggregation of the NPs from uniform-sized discrete particles with an average particle size between 32 nm to 92 nm.

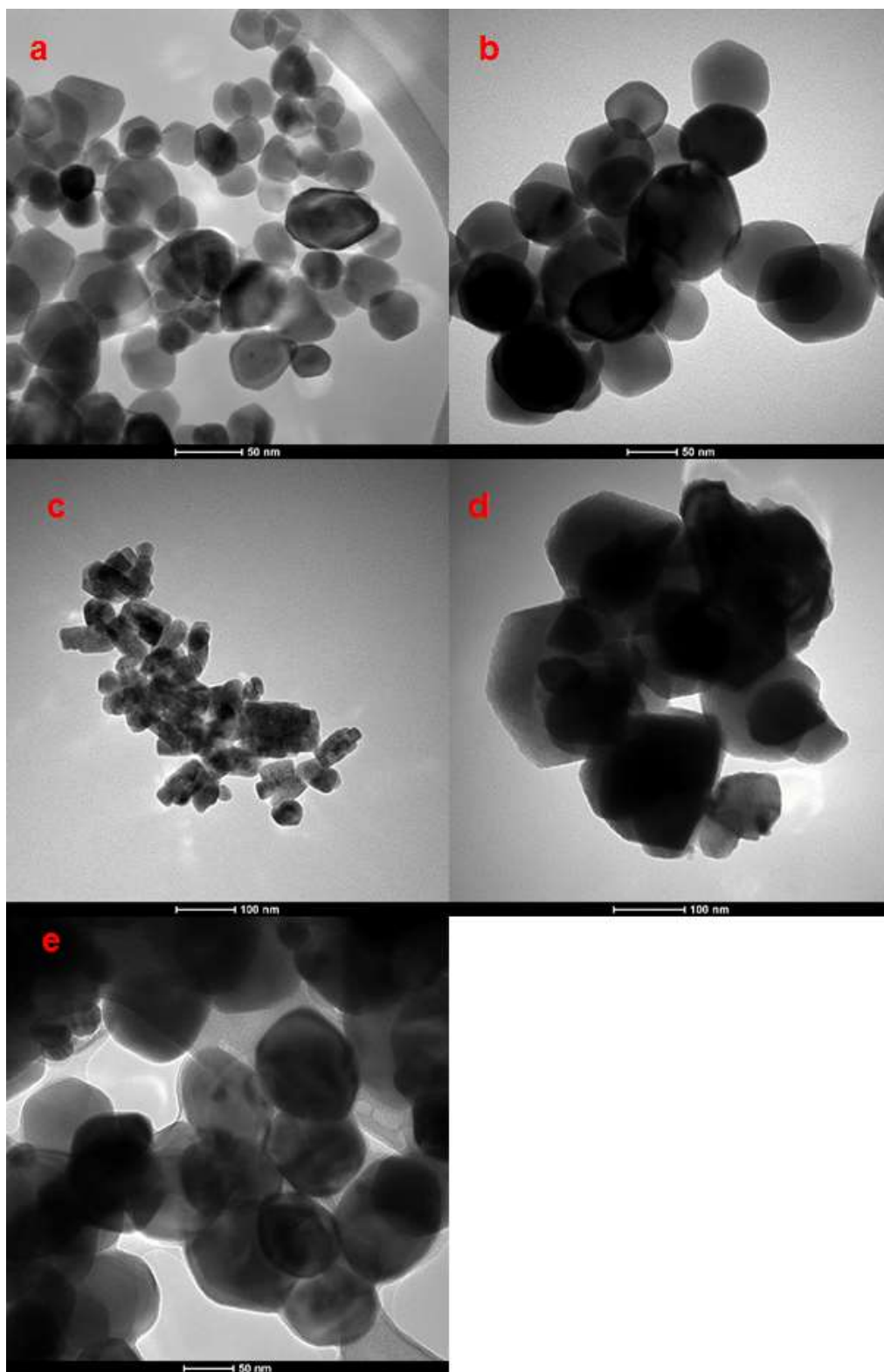


Figure 3 TEM images of ZnO (a), I:ZnO (b), Ag:ZnO (c), I:Ag:ZnO (d) and Ag:I:ZnO (e)

A quasi-spherical morphology is observed from the SEM images of four synthesised NPs (ZnO, I:ZnO, Ag:ZnO, and Ag:I:ZnO) in Figure 4, while a flaky shape is noticed for the I:Ag:ZnO NP sample. The SEM images confirm the aggregation of NPs for all samples.

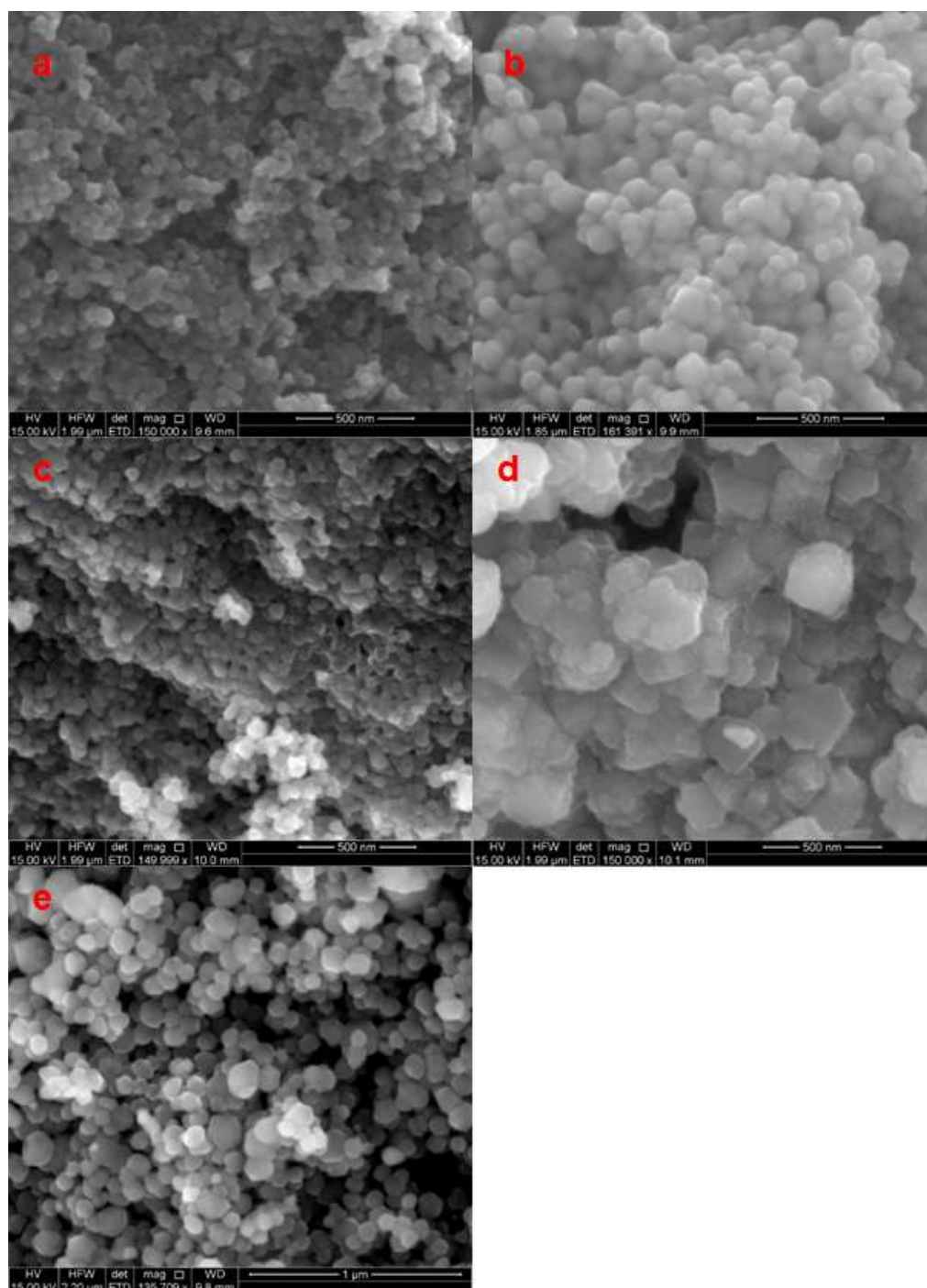


Figure 4 SEM images of ZnO (a), I:ZnO (b), Ag:ZnO (c), I:Ag:ZnO (d) and Ag:I:ZnO (e)

The DLS technique estimates the particle size based on light scattering and the Brownian motion of particles in a solution medium. The DLS results suggest the tendency of the

synthesized NPs for agglomeration/aggregation in an aqueous solution for all five samples as the estimated mean hydrodynamic particle sizes are much higher than TEM measurements. The insertion of Ag into the ZnO NPs (Ag: ZnO) does not have an impact on the size, however Ag:I:ZnO NP size increases after Ag insertion into I:ZnO NPs. The I insertion (I:ZnO) leads to doubling the size of ZnO NPs, and this doubling in size also applies to I insertion into Ag:ZnO NPs(I:Ag:ZnO).

The Zeta potential results reveal a good stability (zeta potential $> + 30$ mV or $< - 30$ mV) for the synthesized NPs apart from I:ZnO NPs. The ZnO and Ag:ZnO NP samples display a positive value for the zeta potential while the I:ZnO, I:Ag:ZnO and Ag:I:ZnO NPs samples show a negative zeta potential. The zeta potential of NPs could be influenced by the precursors used for the synthesis, surfactant and more importantly by pH [180]. The surface charge of NPs may impact their toxicity toward bacteria. The NPs with a stable positive charge may interact better with the bacteria which has a slightly negative charge. However, the surface charge interaction is not considered to be a major factor in the antimicrobial effectiveness of NPs.

Table 3 Dynamic light scattering and zeta potential measurements for the synthesised nanoparticles

Samples	DLS size (nm)	Zeta Potential (mV)
ZnO	131.8 ± 9.7	$+32.9 \pm 11$
I:ZnO	236.3 ± 40.6	-9.2 ± 4.4
Ag:ZnO	144.5 ± 23.5	$+47.3 \pm 5.5$
I:Ag:ZnO	274.9 ± 20.1	-23.3 ± 6.6
Ag:I:ZnO	326.2 ± 50.4	-38.5 ± 6.8

4.3.4 UV-Vis spectroscopy

The UV-Vis diffuse spectra and the corresponding Tauc plot of the synthesised NP samples are shown in Figure 5. The absorption peak at a wavelength less than 400 nm for all synthesised NP samples suggests strong light absorbance of the NP samples in the UV region and the presence of well crystalline ZnO NPs in the samples [181, 182]. The peak at 380 nm is assigned to excitation in ZnO NPs which is due to the electron transition from the valence to the conduction band upon excitation [181, 183, 184]. By comparing the UV-Vis spectra for the I:Ag:ZnO and Ag:I:ZnO NP samples with those of ZnO NP samples, enhancement in the optical absorption is found for both I:Ag:ZnO and Ag:I:ZnO NP samples. The absorption peaks at 426 nm and 433 nm are detected for I:Ag:ZnO and Ag:I:ZnO NP samples respectively, which may be due to the plasma effect of Ag [185]. The band gap for the synthesised NP samples was calculated from the intercept of the tangent of the curves from the Tauc plot as shown in the inset of Figure 5. The band gap energy for the I:Ag:ZnO and Ag:I:ZnO NP samples are found to be 2.28 eV and 3.21 eV, respectively. The Ag:I:ZnO NP sample has a weak peak at around 2.9 eV. The band gap energies for both samples are in agreement with the UV-Vis spectra, indicating that photocatalytic activity of ZnO NPs has been improved by double doping with I

and Ag in two different dopant configurations.

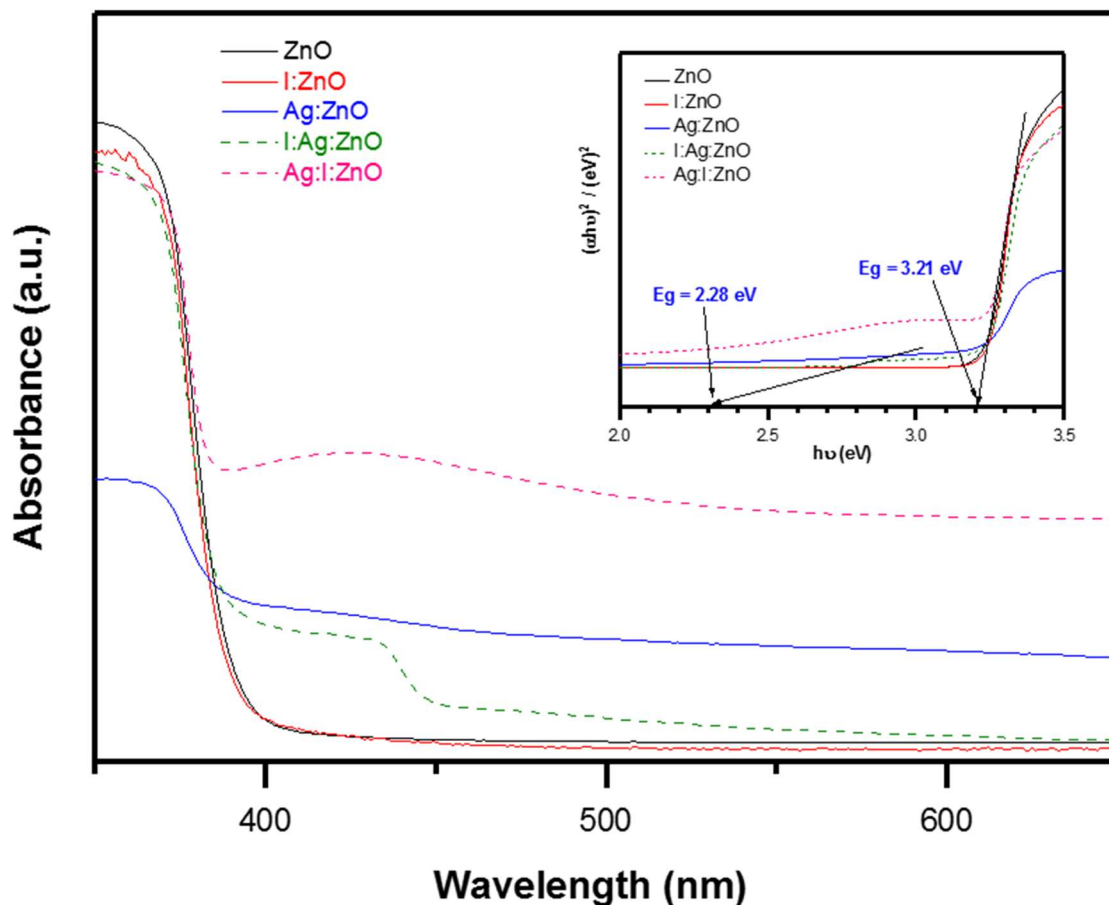


Figure 5 UV-Vis spectra for ZnO, I:ZnO, Ag:ZnO, I:Ag:ZnO and Ag:I:ZnO NP samples. The inset represents the Tauc graphs for the synthesised NP samples.

4.3.5 Photoluminescence (PL)

The PL spectrum reveals the interaction of the NP material with photons after exposure to UV light and provides great insights into the efficiency of the charge carrier. The energy absorption by the NPs leads to light emissions which are interpreted as peaks in the PL graph. This absorption of a photon (excitation) occurs either by the lattice of the NP or the intentionally doped material. As mentioned before, the absorption of photons in ZnO-based NPs leads to the generation of ROS and hence improves antimicrobial properties. Therefore, PL peaks in the visible light region could be positively correlated with the antimicrobial activity of NPs in the visible light region.

Figure 6 below presents the PL spectra of the synthesised NP samples. The ZnO NP sample has a sharp peak at 390 nm and then the PL spectrum becomes flatten in the visible light range between 400 to 700 nm. Other samples also reveal a strong peak at the wavelength of less than 400 nm except for the Ag:ZnO sample from which only a soft peak at 600 nm is detected. Among these five samples tested, I:ZnO has a sharp peak at 388 nm and a broad peak in the visible light range. The PL spectra for the I:Ag:ZnO and Ag:I:ZnO samples are presented in the inset of Figure 6 for better clarity of peak locations. Peaks are seen from both samples in the visible light range. The I:Ag:ZnO NP sample has a broad peak between 470 and 700 nm with a low intensity, while two peaks from Ag:I:ZnO are seen, one at 458 nm and the second at 529 nm with a higher intensity.

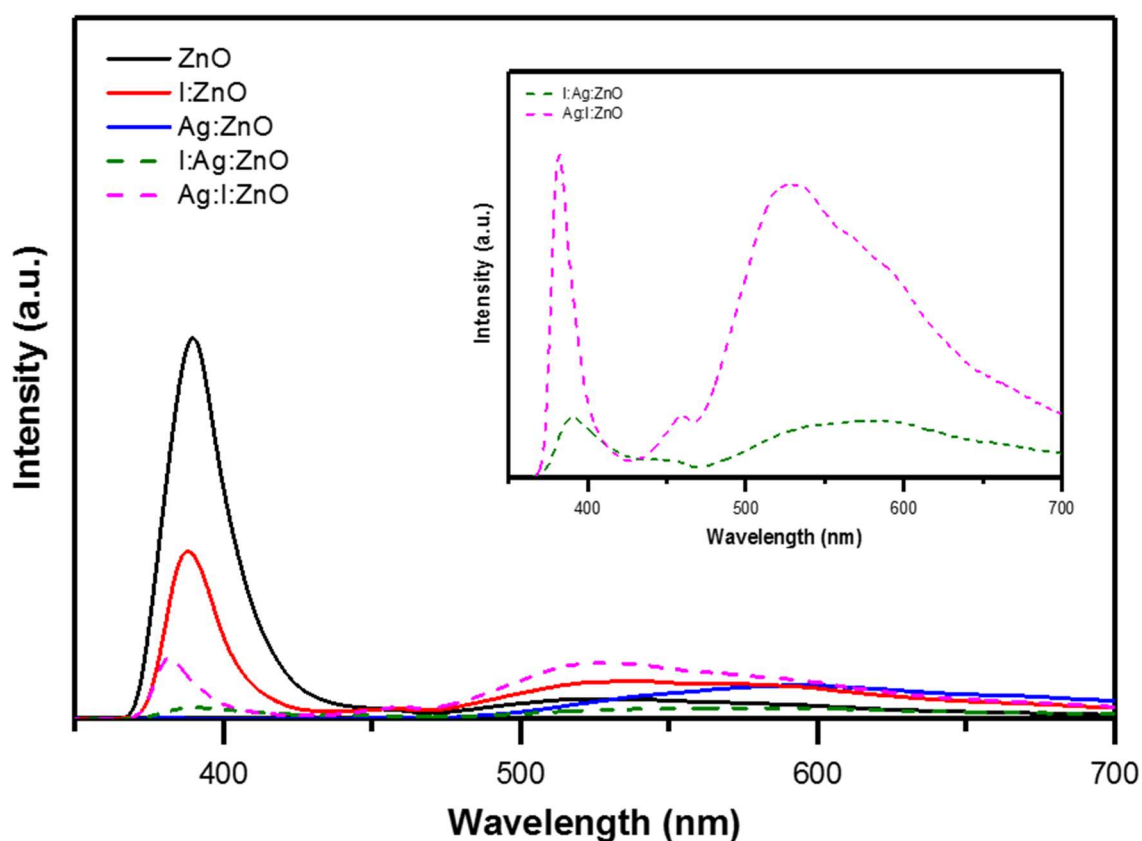


Figure 6 Photoluminescence spectra for ZnO, I:ZnO, Ag:ZnO, I:Ag:ZnO and Ag:I:ZnO NP samples. The inset represents PL spectra for the I:Ag:ZnO and Ag:I:ZnO samples for better clarity of peak locations

4.3.6 Antimicrobial efficacy

The antimicrobial efficacy results for the NP samples evaluated against *E. coli* and *S. aureus* are shown in Figures 7 and 8 respectively. Both microorganisms were treated in visible light and under a dark condition in the presence of the NP samples. The results in Figure 7 demonstrate the Ag:ZnO, I:Ag:ZnO and Ag:I:ZnO NP samples are very effective in killing *E. coli* in the light-illuminated mode, resulting in 5.27 log CFU reduction in survival, while only 0.04 and 0.13 log CFU reduction of *E. coli* in the light-illuminated mode is found for the ZnO and I:ZnO NP samples respectively. Among these five NP samples tested against *E. coli* in the dark condition, the Ag:ZnO and Ag:I:ZnO NP samples outperform other samples with a greater antimicrobial activity: 5.26 and 1.01 log CFU reduction in survival, respectively. On the contrary, ZnO, I:ZnO and I:Ag:ZnO NP samples are less effective, and only 0.02, 0.05 and

0.10 log CFU reduction of bacterial cells are achieved, respectively.

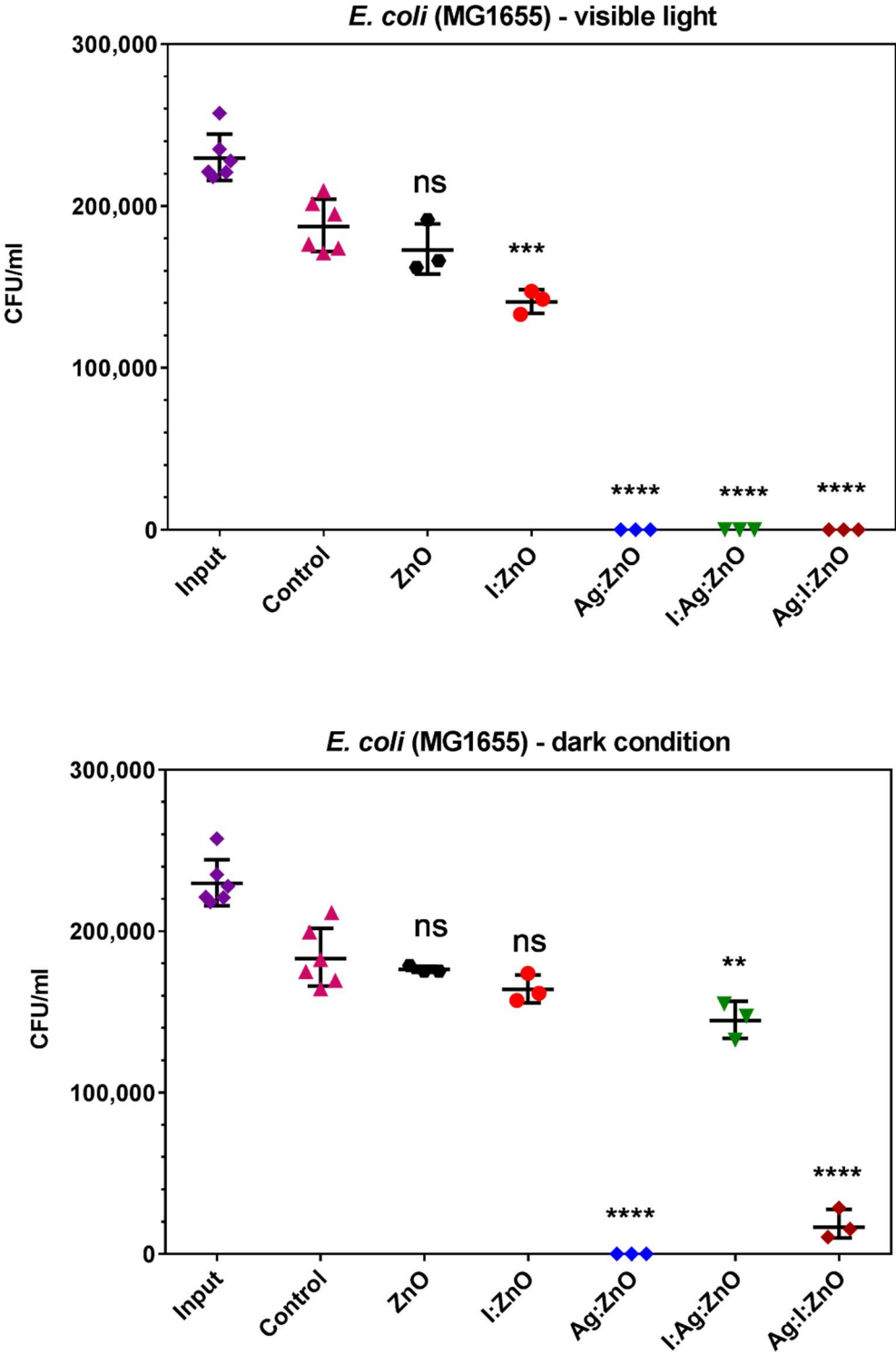


Figure 7 Antimicrobial efficacy of the doped ZnO NPs against *E. coli* (MG1655). Statistical analysis was performed using a one-way ANOVA, with a statistical significance indicated (ns, $P > 0.05$; *, $P < 0.05$; **, $P < 0.01$; ***, $P < 0.001$; and **** for $P < 0.0001$)

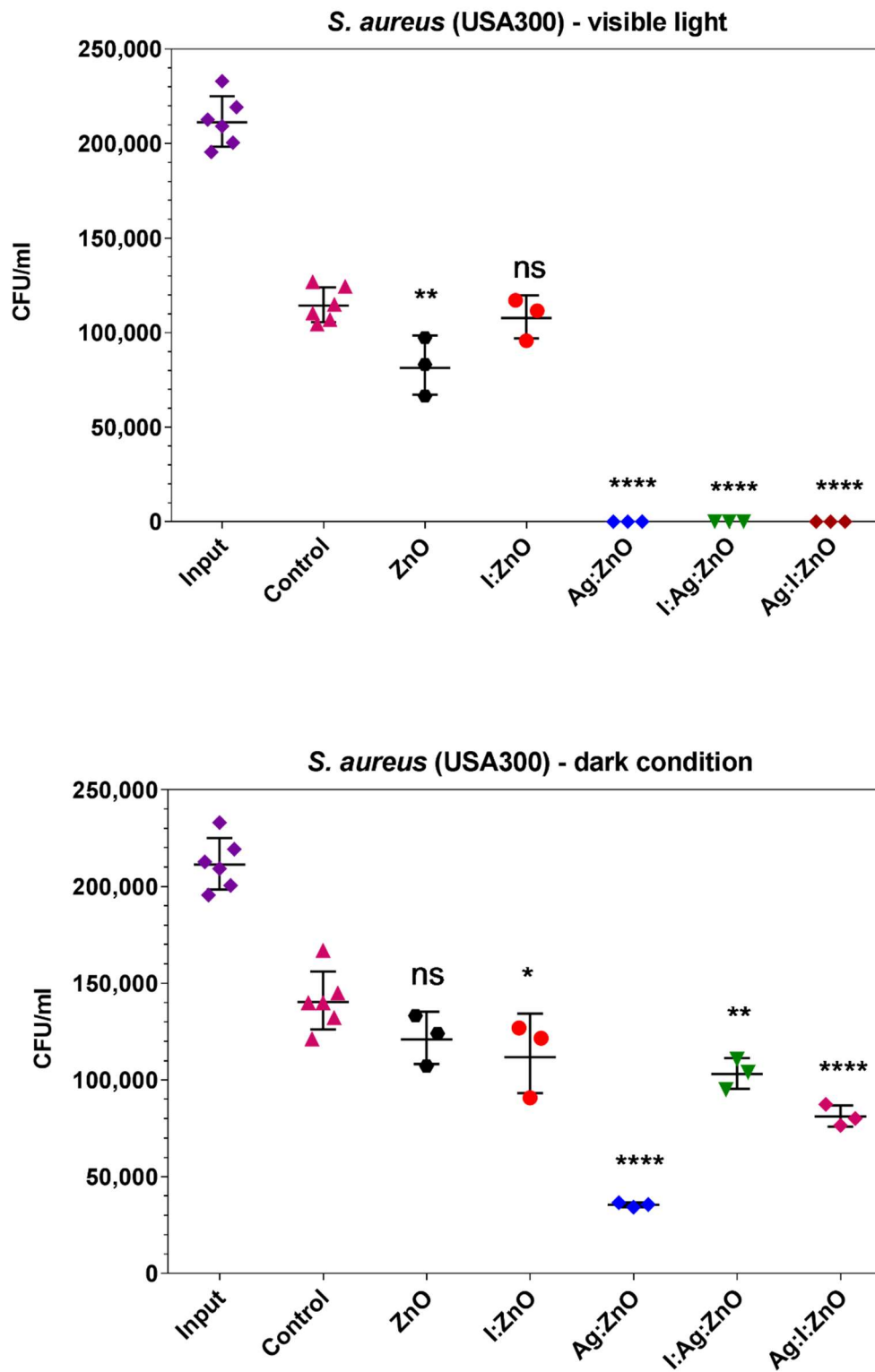


Figure 8 Antimicrobial efficacy of the doped ZnO NPs against *S. aureus* (USA300). Statistical analysis was performed using a one-way ANOVA, with a statistical significance indicated (ns, $P > 0.05$; *, $P < 0.05$; **, $P < 0.01$; ***, $P < 0.001$; and ****, $P < 0.0001$)

The antimicrobial efficacy of the NP samples follows a similar pattern against *S. aureus*. The Ag:ZnO, I:Ag:ZnO and I:Ag:ZnO NP samples are very potent in eliminating *S. aureus* in the light-illuminated mode with 100 % reduction in the CFU, while the other two samples have a lower efficacy, ZnO with 0.14 log CFU reduction and I:ZnO with 0.03 log CFU reduction of bacterial cells after the exposure to visible light. In the dark condition, the Ag:ZnO NP sample is still very potent in eliminating *S. aureus* and has the highest antimicrobial efficacy amongst five NP samples. In contrast, ZnO, I:ZnO, I:Ag:ZnO and Ag:I:ZnO NP samples have minor or moderate antimicrobial activity, with 0.06, 0.10, 0.14 and 0.24 log CFU reduction of *S. aureus*, respectively.

The synthesised NPs showed a rapid antimicrobial efficacy in 1 h compared with other studies which have used a long exposure time up to 24 h [114, 186]. In this study, the antimicrobial efficacy of NPs was based on a quantitative determination by direct contact between NPs and bacteria followed by the agar plate counting. Several other studies have used the disc diffusion technique which is a qualitative (soft-quantitative) method of antimicrobial efficacy evaluation [86, 187].

The above results for the synthesised NPs confirm that the antimicrobial efficacy of ZnO NPs has been significantly enhanced by the doping process. Among all NP samples, ZnO-based NPs doped by Ag (Ag: ZnO) surpass other samples in eliminating both *E. coli* and *S. aureus* bacteria.

4.4 Antimicrobial mechanisms by Ag/I doped ZnO NPs

The antimicrobial mechanisms by ZnO NPs remain debated and these mechanisms include Zn^{2+} release, ROS generation, Ag^+ release, and others. We have designed five ZnO NP samples under illumination or dark conditions in order to illustrate the mechanisms underlying for ZnO NPs.

It has been reported that it is the interaction of the Zn^{2+} ion with the bacterial cell membrane that results in disruption of bacterial metabolism and the eventual death of the bacterial cell because the Zn^{2+} ion enters into the bacterial cell and binds with the sulfhydryl, amino and hydroxyl functional groups [162, 188, 189]. Alternatively, ZnO NPs with a slightly positive charge could attach to the bacterial cell membrane with a slightly negative charge due to electrostatic interaction. The direct contact of ZnO NPs could lead to loss of the charge balance on the cell membrane, or ruptures the cell member, and ultimately breaks the integrity of the cellular structure [154, 162]. However, from our ZnO samples in the dark condition, negligible antimicrobial results are found for both *E. coli* and *S. aureus*, which suggests that Zn ions or positive charge in the ZnO samples do not contribute to the bacterial cell death.

Another possible mechanism is ROS generated from semiconductor NPs after exposure to external light. The photo-generated ROS from ZnO NPs under UV light irradiation has been studied for antimicrobial purposes by Talebian et al. [111]. ZnO NPs are a semiconductor with a band gap of approximately 3.37 eV [190]. Upon irradiation by UV light, ZnO NPs can generate ROS via the photocatalytic process. The ROS have strong antimicrobial toxicity that is correlated with their extremely high oxidizing properties. The ZnO NPs absorb the photons when they are illuminated with photons with an energy equal to and greater than its band-gap ($\lambda \leq 369$ nm). The absorbed photons prompt the electron to be excited from the valence band (VB) to the conduction band (CB), which hence leads to the formation of free electrons (e^-) in CB and holes (h^+) in VB. The combination of the free electron-hole (e^-/h^+) pair could convert the electron-hole pair energy to heat and reduce the photocatalytic activities of the semiconductor NPs [75]. In the presence of water, the electron-hole pair simultaneously splits the water molecule into a hydroxyl radical ($\cdot OH$) and a hydrogen ion (H^+). The electron-hole pair also reacts simultaneously with the dissolved oxygen in water to form superoxide radicals ($\cdot O_2^-$) [75, 154, 157].

The hydroxyl radical and the superoxide anion radical are negatively charged and hence cannot penetrate into the bacterial cell membrane which has a slightly negative charge [191, 192]. Accumulation of the hydroxyl radical, however, results in lipid peroxidation in the bacterial outer membrane, and causes detrimental damage to the bacterial cellular structure [157]. The H_2O_2 has been reported to be the main antimicrobial active agent to be responsible for bacterial non-viability [6, 154]. We have observed that ZnO samples contribute to a slight reduction in both strains after exposure to visible light, which confirms ROS generation is the mechanism for cellular death, not Zn ions. However, the level of reduction is very limited because the photo-generated ROS from ZnO NPs with a wide band-gap requires activation by exposure of NP samples to UV light. The UV light constitutes less than 5 % of the sunlight spectrum, which hampers the utilization of pure ZnO NPs for antimicrobial applications [193].

In general, the band-gap narrowing approach is a common method to shift the photocatalytic activity of wide band-gap photocatalytic NPs from UV light to the visible light range. The band-gap narrowing process is achieved by reducing the conduction band energy, increasing the valence band energy or introducing an intermediate energy level within the band-gap. The doping process is often employed for narrowing the band gap of NPs [169, 194]. A carefully selected multifunctional dopant could enhance the photocatalytic properties in the visible light region for efficient ROS generation also improve the antimicrobial properties of the NP compound, due to the inherent antimicrobial activity of the dopant. In general, dopants are classified into two categories: n-type and p-type. In n-type doping for ZnO NPs, zinc (Zn) or oxygen (O) is substituted with group III elements. The n-type dopants have extra electrons in their valence band which can be donated to the adjacent atoms (Zn cation) in the crystal structure. In contrast, the p-type dopants, such as group I elements, lack electrons in their valence band, hence, they receive an electron from the neighbouring atoms to generate holes in the valence band. Therefore, the donor dopants increase the electron concentration while the

acceptor dopants increase the hole concentration. The p-type doping of ZnO NPs is a challenging process due to several factors including low solubility, high ionization and the formation energy of p-type dopants [194-196].

In this study, we have selected Ag and I elements in either a single or a double dopant form with various arrangements to utilize ZnO-based NPs in the visible light region for antimicrobial applications. Iodine has selected as it has been evaluated as a strong dopant to improve the photocatalytic properties of TiO₂ NPs by modifying the band-gap and reducing the electron-hole pair recombination by trapping the photogenerated electron [96]. Ag has been reported to be effective as an electron trap for delaying the recombination of the electron-hole pair, hence, the Ag dopant can improve the photocatalytic properties of the NP-based semiconductor [197]. Comparison of the antimicrobial efficacy for I:ZnO, Ag:ZnO, I:Ag:ZnO and Ag:I:ZnO samples against *E. coli* and *S. aureus* in both light-illuminated and dark conditions suggests that ROS generation be one antimicrobial mechanism for these NPs. Significant reduction in the CFU of both strains is observed for the I:Ag:ZnO sample after exposure to light in comparison with the dark condition. Although there is no contribution from I:ZnO to *S. aureus* cell death, a slight reduction in *E. coli* cell survival is noticed from this sample after exposure to visible light. ROS contribution from Ag:ZnO and Ag:I:ZnO samples to eliminating *E.coli* cells may not be interpreted from our experiments since in both illuminated and dark conditions, the sample destroys all or most of this type of cells. We do notice that ROS generation from both samples, especially Ag:I:ZnO, explains the further reduction in *S. aureus* cell survival after exposure to visible light. This ROS generation capability and thus the antimicrobial activity of these samples may be well correlated with their photocatalytic activity as shown in Figure 6.

We observe that Ag:ZnO and Ag:I:ZnO samples are able to eliminate most of *E. coli* cells, while some of *S. aureus* cells. This is due to the silver ion (Ag⁺) released from the dissolution of the metallic silver that has been suggested as an antimicrobial mechanism for Ag related

products. Upon interaction of Ag with the water molecules, the dissolved oxygen (O_2) in the water oxidizes Ag to form Ag^+ which is an active antimicrobial ingredient [44, 56, 68, 132]. The Ag^+ ions can cause the bactericidal efficacy by binding them with thiol, sulfur and phosphorus groups of the bacterial cell wall to produce holes on the bacterial cell wall. The holes on the cell wall allow the Ag^+ ions to enter the bacterial cell and bind with DNA which leads to cell death [56, 57, 150-152, 198]. The Gram-negative bacteria have been suggested to be more susceptible toward Ag^+ ions due to their thinner cell membrane and a more negative charge due to their surface lipopolysaccharide (LPS) layer. The favourable electrostatic interactions could lead to the interaction between Ag^+ ions and the cell outer membrane, penetration of the membrane and subsequent death of bacterial cells [5, 154]. However, the use of pure silver as an antimicrobial agent is limited due to high cost and uncontrolled release of the Ag^+ ions, which could also result in localised toxicity to human cells [24]. From our doped ZnO samples, the Ag:ZnO and Ag:I:ZnO samples are very potent against *E. coli* in both light-illuminated mode and dark conditions, which means Ag^+ do contribute to the antimicrobial mechanism. Ag^+ penetration is better for Gram-negative bacteria than Gram-positive bacteria as evidenced by a relatively higher percentage of *S. aureus* CFUs in the dark condition. Silver in the form of AgO is present in the Ag:ZnO and Ag:I:ZnO samples, which has been confirmed through XPS spectra shown in Fig S.F.3-4. This ionic form is released upon contact with bacterial cells. However, I:Ag:ZnO is not effective as Ag:I:ZnO in the dark condition for both strains, and this may be due to the formation of AgI, rather than AgO, in the sample. The Ag^+ release rate from AgI may be much slower than that from AgO. Furthermore, Ag concentration is very low in the doping process and it is not detectable for XRD spectra as shown in Figure 1 for Ag:ZnO samples, however, such a small fraction of Ag in the sample makes a great contribution to the elimination of bacterial cells.

4.5 Conclusions

ZnO-based NPs doped with I and Ag with different doping sequences were synthesised. The XRD characterization of synthesised NPs confirms a crystalline structure for ZnO NPs and the presence of Ag and I dopants in different arrangements. The XPS analysis reveals the chemical binding and elemental compositions, hence shedding light on the forming process of ZnO-based NPs with the selected dopants. The UV-Vis and PL analysis provide direct evidence of the photocatalytic enhancement in double-doped ZnO NPs (I:Ag:ZnO and Ag:I:ZnO) compared with ZnO NPs in the visible light region. The SEM and TEM analysis of the synthesised NPs further reveals a polycrystalline structure consisting of hexagonal prisms for all NPs with an average particle size between 32 nm to 92 nm. I:Ag:ZnO and Ag:I:ZnO NP samples demonstrate a strong antimicrobial efficacy against *E. coli* and *S. aureus* in the visible light region with different dominant mechanisms: ROS generation for the I:Ag:ZnO sample, while Ag⁺ release for the Ag:I:ZnO sample. A very low Ag concentration in the format of AgO for Ag-related products may be enough for completely eliminating pathogenic bacteria.

Conflicts of interest

There are no conflicts to declare.

Acknowledgements

Afshin Karami thanks Dr Victoria Grace Pederick from research centre for infectious diseases, school of molecular and biomedical sciences, the University of Adelaide for her technical support on antimicrobial experiments. Also, support from the Australian Government Research Training Program Scholarship is acknowledged. The funding support from the Australian Research Council is also acknowledged. This work was supported by Australian Research Council Discovery Project (DP160104632) to Z.X. and H.Z.

Chapter 5 : Conclusions and future directions

The nosocomial bacterial infections are a major cause of mortality mainly because overuse and/or inappropriate usage of antibiotic agents leads to the development of antimicrobial resistant bacteria. The antimicrobial resistance is less likely to occur for nanomaterials due to their nature and mechanism of fighting against bacteria. In this study, two strategies were evaluated for the antimicrobial applications including nanostructured coatings and nanoparticles.

In the first study, magnetron sputtering was used to produce a very thin Cr-Ag coating. The results of the nanoindentation measurements exhibit acceptable mechanical properties for the coatings. The study confirms the antimicrobial properties of Cr-Ag coatings can be tuned by varying the Ag content. However, in contrary to expectations, the 15.23 % Ag coating did not have a greater antimicrobial efficacy than the 4.83 % Ag coating against either *Escherichia coli* (MG1655) or *Staphylococcus aureus* (USA300). Several hypotheses have been proposed, but more samples of Cr-Ag coatings with different Ag concentrations are required in order to validate these hypotheses. A further investigation into the mechanism of antimicrobial action and the relationship with the concentration of silver in the Cr-Ag coating needs to be studied in future. Also, evaluating different elements such as tungsten (W) or copper (Cu) with various concentrations may assist in producing more efficient coatings.

In the second study, ZnO-based nanoparticles were synthesized via a Solvothermal method. Iodine and silver were used as a single and double dopants with different combinations (I-ZnO, Ag-ZnO, I-Ag-ZnO, and Ag-I-ZnO) in order to improve the antimicrobial properties of ZnO NPs and study the antimicrobial mechanism of ZnO nanoparticles derivatives under visible light. The characterization tests on the synthesised samples have confirmed the improved photocatalytic activity of double doped ZnO NPs with I:Ag:ZnO and Ag:I:ZnO arrangement compared with ZnO NPs. The synthesised I:Ag:ZnO and Ag:I:ZnO NPs had demonstrated their potent efficacy against *Escherichia coli* (MG1655) and *Staphylococcus aureus*(USA300)

and they may have great potential application in combating infectious diseases. More importantly, the mechanisms underlying the antimicrobial samples were revealed: synergistic effect of reactive oxygen species (ROS) generation and Ag^+ release. However, ROS generation was more dominant in the I:Ag:ZnO sample, while Ag^+ release played an important role in the Ag:I:ZnO. We also confirmed that a small fraction of Ag in the AgO form in the sample was enough to eliminate these pathogenic bacteria.

The future study will be focussed on synthesis and optimization of novel semiconductor based (e.g. ZnO, TiO_2 , etc) NPs with different dopants suitable for specific biomedical applications. The antimicrobial mechanisms of action and biocompatibility of as-synthesized NPs will be investigated more in depth. The optimizations may include evaluation of different surfactants, annealing at various temperatures and the other NP synthesis methods.

Appendix

Supporting information for antimicrobial coating surfaces paper

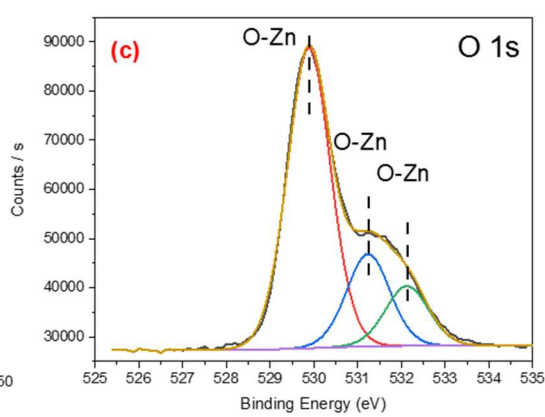
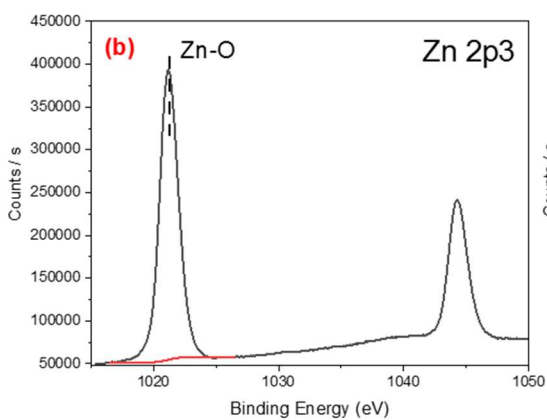
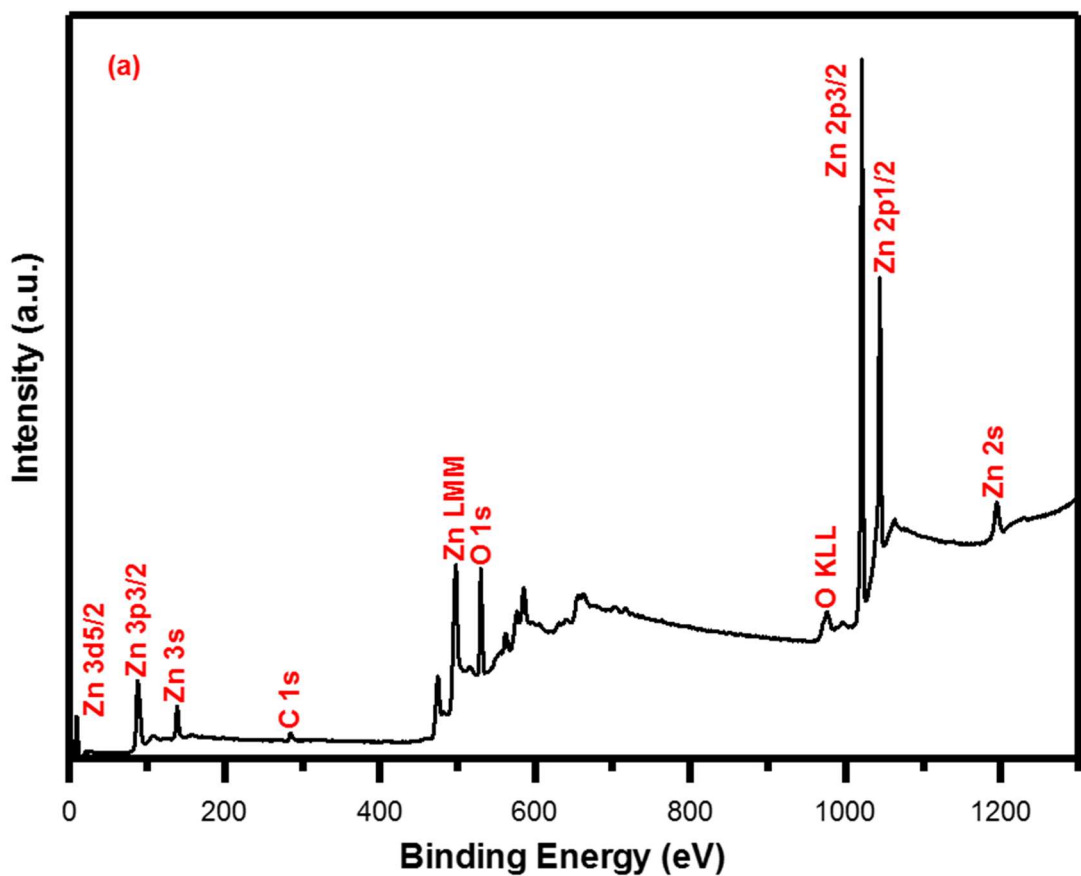


Figure S.F.1 - XPS spectra, ZnO XPS survey (a), ZnO XPS spectra (b-c)

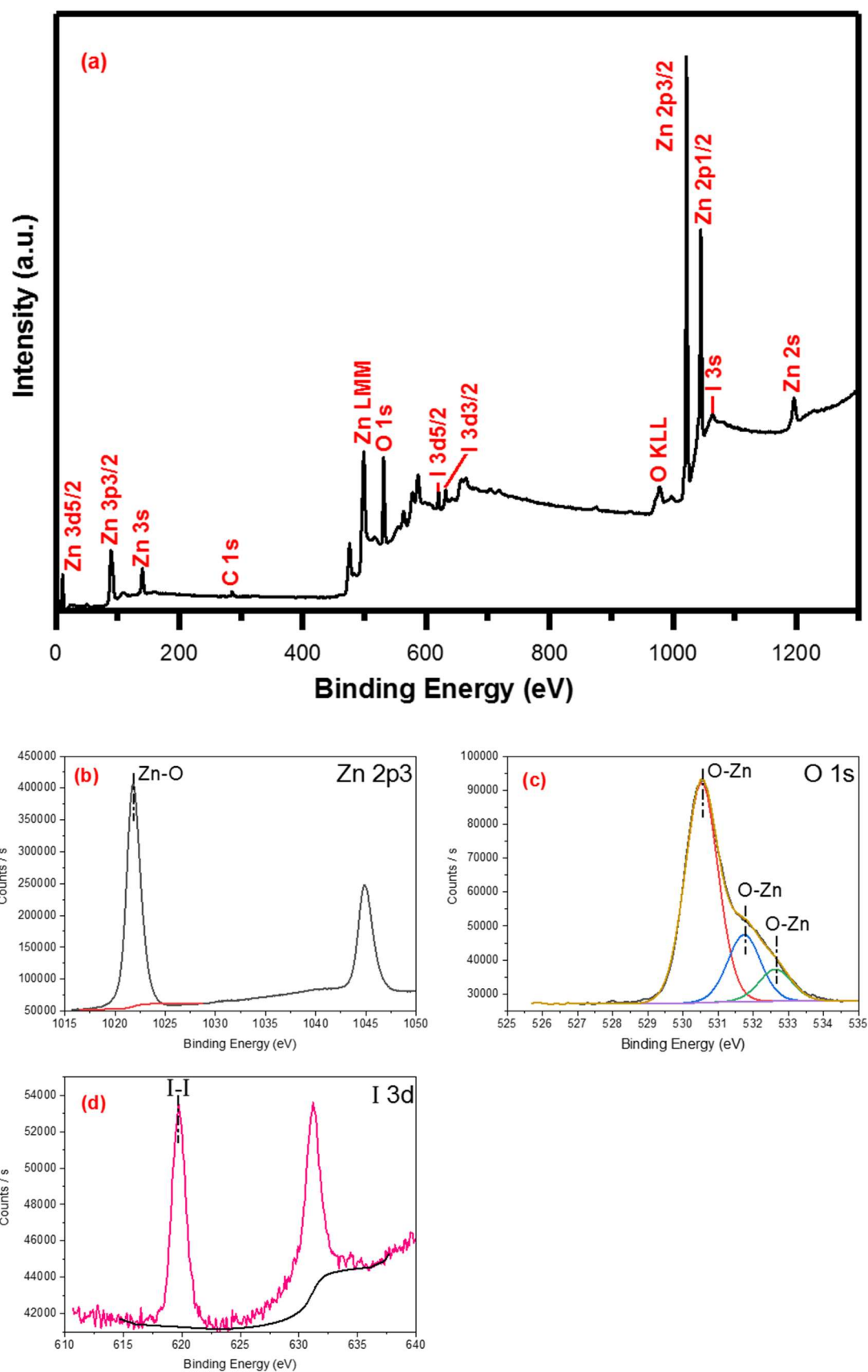


Figure S.F.2 - XPS spectra, I:ZnO XPS survey (a), I:ZnO XPS spectra (b-d)

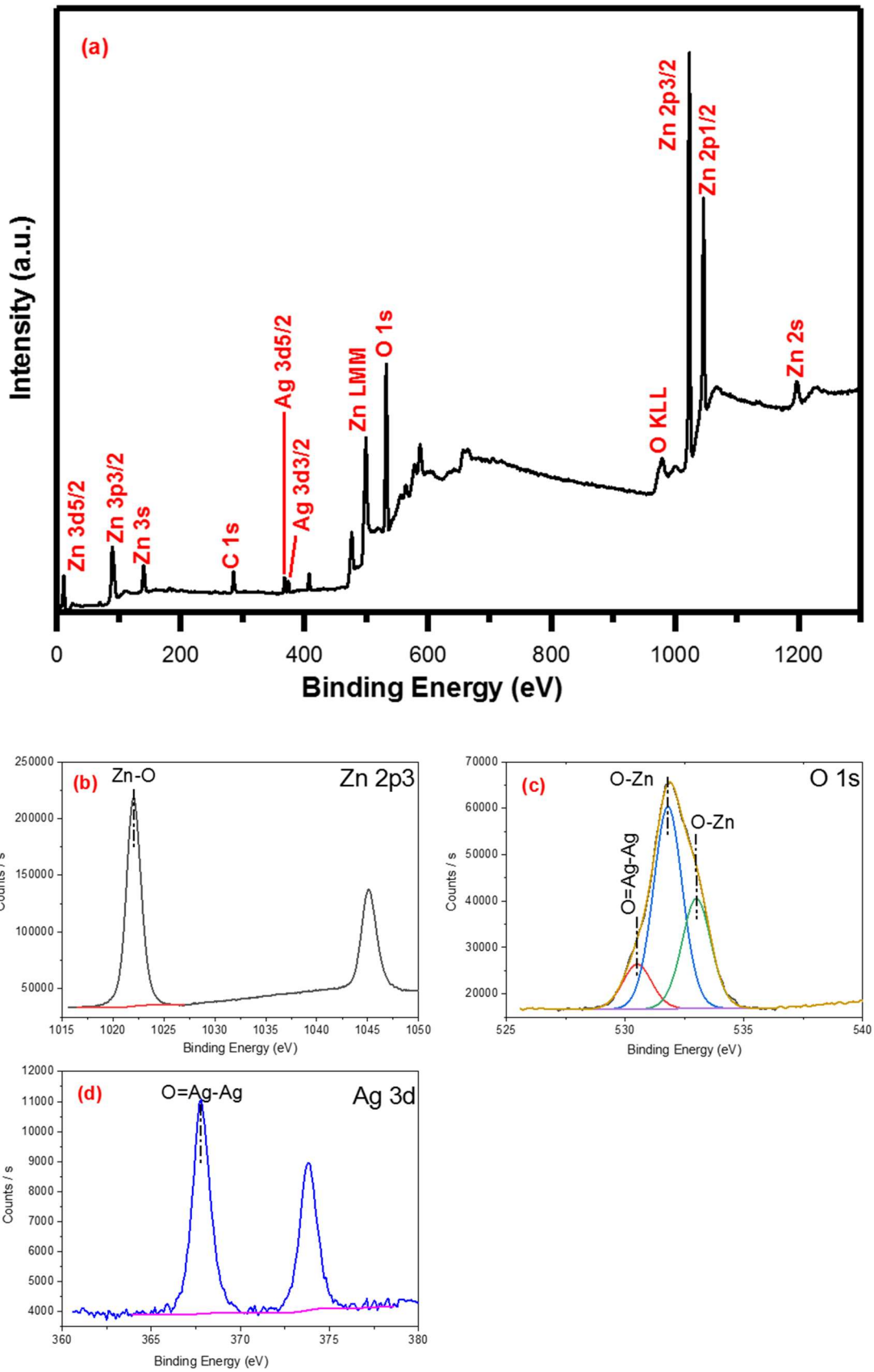


Figure S.F.3 - XPS spectra, Ag:ZnO XPS survey (a), Ag:ZnO XPS spectra (b-d)

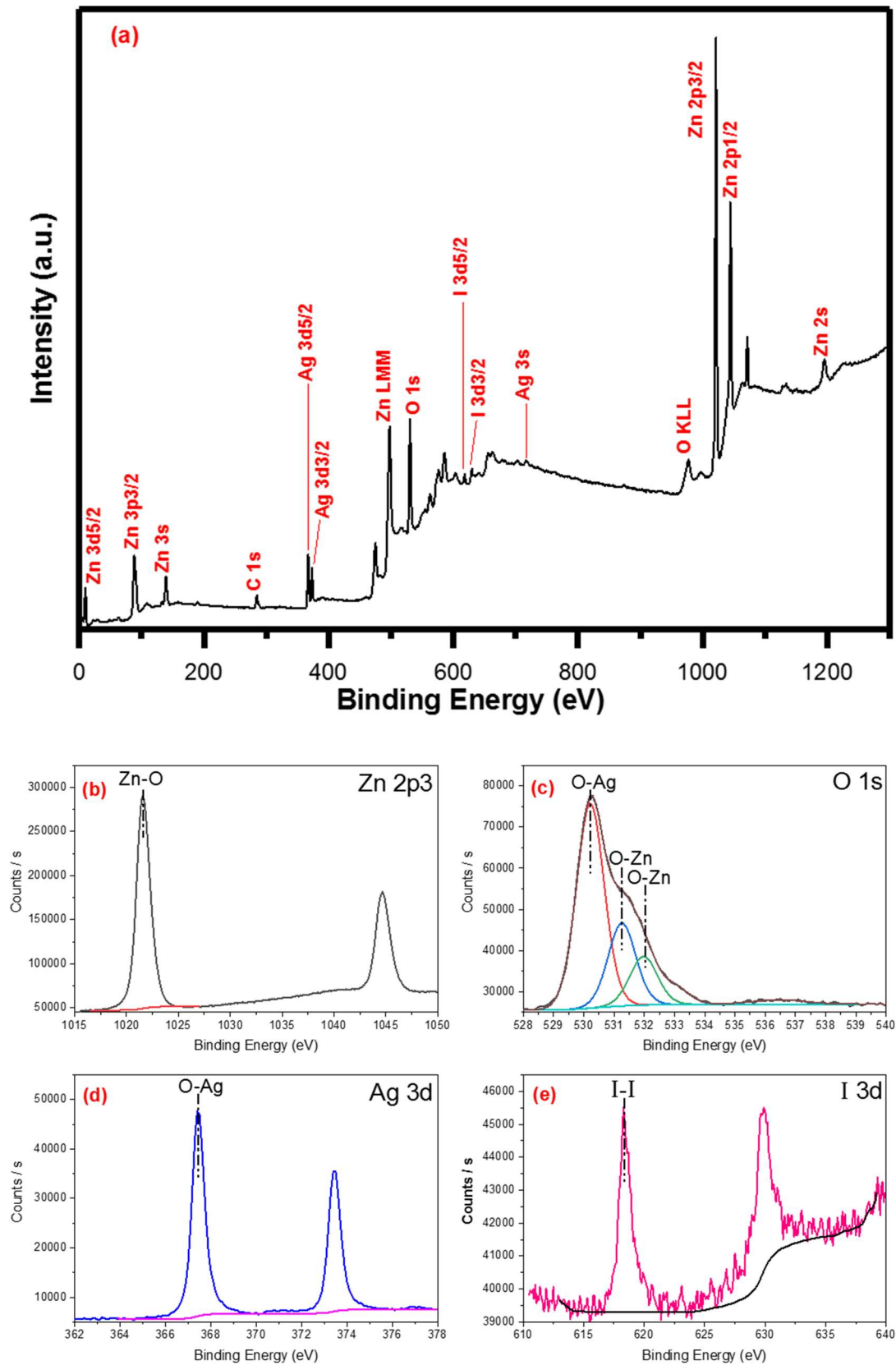


Figure 4 S.F.4 - XPS spectra, Ag:I:ZnO XPS survey (a), Ag:I:ZnO XPS spectra (b-e). The binding energy spectra for Zn 2P3 (b), binding energy spectra for O 1s (c), binding energy spectra for Ag 3d (d) and binding energy spectra for I 3d (e).

References

1. European Centre for Disease Prevention and Control, 2013 "Point prevalence survey of healthcare-associated infections and antimicrobial use in European hospitals 2011-2012". 2013.
2. Organization, W.H., *Report on the burden of endemic health care-associated infection worldwide*. 2011: Geneva.
3. Tortora, G.J., B.R. Funke, and C.L. Case, *Microbiology: An Introduction*. 2015: Pearson Education.
4. Doelle, H.W., et al., *Biotechnology, I. General*, in *Ullmann's Encyclopedia of Industrial Chemistry*. 2000, Wiley-VCH Verlag GmbH & Co. KGaA.
5. Cabeen, M.T. and C. Jacobs-Wagner, *Bacterial cell shape*. *Nature Reviews Microbiology*, 2005. **3**(8): p. 601-10.
6. Sirelkhatim, A., et al., *Review on Zinc Oxide Nanoparticles: Antibacterial Activity and Toxicity Mechanism*. *Nano-Micro Letters*, 2015. **7**(3): p. 219-242.
7. Fu, G., P.S. Vary, and C.-T. Lin, *Anatase TiO₂ Nanocomposites for Antimicrobial Coatings*. *The Journal of Physical Chemistry B*, 2005. **109**(18): p. 8889-8898.
8. Laudano, J.B., *Ceftaroline fosamil: a new broad-spectrum cephalosporin*. *Journal of Antimicrobial Chemotherapy*, 2011. **66**(suppl_3): p. iii11-iii18.
9. Duplessis, C. and N.F. Crum-Cianflone, *Ceftaroline: A New Cephalosporin with Activity against Methicillin-Resistant Staphylococcus aureus (MRSA)*. *Clinical medicine reviews in therapeutics*, 2011. **3**: p. a2466.
10. Mandal, S.M., R.O. Dias, and O.L. Franco, *Phenolic Compounds in Antimicrobial Therapy*. *J Med Food*, 2017. **20**(10): p. 1031-1038.
11. Mafra, C.S.P., et al., *Antimicrobial Action of Biguanides on the Viability of Acanthamoeba Cysts and Assessment of Cell Toxicity*. *Investigative Ophthalmology & Visual Science*, 2013. **54**(9): p. 6363-6372.
12. Day, C. and C.J. Bailey, *Biguanides*, in *xPharm: The Comprehensive Pharmacology Reference*, S.J. Enna and D.B. Bylund, Editors. 2007, Elsevier: New York. p. 1-3.
13. Arteagoitia, I., C. Rodriguez Andres, and E. Ramos, *Does chlorhexidine reduce bacteremia following tooth extraction? A systematic review and meta-analysis*. *PLoS One*, 2018. **13**(4): p. e0195592.
14. Tennen, R., et al., *Mechanisms of killing of spores of Bacillus subtilis by iodine, glutaraldehyde and nitrous acid*. *Journal of Applied Microbiology*, 2000. **89**(2): p. 330-338.
15. Leaper, D.J. and P. Durani, *Topical antimicrobial therapy of chronic wounds healing by secondary intention using iodine products*. *International Wound Journal*, 2008. **5**(2): p. 361-368.
16. Bigliardi, P.L., et al., *Povidone iodine in wound healing: A review of current concepts and practices*. *International Journal of Surgery*, 2017. **44**: p. 260-268.

17. Orsi, I.A., et al., *Antimicrobial efficacy of chemical disinfectants on contaminated full metal crowns*. Braz Dent J, 2010. **21**(3): p. 241-6.
18. Gorman, S.P., E.M. Scott, and A.D. Russell, *Antimicrobial activity, uses and mechanism of action of glutaraldehyde*. Journal of Applied Bacteriology, 1980. **48**(2): p. 161-190.
19. Colon, G., B.C. Ward, and T.J. Webster, *Increased osteoblast and decreased Staphylococcus epidermidis functions on nanophase ZnO and TiO₂*. Journal of Biomedical Materials Research Part A, 2006. **78A**(3): p. 595-604.
20. Otter, J.A., et al., *Surface-attached cells, biofilms and biocide susceptibility: implications for hospital cleaning and disinfection*. Journal of Hospital Infection, 2015. **89**(1): p. 16-27.
21. Kumar, A., et al., *Biofilms: Survival and defense strategy for pathogens*. International Journal of Medical Microbiology, 2017. **307**(8): p. 481-489.
22. Arciola, C.R., et al., *Biofilm formation in Staphylococcus implant infections. A review of molecular mechanisms and implications for biofilm-resistant materials*. Biomaterials, 2012. **33**(26): p. 5967-5982.
23. Hasan, J., R.J. Crawford, and E.P. Ivanova, *Antibacterial surfaces: the quest for a new generation of biomaterials*. Trends in Biotechnology, 2013. **31**(5): p. 295-304.
24. Campoccia, D., L. Montanaro, and C.R. Arciola, *A review of the biomaterials technologies for infection-resistant surfaces*. Biomaterials, 2013. **34**(34): p. 8533-8554.
25. Tiller, J.C., et al., *Designing surfaces that kill bacteria on contact*. Proceedings of the National Academy of Sciences of the United States of America, 2001. **98**(11): p. 5981-5985.
26. Waschinski, C.J., et al., *Insights in the antibacterial action of poly(methyloxazoline)s with a biocidal end group and varying satellite groups*. Biomacromolecules, 2008. **9**(7): p. 1764-1771.
27. Hume, E.B.H., et al., *The control of Staphylococcus epidermidis biofilm formation and in vivo infection rates by covalently bound furanones*. Biomaterials, 2004. **25**(20): p. 5023-5030.
28. Roosjen, A., et al., *Inhibition of adhesion of yeasts and bacteria by poly(ethylene oxide)-brushes on glass in a parallel plate flow chamber*. Microbiology, 2003. **149**(11): p. 3239-3246.
29. Murata, H., et al., *Permanent, non-leaching antibacterial surface--2: how high density cationic surfaces kill bacterial cells*. Biomaterials, 2007. **28**(32): p. 4870-9.
30. Shah, N.J., et al., *Osteophilic multilayer coatings for accelerated bone tissue growth*. Adv Mater, 2012. **24**(11): p. 1445-50.
31. Li, Z., et al., *Two-level antibacterial coating with both release-killing and contact-killing capabilities*. Langmuir, 2006. **22**(24): p. 9820-9823.
32. Fujii, K., et al., *Prevention of Biofilm Formation with a Coating of 2-Methacryloyloxyethyl Phosphorylcholine Polymer*. Journal of Veterinary Medical Science, 2008. **70**(2): p. 167-173.

33. Ma, Y., et al., *Inhibition of *Staphylococcus epidermidis* Biofilm by Trimethylsilane Plasma Coating*. *Antimicrobial Agents and Chemotherapy*, 2012. **56**(11): p. 5923.
34. Popelka, A., et al., *Anti-bacterial Treatment of Polyethylene by Cold Plasma for Medical Purposes*. *Molecules*, 2012. **17**(1): p. 762.
35. Qu, J., et al., *Silver/hydroxyapatite composite coatings on porous titanium surfaces by sol-gel method*. *Journal of Biomedical Materials Research Part B: Applied Biomaterials*, 2011. **97B**(1): p. 40-48.
36. Fox, S., et al., *NO-loaded Zn²⁺-exchanged zeolite materials: A potential bifunctional anti-bacterial strategy*. *Acta Biomaterialia*, 2010. **6**(4): p. 1515-1521.
37. Carpenter, A.W., et al., *Dual Action Antimicrobials: Nitric Oxide Release from Quaternary Ammonium-Functionalized Silica Nanoparticles*. *Biomacromolecules*, 2012. **13**(10): p. 3334-3342.
38. Wang, J., et al., *Oxygen-Generating Nanofiber Cell Scaffolds with Antimicrobial Properties*. *ACS Applied Materials & Interfaces*, 2011. **3**(1): p. 67-73.
39. Cai, W., et al., *Carboxyl-epselen-based layer-by-layer films as potential antithrombotic and antimicrobial coatings*. *Biomaterials*, 2011. **32**(31): p. 7774-7784.
40. Fan, F.R.F. and A.J. Bard, *Chemical, electrochemical, gravimetric, and microscopic studies on antimicrobial silver films*. *Journal of Physical Chemistry B*, 2002. **106**(2): p. 279-287.
41. Pollini, M., et al., *Antibacterial coatings on haemodialysis catheters by photochemical deposition of silver nanoparticles*. *Journal of Materials Science-Materials in Medicine*, 2011. **22**(9): p. 2005-2012.
42. Eby, D.M., H.R. Luckarift, and G.R. Johnson, *Hybrid Antimicrobial Enzyme and Silver Nanoparticle Coatings for Medical Instruments*. *Acs Applied Materials & Interfaces*, 2009. **1**(7): p. 1553-1560.
43. Ivanova, E.P., et al., *The influence of nanoscopically thin silver films on bacterial viability and attachment*. *Applied Microbiology and Biotechnology*, 2011. **91**(4): p. 1149-1157.
44. Chernousova, S. and M. Epple, *Silver as Antibacterial Agent: Ion, Nanoparticle, and Metal*. *Angewandte Chemie International Edition*, 2013. **52**(6): p. 1636-1653.
45. Coeling, K.J., *Coating Processes, Spray Coating*, in *Kirk-Othmer Encyclopedia of Chemical Technology*. 2000.
46. Righetti, P.G. and C. Gelfi, *Electrophoresis*, in *Ullmann's Encyclopedia of Industrial Chemistry*. 2000.
47. Sarkar, P. and P.S. Nicholson, *Electrophoretic Deposition (EPD): Mechanisms, Kinetics, and Application to Ceramics*. *Journal of the American Ceramic Society*, 1996. **79**(8): p. 1987-2002.
48. Carlsson, J.-O. and P.M. Martin, *Chapter 7 - Chemical Vapor Deposition*, in *Handbook of Deposition Technologies for Films and Coatings (Third Edition)*, P.M. Martin, Editor. 2010, William Andrew Publishing: Boston. p. 314-363.
49. *Thin Films*, in *Van Nostrand's Scientific Encyclopedia*. 2006.

50. Rumaiz, A.K., et al., *Thin Film Formation Techniques*, in *Kirk-Othmer Encyclopedia of Chemical Technology*. 2000, John Wiley & Sons, Inc.
51. Juhasz, J.A. and S.M. Best, *6 - Surface modification of biomaterials by calcium phosphate deposition*, in *Surface Modification of Biomaterials*, R. Williams, Editor. 2011, Woodhead Publishing. p. 143-169.
52. Milev, A.S., G.S.K. Kannangara, and M.A. Wilson, *Nanotechnology*, in *Kirk-Othmer Encyclopedia of Chemical Technology*. 2000, John Wiley & Sons, Inc.
53. Stankic, S., et al., *Pure and multi metal oxide nanoparticles: synthesis, antibacterial and cytotoxic properties*. *Journal of Nanobiotechnology*, 2016. **14**: p. 20.
54. Pierre, A.C., *Sol-Gel Technology*, in *Kirk-Othmer Encyclopedia of Chemical Technology*. 2007, John Wiley & Sons, Inc.
55. Chun, A.L., *Playing tricks on bacteria*. *Nature Nanotechnology*, 2009.
56. Pelgrift, R.Y. and A.J. Friedman, *Nanotechnology as a therapeutic tool to combat microbial resistance*. *Adv Drug Deliv Rev*, 2013. **65**(13-14): p. 1803-15.
57. Blecher, K., A. Nasir, and A. Friedman, *The growing role of nanotechnology in combating infectious disease*. *Virulence*, 2011. **2**(5): p. 395-401.
58. Vigneshwaran, N., et al., *A novel one-pot 'green' synthesis of stable silver nanoparticles using soluble starch*. *Carbohydrate Research*, 2006. **341**(12): p. 2012-2018.
59. Xu, G.n., et al., *Preparation and characterization of stable monodisperse silver nanoparticles via photoreduction*. *Colloids and Surfaces A: Physicochemical and Engineering Aspects*, 2008. **320**(1-3): p. 222-226.
60. Huh, A.J. and Y.J. Kwon, "Nanoantibiotics": *A new paradigm for treating infectious diseases using nanomaterials in the antibiotics resistant era*. *Journal of Controlled Release*, 2011. **156**(2): p. 128-145.
61. Alexander, J.W., *History of the Medical Use of Silver*. *Surgical Infections*, 2009. **10**(3): p. 289-292.
62. Dibrov, P., et al., *Chemiosmotic mechanism of antimicrobial activity of Ag⁺ in Vibrio cholerae*. *Antimicrobial Agents and Chemotherapy*, 2002. **46**(8): p. 2668-2670.
63. Johnston, H.J., et al., *A review of the in vivo and in vitro toxicity of silver and gold particulates: Particle attributes and biological mechanisms responsible for the observed toxicity*. *Critical Reviews in Toxicology*, 2010. **40**(4): p. 328-346.
64. Prabhu, S. and E.K. Poulouse, *Silver nanoparticles: Mechanism of antimicrobial action, synthesis, medical applications, and toxicity effects*. *Int. Nano Lett.*, 2012. **2**(1).
65. Lemire, J.A., J.J. Harrison, and R.J. Turner, *Antimicrobial activity of metals: mechanisms, molecular targets and applications*. *Nature Reviews Microbiology*, 2013. **11**: p. 371.
66. McShan, D., P.C. Ray, and H. Yu, *Molecular toxicity mechanism of nanosilver*. *Journal of Food and Drug Analysis*, 2014. **22**(1): p. 116-127.
67. Sondi, I. and B. Salopek-Sondi, *Silver nanoparticles as antimicrobial agent: a case study on E. coli as a model for Gram-negative bacteria*. *Journal of Colloid and Interface Science*, 2004. **275**(1): p. 177-182.

68. Le Ouay, B. and F. Stellacci, *Antibacterial activity of silver nanoparticles: A surface science insight*. Nano Today, 2015. **10**(3): p. 339-354.
69. Cho, K.-H., et al., *The study of antimicrobial activity and preservative effects of nanosilver ingredient*. Electrochimica Acta, 2005. **51**(5): p. 956-960.
70. Hadrup, N. and H.R. Lam, *Oral toxicity of silver ions, silver nanoparticles and colloidal silver – A review*. Regulatory Toxicology and Pharmacology, 2014. **68**(1): p. 1-7.
71. de Lima, R., A.B. Seabra, and N. Durán, *Silver nanoparticles: a brief review of cytotoxicity and genotoxicity of chemically and biogenically synthesized nanoparticles*. Journal of Applied Toxicology, 2012. **32**(11): p. 867-879.
72. Pal, S., Y.K. Tak, and J.M. Song, *Does the antibacterial activity of silver nanoparticles depend on the shape of the nanoparticle? A study of the gram-negative bacterium Escherichia coli*. Applied and Environmental Microbiology, 2007. **73**(6): p. 1712-1720.
73. Li, Q., et al., *Antimicrobial nanomaterials for water disinfection and microbial control: Potential applications and implications*. Water Research, 2008. **42**(18): p. 4591-4602.
74. Sondi, I. and B. Salopek-Sondi, *Silver nanoparticles as antimicrobial agent: A case study on E. coli as a model for Gram-negative bacteria*. Journal of Colloid and Interface Science, 2004. **275**(1): p. 177-182.
75. Herrmann, J.-M., *Photocatalysis*, in *Kirk-Othmer Encyclopedia of Chemical Technology*. 2017, Kirk-Othmer Encyclopedia of Chemical Technology, John Wiley & Sons, Inc (Ed.).
76. Adriana, Z., *Doped-TiO₂: A Review*. Recent Patents on Engineering, 2008. **2**(3): p. 157-164.
77. Asahi, R., et al., *Visible-Light Photocatalysis in Nitrogen-Doped Titanium Oxides*. Science, 2001. **293**(5528): p. 269-271.
78. Duran-Alvares, J.C., et al., *Photocatalytic degradation of ciprofloxacin using mono- (Au, Ag and Cu) and bi- (Au-Ag and Au-Cu) metallic nanoparticles supported on TiO₂ under UV-C and simulated sunlight*. Catalysis Today, 2016. **266**: p. 175-187.
79. Gopinath, K., et al., *Eco-friendly synthesis of TiO₂, Au and Pt doped TiO₂ nanoparticles for dye sensitized solar cell applications and evaluation of toxicity*. Superlattices and Microstructures, 2016. **92**: p. 100-110.
80. Hamad, A., et al., *The characteristics of novel bimodal Ag-TiO₂ nanoparticles generated by hybrid laser-ultrasonic technique*. Applied Physics a-Materials Science & Processing, 2016. **122**(4).
81. Jia, Y., et al., *Fabrication of TiO₂-Bi₂WO₆ Binanosheet for Enhanced Solar Photocatalytic Disinfection of E-coli: Insights on the Mechanism*. Acs Applied Materials & Interfaces, 2016. **8**(11): p. 6841-6851.
82. Sood, S., et al., *Bi₂O₃/TiO₂ heterostructures: Synthesis, characterization and their application in solar light mediated photocatalyzed degradation of an antibiotic, ofloxacin*. Chemical Engineering Journal, 2016. **290**: p. 45-52.
83. Dhanapandian, S., A. Arunachalam, and C. Manoharan, *Highly oriented and physical properties of sprayed anatase Sn-doped TiO₂ thin films with an enhanced antibacterial activity*. Applied Nanoscience, 2016. **6**(3): p. 387-397.

84. Dhineshababu, N.R., et al., *Enhanced functional properties of cotton fabrics using TiO₂/SiO₂ nanocomposites*. Journal of Industrial Textiles, 2016. **45**(5): p. 674-692.
85. Leyland, N.S., et al., *Highly Efficient F, Cu doped TiO₂ anti-bacterial visible light active photocatalytic coatings to combat hospital-acquired infections*. Sci Rep, 2016. **6**: p. 24770.
86. Parvathi V, P., et al., *Synergistic effect of MgO/Ag co-doping on TiO₂ for efficient antibacterial agents*. Materials Letters, 2016. **184**: p. 82-87.
87. Yuzheng, W., et al., *Co-doping TiO₂ with boron and/or yttrium elements: effects on antimicrobial activity*. Materials Science and Engineering: B (Advanced Functional Solid-State Materials), 2016. **211**: p. 149-55.
88. Na Phattalung, S., S. Limpijumnong, and J. Yu, *Passivated co-doping approach to bandgap narrowing of titanium dioxide with enhanced photocatalytic activity*. Applied Catalysis B: Environmental, 2017. **200**: p. 1-9.
89. Xiaojing, H., et al., *Antibacterial ability and osteogenic activity of porous Sr/Ag-containing TiO₂ coatings*. Biomedical Materials, 2016. **11**(4): p. 045008 (18 pp.).
90. Wang, Y.Z., et al., *Microstructure and antibacterial activity of ions (Ce, Y, or B)-doped Zn-TiO₂: a comparative study*. 2016: p. 1-11.
91. Raja, V., et al., *A study on the free radical generation and photocatalytic yield in extended surfaces of visible light active TiO₂ compounds*. Solar Energy Materials & Solar Cells, 2016. **152**: p. 125-32.
92. Duo, F., et al., *Low temperature one-step synthesis of rutile TiO₂/BiOCl composites with enhanced photocatalytic activity*. Materials Characterization, 2015. **99**: p. 8-16.
93. Tobaldi, D.M., et al., *Cu-TiO₂ Hybrid Nanoparticles Exhibiting Tunable Photochromic Behavior*. Journal of Physical Chemistry C, 2015. **119**(41): p. 23658-23668.
94. Naghibi, S., et al., *Exploring a new phenomenon in the bactericidal response of TiO₂ thin films by Fe doping: Exerting the antimicrobial activity even after stoppage of illumination*. Applied Surface Science, 2015. **327**: p. 371-378.
95. Prabha, S., et al., *Activated charcoal supported cadmium doped TiO₂ for photocatalytic and antibacterial applications*. International Letters of Chemistry, Physics and Astronomy, 2015. **44**: p. 108-23.
96. Lin, H., et al., *Iodine-modified nanocrystalline titania for photo-catalytic antibacterial application under visible light illumination*. Applied Catalysis B: Environmental, 2015. **176-177**: p. 36-43.
97. Zhang, C., et al., *Sodium-promoted Pd/TiO₂ for catalytic oxidation of formaldehyde at ambient temperature*. Environ Sci Technol, 2014. **48**(10): p. 5816-22.
98. Yang, H., Y. Wang, and X. Xue, *Influences of glycerol as an efficient doping agent on crystal structure and antibacterial activity of B-TiO₂ nano-materials*. Colloids and Surfaces B: Biointerfaces, 2014. **122**: p. 701-8.
99. Wang, Y., X. Xue, and H. Yang, *Synthesis and antimicrobial activity of boron-doped titania nano-materials*. Chinese Journal of Chemical Engineering, 2014. **22**(4): p. 474-479.

100. Wang, Y., X. Xue, and H. Yang, *Modification of the antibacterial activity of Zn/TiO₂ nano-materials through different anions doped*. Vacuum, 2014. **101**: p. 193-199.
101. Kongsong, P., et al., *Photocatalytic Antibacterial Performance of Glass Fibers Thin Film Coated with N-Doped SnO₂/TiO₂*. Scientific World Journal, 2014: p. 869706 (9 pp.).
102. Yuzheng, W., X. Xiangxin, and Y. He, *Preparation and characterization of carbon or/and boron-doped titania nano-materials with antibacterial activity*. Ceramics International, 2014. **40**(8): p. 12533-7.
103. Wang, C. and Y. Li, *Preparation and characterisation of S doped TiO₂/natural zeolite with photocatalytic and adsorption activities*. Materials Technology, 2014. **29**(4): p. 204-9.
104. Amna, T., et al., *Characterization and potent bactericidal effect of Cobalt doped Titanium dioxide nanofibers*. Ceramics International, 2013. **39**(3): p. 3189-3193.
105. Ramya, S., et al., *Antibacterial studies on Eu-Ag codoped TiO₂ surfaces*. Ceramics International, 2013. **39**(2): p. 1695-1705.
106. Yu, B., W.M. Lau, and J. Yang, *Preparation and characterization of N-TiO₂ photocatalyst with high crystallinity and enhanced photocatalytic inactivation of bacteria*. Nanotechnology, 2013. **24**(33).
107. Jalal, R., et al., *ZnO nanofluids: Green synthesis, characterization, and antibacterial activity*. Materials Chemistry and Physics, 2010. **121**(1-2): p. 198-201.
108. Ramani, M., S. Ponnusamy, and C. Muthamizhchelvan, *From zinc oxide nanoparticles to microflowers: A study of growth kinetics and biocidal activity*. Materials Science and Engineering: C, 2012. **32**(8): p. 2381-2389.
109. Hafez, E.E., et al., *Assessment of antibacterial activity for synthesized Zinc Oxide nanorods against plant pathogenic strains*. International journal of scientific & technology research, 2014. **3**(9).
110. Kumar, S.S., et al., *Synthesis, characterization and optical properties of zinc oxide nanoparticles*. International Nano Letters, 2013. **3**(1): p. 30.
111. Talebian, N., S.M. Amininezhad, and M. Douidi, *Controllable synthesis of ZnO nanoparticles and their morphology-dependent antibacterial and optical properties*. J Photochem Photobiol B, 2013. **120**: p. 66-73.
112. Azizi, S., et al., *ZnO-Ag core shell nanocomposite formed by green method using essential oil of wild ginger and their bactericidal and cytotoxic effects*. Applied Surface Science, 2016. **384**: p. 517-524.
113. Sharma, N., et al., *Synthesis, characterisation and antimicrobial activity of manganese- and iron-doped zinc oxide nanoparticles*. Journal of Experimental Nanoscience, 2016. **11**(1): p. 54-71.
114. Arul Mary, J., et al., *Microwave-assisted synthesis, characterization and antibacterial properties of Ce-Cu dual doped ZnO nanostructures*. Optik, 2016. **127**(4): p. 2360-2365.
115. Ravichandran, K., et al., *Influence of a novel triple doping (Ag+Mn+F) on the magnetic and antibacterial properties of ZnO nanopowders*. Ceramics International, 2016. **42**(2): p. 2349-2356.

116. Vreuls, C., et al., *Biomolecules in multilayer film for antimicrobial and easy-cleaning stainless steel surface applications*. *Biofouling*, 2010. **26**(6): p. 645-656.
117. Konradi, R., C. Acikgoz, and M. Textor, *Polyoxazolines for Nonfouling Surface Coatings — A Direct Comparison to the Gold Standard PEG*. *Macromolecular Rapid Communications*, 2012. **33**(19): p. 1663-1676.
118. Wang, Q., et al., *Self-Assembled Poly(ethylene glycol)-co-Acrylic Acid Microgels to Inhibit Bacterial Colonization of Synthetic Surfaces*. *ACS Applied Materials & Interfaces*, 2012. **4**(5): p. 2498-2506.
119. Carvalho, I., et al., *Influence of surface features on the adhesion of Staphylococcus epidermidis to Ag-TiCN thin films*. *Science and Technology of Advanced Materials*, 2013. **14**(3): p. 035009.
120. Veiga, A.S., et al., *Arginine-rich self-assembling peptides as potent antibacterial gels*. *Biomaterials*, 2012. **33**(35): p. 8907-8916.
121. Mohamed, N.A. and N.A. Abd El-Ghany, *Preparation and antimicrobial activity of some carboxymethyl chitosan acyl thiourea derivatives*. *International Journal of Biological Macromolecules*, 2012. **50**(5): p. 1280-1285.
122. Sun, B., et al., *Nitric Oxide-Releasing Dendrimers as Antibacterial Agents*. *Biomacromolecules*, 2012. **13**(10): p. 3343-3354.
123. Dunnill, C.W. and I.P. Parkin, *Nitrogen-doped TiO₂ thin films: photocatalytic applications for healthcare environments*. *Dalton Transactions*, 2011. **40**(8): p. 1635-1640.
124. Kim, B.H., et al., *Study in Bactericidal Properties of Chlorhexidine Grafting on the Modified Titanium*. *Journal of Nanoscience and Nanotechnology*, 2011. **11**(2): p. 1530-1533.
125. Vukčević, M., et al., *Surface characteristics and antibacterial activity of a silver-doped carbon monolith*. *Science and Technology of Advanced Materials*, 2008. **9**(1): p. 015006.
126. Dutta, S., et al., *Counterion-Induced Modulation in the Antimicrobial Activity and Biocompatibility of Amphiphilic Hydrogelators: Influence of in-Situ-Synthesized Ag-Nanoparticle on the Bactericidal Property*. *Langmuir*, 2011. **27**(8): p. 5000-5008.
127. Grandi, S., et al., *Bone Reconstruction: Au Nanocomposite Bioglasses with Antibacterial Properties*. *The International Journal of Artificial Organs*, 2011. **34**(9): p. 920-928.
128. Brackman, G., et al., *Quorum Sensing Inhibitors Increase the Susceptibility of Bacterial Biofilms to Antibiotics In Vitro and In Vivo*. *Antimicrobial Agents and Chemotherapy*, 2011. **55**(6): p. 2655-2661.
129. Hochbaum, A.I., et al., *Inhibitory Effects of d-Amino Acids on Staphylococcus aureus Biofilm Development*. *Journal of Bacteriology*, 2011. **193**(20): p. 5616-5622.
130. Peran, J., et al., *Antimicrobial effectiveness of cellulose based fabrics treated with silver nitrate solution using plasma processes*. *Tekstilec*, 2017. **60**(4): p. 247-253.
131. Nowack, B., H.F. Krug, and M. Height, *120 Years of Nanosilver History: Implications for Policy Makers*. *Environmental Science & Technology*, 2011. **45**(4): p. 1177-1183.

132. Marambio-Jones, C. and E.M.V. Hoek, *A review of the antibacterial effects of silver nanomaterials and potential implications for human health and the environment*. Journal of Nanoparticle Research, 2010. **12**(5): p. 1531-1551.
133. Haynes, W.M., *CRC handbook of chemistry and physics*. 1978: Cleveland, Ohio : CRC Press.
134. Mahltig, B., D. Fiedler, and P. Simon, *Silver-containing sol-gel coatings on textiles: antimicrobial effect as a function of curing treatment*. Journal of the Textile Institute, 2011. **102**(9): p. 739-745.
135. Meininger, M., et al., *Silver and copper addition enhances the antimicrobial activity of calcium hydroxide coatings on titanium*. J Mater Sci Mater Med, 2018. **29**(5): p. 61.
136. Tran, N., et al., *Silver doped titanium oxide-PDMS hybrid coating inhibits Staphylococcus aureus and Staphylococcus epidermidis growth on PEEK*. Materials Science & Engineering C-Materials for Biological Applications, 2015. **49**: p. 201-209.
137. Shende, P., B. Oza, and R.S. Gaud, *Silver-doped titanium dioxide nanoparticles encapsulated in chitosan/PVA film for synergistic antimicrobial activity*. 2018: p. 1-7.
138. Ibanescu, M., et al., *Photocatalytic and antimicrobial Ag/ZnO nanocomposites for functionalization of textile fabrics*. Journal of Alloys and Compounds, 2014. **610**: p. 244-9.
139. Hans, M., et al., *Laser cladding of stainless steel with a copper-silver alloy to generate surfaces of high antimicrobial activity*. Applied Surface Science, 2014. **320**: p. 195-199.
140. Cong, F., et al., *Antimicrobial silver-hydroxyapatite composite coatings through two-stage electrochemical synthesis*. Surface and Coatings Technology, 2016. **301**: p. 13-19.
141. *NIST X-ray Photoelectron Spectroscopy Database, Version 4.1 (National Institute of Standards and Technology, Gaithersburg, 2012)*; <http://srdata.nist.gov/xps/>. Available from: <http://srdata.nist.gov/xps/>.
142. *NIST Chemistry WebBook, NIST Standard Reference Database Number 69, Eds. P.J. Linstrom and W.G. Mallard*.
143. Hindrichs, G., *Metallographische Mitteilungen aus dem Institut für physikalische Chemie der Universität Göttingen. LXVII. Über einige Chrom- und Manganlegierungen*. Zeitschrift für anorganische Chemie, 1908. **59**(1): p. 414-449.
144. Allen, B.C., *Solubility of chromium in liquid silver and molybdenum and tungsten in liquid tin*. Trans. Met. Soc. AIME, 239: 1026-29 (July 1967). 1967: p. Medium: X.
145. Grigorev, A.T., E.M. Sokolovskaya, and M.I. Kruglova, *Alloys of Silver and Chromium*. Vestn. Mosk. Univ. Ser. Fiz. Mat. Estest. Nauk, 9 (1954) 77-81., 1954.
146. Oliver, W.C. and G.M. Pharr, *An improved technique for determining hardness and elastic-modulus using load and displacement sensing indentation experiments*. Journal of Materials Research, 1992. **7**(6): p. 1564-1583.
147. Pharr, G.M. and W.C. Oliver, *Measurement of thin-film mechanical-properties using nanoindentation*. MRS Bulletin, 1992. **17**(7): p. 28-33.

148. Tsui, T.Y., et al., *Nanoindentation and nanoscratching of hard carbon coatings for magnetic disks*, in *Mechanical Behavior of Diamond and Other Forms of Carbon*, M.D. Drory, et al., Editors. 1995, Materials Research Soc: Pittsburgh. p. 447-452.
149. *JIS Z 2801:2010 Antibacterial products -Test for antibacterial activity and efficacy*. 2010.
150. Knetsch, M.L.W. and L.H. Koole, *New Strategies in the Development of Antimicrobial Coatings: The Example of Increasing Usage of Silver and Silver Nanoparticles*. *Polymers*, 2011. **3**(1): p. 340.
151. Lara, H.H., et al., *Bactericidal effect of silver nanoparticles against multidrug-resistant bacteria*. *World Journal of Microbiology and Biotechnology*, 2010. **26**(4): p. 615-621.
152. Huang, L., et al., *Synergistic Combination of Chitosan Acetate with Nanoparticle Silver as a Topical Antimicrobial: Efficacy against Bacterial Burn Infections*. *Antimicrobial Agents and Chemotherapy*, 2011. **55**(7): p. 3432-3438.
153. Randall, C.P., et al., *The silver cation (Ag⁺): antistaphylococcal activity, mode of action and resistance studies*. *Journal of Antimicrobial Chemotherapy*, 2013. **68**(1): p. 131-138.
154. Arakha, M., et al., *The effects of interfacial potential on antimicrobial propensity of ZnO nanoparticle*. *Scientific Reports*, 2015. **5**: p. 9578.
155. (ACSQHC), A.C.o.S.a.Q.i.H.C., *AURA 2016: first Australian report on antimicrobial use and resistance in human health*. 2016.
156. Allaker, R.P. and G. Ren, *Potential impact of nanotechnology on the control of infectious diseases*. *Trans R Soc Trop Med Hyg*, 2008. **102**(1): p. 1-2.
157. Feng, Y., et al., *Photoactive antimicrobial nanomaterials*. *Journal of Materials Chemistry B*, 2017. **5**(44): p. 8631-8652.
158. Liu, S., et al., *Porous Fluorinated SnO₂ Hollow Nanospheres: Transformative Self-assembly and Photocatalytic Inactivation of Bacteria*. *ACS Applied Materials & Interfaces*, 2014. **6**(4): p. 2407-2414.
159. Khan, M.M., S.F. Adil, and A. Al-Mayouf, *Metal oxides as photocatalysts*. *Journal of Saudi Chemical Society*, 2015. **19**(5): p. 462-464.
160. Thill, A., et al., *Cytotoxicity of CeO₂ Nanoparticles for Escherichia coli. Physico-Chemical Insight of the Cytotoxicity Mechanism*. *Environmental Science & Technology*, 2006. **40**(19): p. 6151-6156.
161. Sawai, J., *Quantitative evaluation of antibacterial activities of metallic oxide powders (ZnO, MgO and CaO) by conductimetric assay*. *Journal of Microbiological Methods*, 2003. **54**(2): p. 177-182.
162. Qi, K., et al., *Review on the improvement of the photocatalytic and antibacterial activities of ZnO*. *Journal of Alloys and Compounds*, 2017. **727**: p. 792-820.
163. Djurišić, A.B., et al., *Toxicity of metal oxide nanoparticles: Mechanisms, characterization, and avoiding experimental artefacts*. *Small*, 2015. **11**(1): p. 26-44.
164. Raghupathi, K.R., R.T. Koodali, and A.C. Manna, *Size-dependent bacterial growth inhibition and mechanism of antibacterial activity of zinc oxide nanoparticles*. *Langmuir*, 2011. **27**(7): p. 4020-4028.

165. Bellanger, X., et al., *Stability and toxicity of ZnO quantum dots: Interplay between nanoparticles and bacteria*. Journal of Hazardous Materials, 2015. **283**: p. 110-116.
166. Heinlaan, M., et al., *Toxicity of nanosized and bulk ZnO, CuO and TiO₂ to bacteria *Vibrio fischeri* and crustaceans *Daphnia magna* and *Thamnocephalus platyurus**. Chemosphere, 2008. **71**(7): p. 1308-1316.
167. Zhang, L., et al., *ZnO nanofluids-A potential antibacterial agent*. Progress in Natural Science, 2008. **18**(8): p. 939-944.
168. Kolodziejczak-Radzimska, A. and T. Jesionowski, *Zinc Oxide-From Synthesis to Application: A Review*. Materials, 2014. **7**(4): p. 2833-2881.
169. Samadi, M., et al., *Recent progress on doped ZnO nanostructures for visible-light photocatalysis*. Thin Solid Films, 2016. **605**: p. 2-19.
170. Ong, C.B., L.Y. Ng, and A.W. Mohammad, *A review of ZnO nanoparticles as solar photocatalysts: Synthesis, mechanisms and applications*. Renewable and Sustainable Energy Reviews, 2018. **81**: p. 536-551.
171. V, L.P. and R. Vijayaraghavan, *Chemical manipulation of oxygen vacancy and antibacterial activity in ZnO*. Materials Science and Engineering: C, 2017. **77**: p. 1027-1034.
172. Wang, W., T. Ai, and Q. Yu, *Electrical and photocatalytic properties of boron-doped ZnO nanostructure grown on PET-ITO flexible substrates by hydrothermal method*. Scientific Reports, 2017. **7**: p. 42615.
173. Ravichandran, K., N. Chidhambaram, and S. Gobalakrishnan, *Copper and Graphene activated ZnO nanopowders for enhanced photocatalytic and antibacterial activities*. Journal of Physics and Chemistry of Solids, 2016. **93**: p. 82-90.
174. Hui, A., J. Liu, and J. Ma, *Synthesis and morphology-dependent antimicrobial activity of cerium doped flower-shaped ZnO crystallites under visible light irradiation*. Colloids and Surfaces A: Physicochemical and Engineering Aspects, 2016. **506**: p. 519-525.
175. Tauc, J., R. Grigorovici, and A. Vancu, *Optical Properties and Electronic Structure of Amorphous Germanium*. physica status solidi (b), 1966. **15**(2): p. 627-637.
176. Abeles, F., *Optical properties of solids*. 1972, Amsterdam, New York: Amsterdam : North-Holland Pub. Co. ; New York : American Elsevier.
177. Zak, A.K., et al., *Synthesis and characterization of ZnO nanoparticles prepared in gelatin media*. Materials Letters, 2011. **65**(1): p. 70-73.
178. Darroudi, M., et al., *Sol-gel synthesis, characterization, and neurotoxicity effect of zinc oxide nanoparticles using gum tragacanth*. Ceramics International, 2013. **39**(8): p. 9195-9199.
179. Kumar, R., et al., *Efficient ZnO-based visible-light-driven photocatalyst for antibacterial applications*. ACS Applied Materials & Interfaces, 2014. **6**(15): p. 13138-13148.
180. Marsalek, R., *Particle Size and Zeta Potential of ZnO*. APCBEE Procedia, 2014. **9**: p. 13-17.

181. Xitao, W., L. Rong, and W. Kang, *Synthesis of ZnO@ZnS-Bi₂S₃ core-shell nanorod grown on reduced graphene oxide sheets and its enhanced photocatalytic performance*. Journal of Materials Chemistry A, 2014. **2**(22): p. 8304-8313.
182. Sang, H.X., et al., *Enhanced photocatalytic H₂ production from glycerol solution over ZnO/ZnS core/shell nanorods prepared by a low temperature route*. International Journal of Hydrogen Energy, 2012. **37**(2): p. 1348-1355.
183. Yu, H., et al., *Effects of hydrothermal post-treatment on microstructures and morphology of titanate nanoribbons*. Journal of Solid State Chemistry, 2006. **179**(2): p. 349-354.
184. Zak, A.K., et al., *Effects of annealing temperature on some structural and optical properties of ZnO nanoparticles prepared by a modified sol-gel combustion method*. Ceramics International, 2011. **37**(1): p. 393-398.
185. Yin, X.T., et al., *Ag-ZnO composite nanocrystals: synthesis, characterisation and photocatalytic properties*. Materials Research Innovations, 2012. **16**(3): p. 213-218.
186. Vijayaprasath, G., et al., *Structural, optical and antibacterial activity studies of neodymium doped ZnO nanoparticles*. Journal of Materials Science: Materials in Electronics, 2015. **26**(10): p. 7564-7576.
187. Aytekin Aydın, M.T., et al., *Synthesis, characterization and antibacterial activity of silver-doped TiO₂ nanotubes*. Spectrochimica Acta Part A: Molecular and Biomolecular Spectroscopy, 2018. **205**: p. 503-507.
188. Awad, A., et al., *Polymer nanocomposites part I: Structural characterization of zinc oxide nanoparticles synthesized via novel calcination method*. Journal of Thermoplastic Composite Materials, 2015. **28**(9): p. 1343-1358.
189. Pasquet, J., et al., *The contribution of zinc ions to the antimicrobial activity of zinc oxide*. Colloids and Surfaces A: Physicochemical and Engineering Aspects, 2014. **457**: p. 263-274.
190. Djurišić, A.B., et al., *Photoluminescence and Electron Paramagnetic Resonance of ZnO Tetrapod Structures*. Advanced Functional Materials, 2004. **14**(9): p. 856-864.
191. Padmavathy, N. and R. Vijayaraghavan, *Enhanced bioactivity of ZnO nanoparticles—an antimicrobial study*. Science and Technology of Advanced Materials, 2008. **9**(3): p. 035004.
192. Xie, Y., et al., *Antibacterial Activity and Mechanism of Action of Zinc Oxide Nanoparticles against Campylobacter jejuni*. Applied and Environmental Microbiology, 2011. **77**(7): p. 2325-2331.
193. Basu, M., N. Garg, and A.K. Ganguli, *A type-II semiconductor (ZnO/CuS heterostructure) for visible light photocatalysis*. Journal of Materials Chemistry A, 2014. **2**(20): p. 7517-7525.
194. Coronado, J.M., et al., *Design of Advanced Photocatalytic Materials for Energy and Environmental Applications*. 2013: Springer London.
195. Klingshirn, C., *ZnO: From basics towards applications*. physica status solidi (b), 2007. **244**(9): p. 3027-3073.
196. Pierret, R.F., *Advanced Semiconductor Fundamentals*. 2003: Prentice Hall.

197. Fagan, R., et al., *A review of solar and visible light active TiO₂ photocatalysis for treating bacteria, cyanotoxins and contaminants of emerging concern*. *Materials Science in Semiconductor Processing*, 2016. **42**: p. 2-14.
198. Hindi, K.M., et al., *The antimicrobial efficacy of sustained release silver–carbene complex-loaded l-tyrosine polyphosphate nanoparticles: Characterization, in vitro and in vivo studies*. *Biomaterials*, 2009. **30**(22): p. 3771-3779.